AD-A029 456

Methods for Controlling the Sideforce on Surface Piercing Hydrofoil Struts

David W. Taylor Naval Ship Res & Dev Center

July 1976

DAVID W. TAYLOR NAVAL SHIP RESEARCH AND DEVELOPMENT CENTER

Bethesda, Md. 20084

Methods for Controlling the Sideforce on Surface-Piercing Hydrofoil Struts

by

Richard S. Rothblum
Michael F. Jeffers
Russel P. Smith

Ship Performance Department
Departmental Report

July 1976

SPD-700-01

MAJOR DTNSRDC ORGANIZATIONAL COMPONENTS

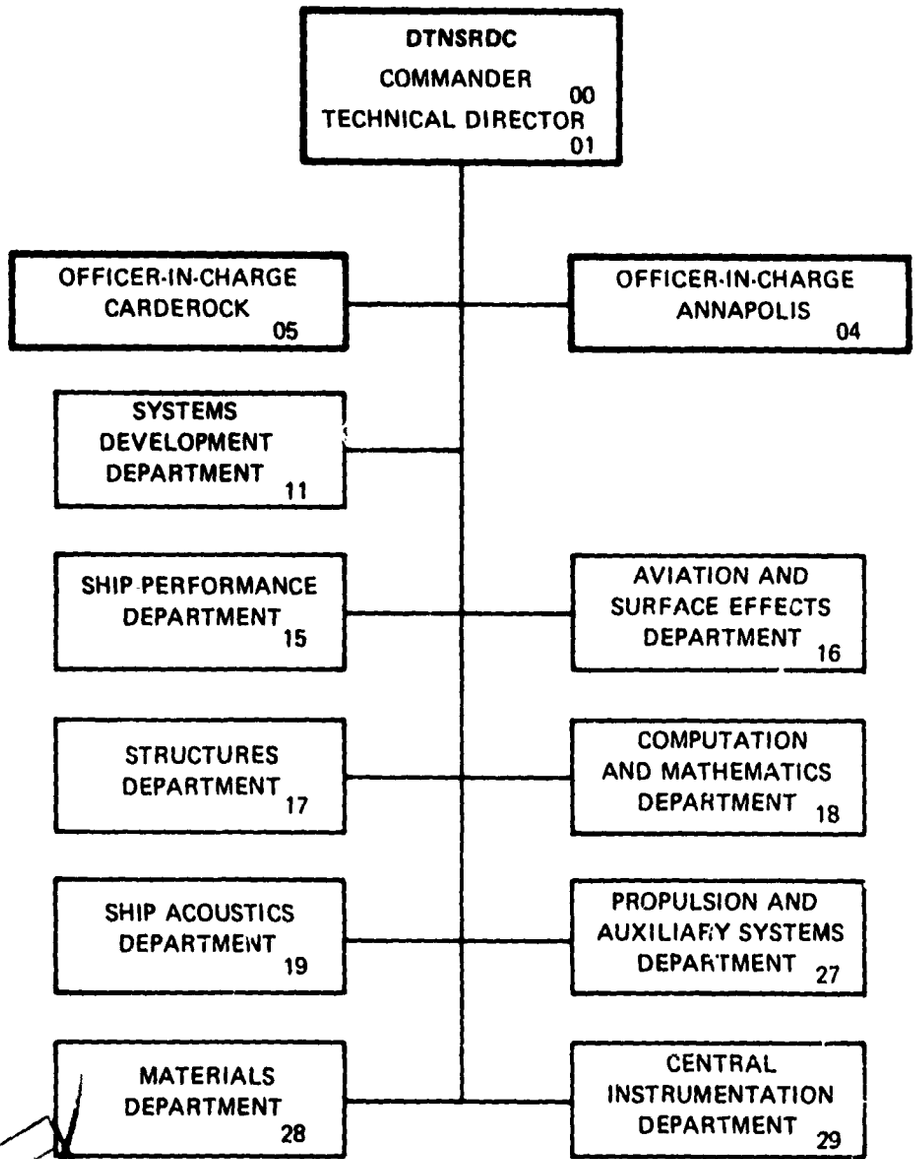

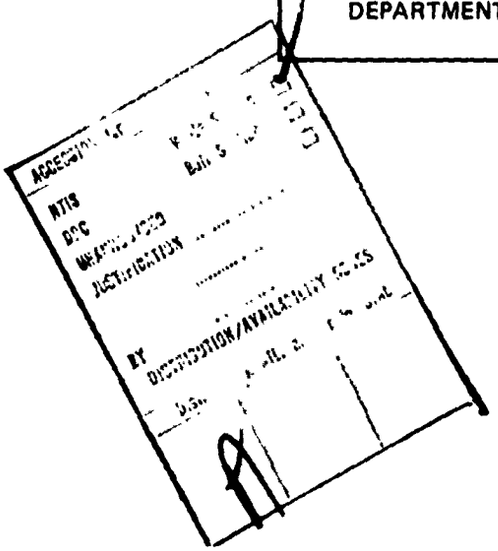

UNCLASSIFIED

SECURITY CLASSIFICATION OF THIS PAGE *(When Data Entered)*

REPORT DOCUMENTATION PAGE		READ INSTRUCTIONS BEFORE COMPLETING FORM
1. REPORT NUMBER SPD-700-01	2. GOVT ACCESSION NO.	3. RECIPIENT'S CATALOG NUMBER
4. TITLE *(and Subtitle)* Methods for Controlling the Sideforce on Surface-Piercing Hydrofoil Struts		5. TYPE OF REPORT & PERIOD COVERED Final 6. PERFORMING ORG. REPORT NUMBER
7. AUTHOR(s) Richard S. Rothblum Michael F. Jeffers Russell P. Smith		8. CONTRACT OR GRANT NUMBER(s)
9. PERFORMING ORGANIZATION NAME AND ADDRESS David W. Taylor Naval Ship R&D Center Bethesda, Maryland 20084		10. PROGRAM ELEMENT, PROJECT, TASK AREA & WORK UNIT NUMBERS
11. CONTROLLING OFFICE NAME AND ADDRESS Systems Development Department. Advanced Hydrofoil Systems Office, David W. Taylor Naval Ship R&D Center, Bethesda, Maryland 20084		12. REPORT DATE July 1976 13. NUMBER OF PAGES 127
14. MONITORING AGENCY NAME & ADDRESS(if different from Controlling Office)		15. SECURITY CLASS. (of this report) UNCLASSIFIED 15a. DECLASSIFICATION/DOWNGRADING SCHEDULE

16. DISTRIBUTION STATEMENT *(of this Report)*

APPROVED FOR PUBLIC RELEASE: DISTRIBUTION UNLIMITED

17. DISTRIBUTION STATEMENT *(of the abstract entered in Block 20, if different from Report)*

18. SUPPLEMENTARY NOTES

19. KEY WORDS *(Continue on reverse side if necessary and identify by block number)*

Hydrofoil, Struts, Ventilation, Lift, Drag, Sideforce, Aeration, Airbleed, Air injection, Cavitation, Ventilation fences, Fences, Cavitation plate, Endplate, Flaps, Split flaps, Trailing edge flaps, Nose flaps

20. ABSTRACT *(Continue on reverse side if necessary and identify by block number)*

Possible means of reducing the sideforce due to sideslip angle on a surface-piercing hydrofoil strut were investigated. An experimental program was performed to test the effect on strut sideforce and ventilation characteristics of 50-percent chord trailing edge flaps, midchord spoilers (split flaps), and airbleed (air injection). The effect of fences was tested in combination with the trailing edge flap and airbleed. All systems were found to be effective in reducing or changing sideforce. None of the methods

DD FORM 1 JAN 73 1473 EDITION OF 1 NOV 65 IS OBSOLETE
S/N 0102-014-6601

UNCLASSIFIED

SECURITY CLASSIFICATION OF THIS PAGE *(When Data Entered)*

significantly improved strut resistance to ventilation, but airbleed and spoilers reduced the abruptness of transition to the ventilated state under certain circumstances. Power requirements were evaluated for the case of flapped struts. Drag penalties varied from nothing for a midchord spoiler on one side to 200 percent of baseline drag for continuous airbleed. Fences slightly increased drag, and had a smoothing influence on transition between ventilated and unventilated flow states.

TABLE OF CONTENTS

LIST OF FIGURES

ABSTRACT

Possible means of reducing the sideforce due to sideslip angle on a surface-piercing hydrofoil strut were investigated. An experimental program was performed to test the effect on strut sideforce and ventilation characteristics of 50-percent chord trailing edge flaps, midchord spoilers (split flaps), and airbleed (air injection). The effect of fences was tested in combination with the trailing edge flap and airbleed. All systems were found to be effective in reducing or changing sideforce. None of the methods significantly improved strut resistance to ventilation, but airbleed and spoilers reduced the abruptness of transition to the ventilated state under certain circumstances. Power requirements were evaluated for the case of flapped struts. Drag penalties varied from nothing for a midchord spoiler on one side to 200 percent of baseline drag for continuous airbleed. Fences slightly increased drag, and had a smoothing influence on transition between ventilated and unventilated flow states.

ADMINISTRATIVE INFORMATION

This work was funded by the Systems Development Department, Advanced Hydrofoil Systems Office, David W. Taylor Naval Ship Research and Development Center.

INTRODUCTION

The Advanced Hydrofoil Systems Office of the David W. Taylor Naval Ship R&D Center is considering the design of a large, ocean-going hydrofoil ship (HOC) with the following approximate characteristics:

hullborne displacement	750 – 1200 metric tons
length overall	60 – 80 m
longitudinal strut spacing	50 – 70 m
forward strut chord length	5 – 7 m
max turn rate	5 – 6 deg/s (c.f. PHM, TUCUMCARI, 8 deg/s, 12 deg/s, respectively)
design speed	50 knots

It is envisioned that turns will be fully coordinated. That is, the craft will heel in a turn such that the centrifugal and gravitational forces are exactly compensated by the lift force on the foil system. It can be assumed for purposes of estimating strut side slip angle during turns that the craft will pivot virtually on the after struts. In these circumstances, the forward strut will experience a sideslip angle even in a perfectly coordinated, calm water turn. The sideslip angle, β, the heel angle, γ, the radius of the turn, r, and the apparent sideslip angle at the strut (reduced because of the heel) β', are related by straightforward geometric formulas to the craft velocity, V, the strut spacing, s, and the turn rate. $\dot{\psi}$ (deg/s) or ω (rad/s):

$$r = \frac{V}{\omega}$$

$$\beta = \tan^{-1} \frac{s\omega}{V}$$

$$\tan \beta' = \tan \beta \cos \gamma$$

$$\tan \gamma = \frac{V\omega}{g}$$

$$\tan \beta' = \frac{s\omega}{V} \cos \left\{ \tan^{-1} \frac{V\omega}{g} \right\}$$

A useful approximation, for small heel angles and sideslip angles is

$$\beta = \frac{s}{r} \text{ (units of } \beta \text{ are radians)}$$

Figure 1 shows the geometry. Figures 2 – 4 show sideslip angle at the strut, β', versus strut spacing, s, for various values of V and $\dot{\psi}$. The corresponding values of γ and r are also noted. Figure 3 also shows the values of the approximation, $\beta = s/r$, for comparison with the exact formula. It can be seen from the figures that β' will be well above 10 degrees even for modest values of s and $\dot{\psi}$ at the design speed.

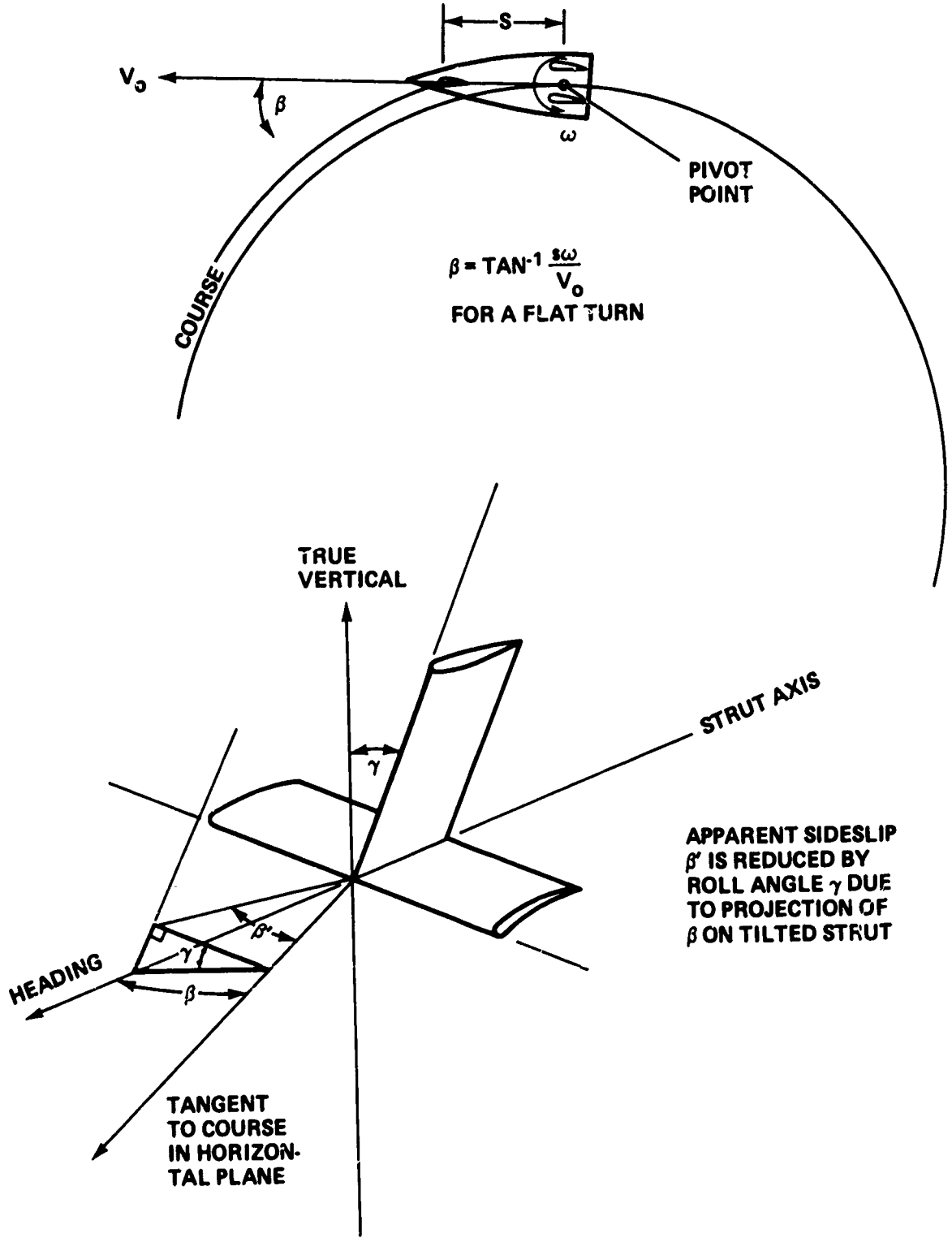

Figure 1 – Diagram of Sideslip Angle, β, Induced by Turn

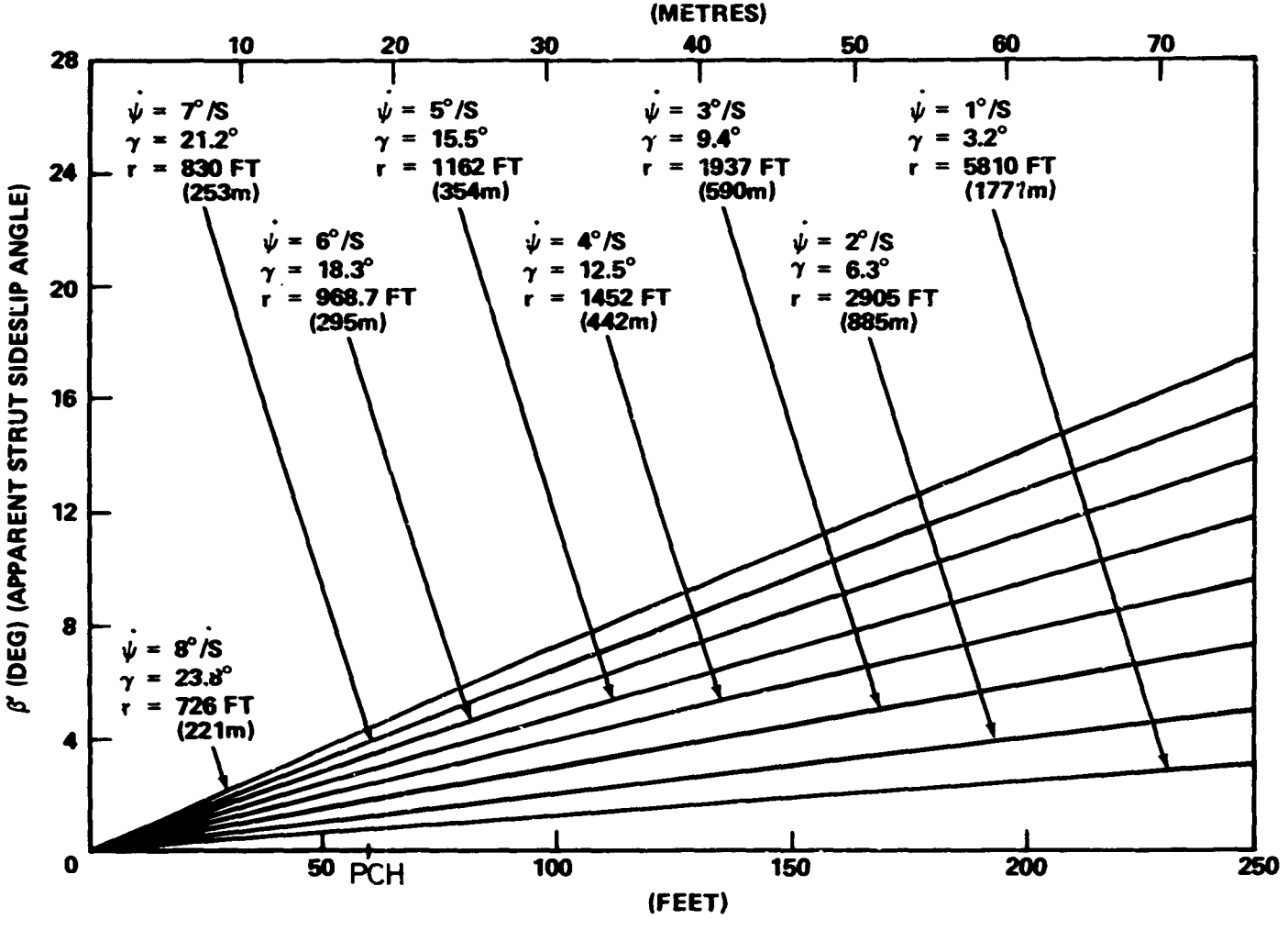

Figure 2 – Apparent Sideslip Angle versus Strut Separation for Various Turn Rates, 60 kts.

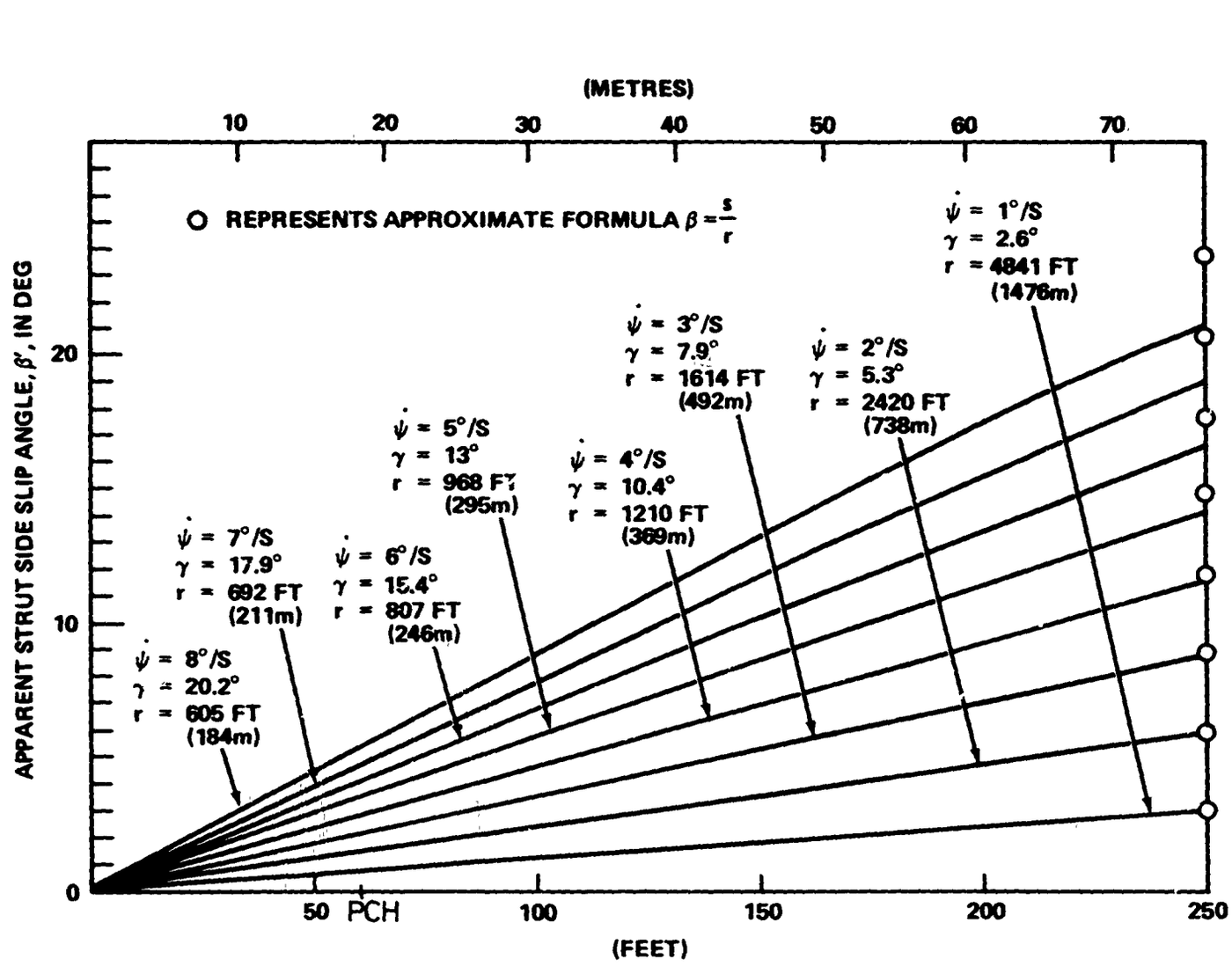

Figure 3 – Apparent Sideslip Angle versus Strut Separation for Various Turn Rates, 50 kts

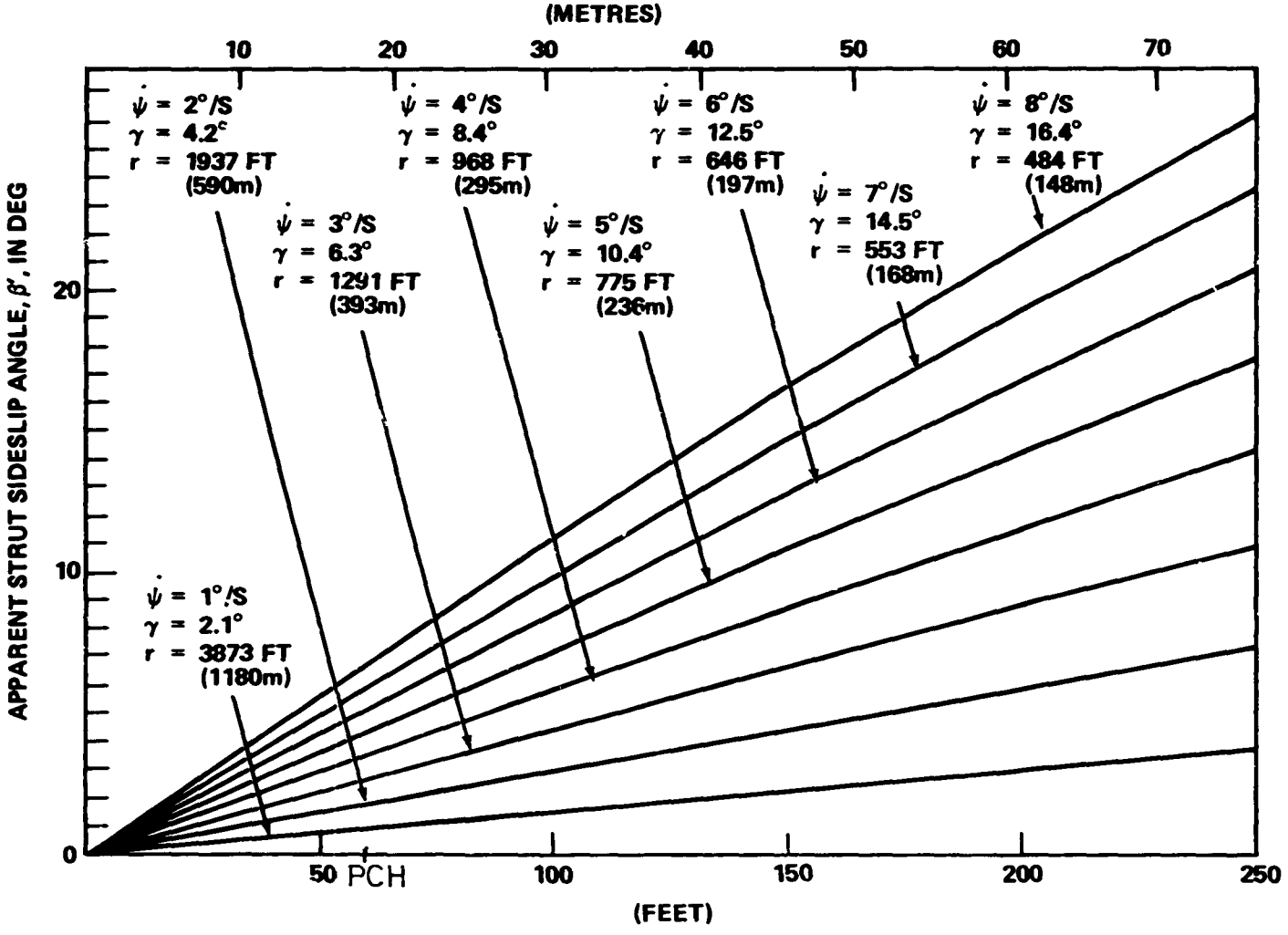

Figure 4 — Apparent Sideslip Angle versus Strut Separation for Various Turn Rates, 40 kts

For sideslip angles of 10 degrees and speeds of 50 kts, it is unlikely that conventionally shaped surface piercing struts will not become ventilated, with undesirable consequences of discontinuous side force. Aside from the problem of ventilation, the large sideslip angle induced on the forward strut would tend to throw the boat out of the turn, or prevent it from turning at all. It would be desirable to be able to control the amount of sideforce on the forward strut as well as to ensure that the force was a well-behaved function of sideslip angle.

On the HIGHPOINT (PCH-1), the problem of turn-induced sideslip angle was solved by steering the forward strut along the course tangent, or true heading at the strut. For HOC, this may not be feasible because of structural limitations. Therefore it is necessary to examine alternative solutions. In this study, the following are considered:

1. Controllable flap
2. Air bleed
3. Spoilers
4. Fences

Each of these techniques are evaluated in terms of the following criteria:

1. effectiveness in reducing adverse side forces
2. suppression of ventilation
   or
   smoothness of transistion between ventilated and fully wetted state
3. drag or auxiliary power penalty
4. potential reliability
5. complexity of implementation
6. adverse or favorable associated effects

In order to resolve some of the unknowns encountered in the study, a rather extensive experimental program was conducted, the results of which are incorporated herein.

CONTROLLABLE FLAP

If aligning the entire strut to the flow is impractical, a possible alternative is to align a portion of the strut with the flow. This could be accomplished by a leading or trailing edge flap. Generally, moving a flap does not change the force as greatly as moving the entire foil, per degree of rotation. Figure 5 shows the average effectiveness of several trailing edge airfoil flaps.[1] Effectiveness is defined as $\Delta\alpha_0/\Delta\delta$ where α_0 is the angle of attack at zero lift and δ is the flap deflection. In this text, when reference to airfoil data is made, the standard geometric orientation of a wing in air will be assumed, rather than that of a vertical strut.

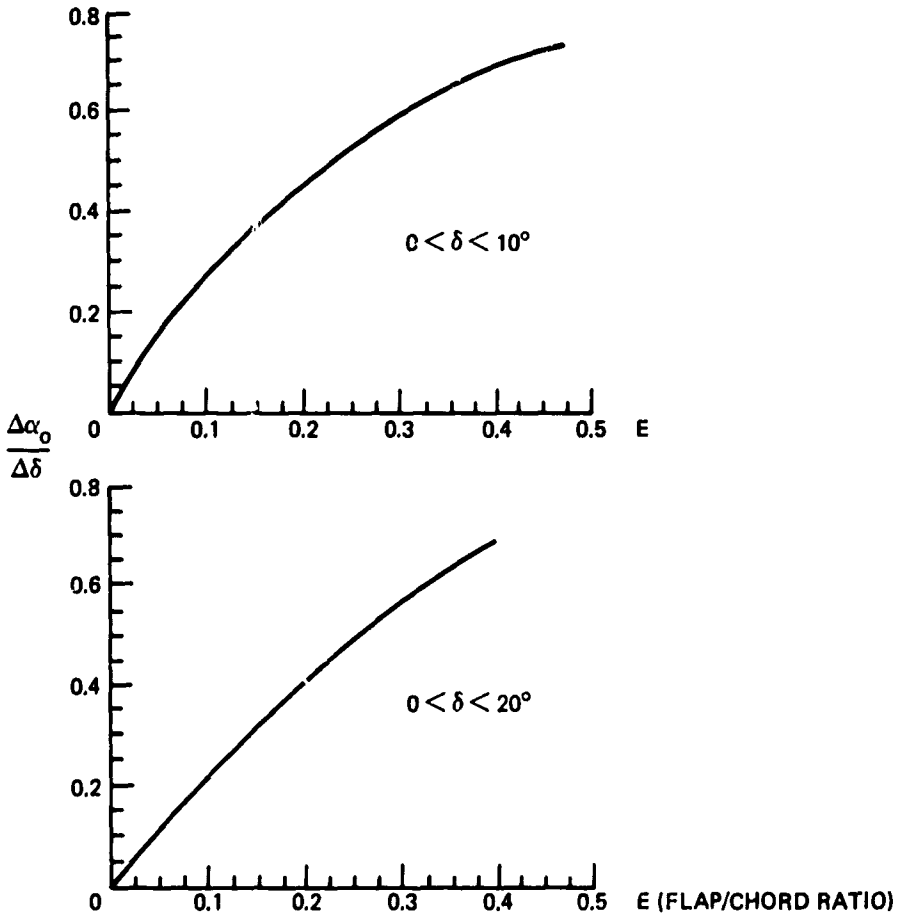

Figure 5 – Flap Effectiveness vs Flap/Chord Ratio[1]

[1] Abbott, I.H., and A.E. von Doenhoff, *"Theory of Wing Sections,"* Dover Publications, Inc., New York (1959).

Thus, angle of attack is α rather than β, and the crossforce is lift rather than sideforce. The difference in the physics of the two situations is thereby emphasized. Experience with flapped hydrofoil has not confirmed the effectiveness predicted by Figure 5. This may be because the hydrofoil sections were not specifically designed for flap effectiveness. Cavitation and the higher susceptibility of foils in water to roughness effects may also be significant. Whether the forward strut sideforce could be reduced to near zero at sideslip angles of 10 degrees at 50 knots will depend upon the effect of cavitation and ventilation on a surface-piercing flap. Chances for success are enhanced since the flap will be working to reduce rather than increase lift. Figure 6 shows the pressure distribution on a flapped symetric foil at an angle of attack.[2] Notice that the upper surface distribution has crossed over the lower surface distribution to become slightly positive, and the converse has happened to the lower surface distribution. Because a region of lower-than-atmospheric pressure is a prerequisite for spontaneous ventilation inception,[3] ventilation as it usually occurs on the low pressure face of a surface-piercing strut could be prevented by use of a flap, and probably the loads could be reduced to near zero or made somewhat negative. A more complete examination of pressure distribution on flapped struts[2] reveals that for many combinations of flap angle and

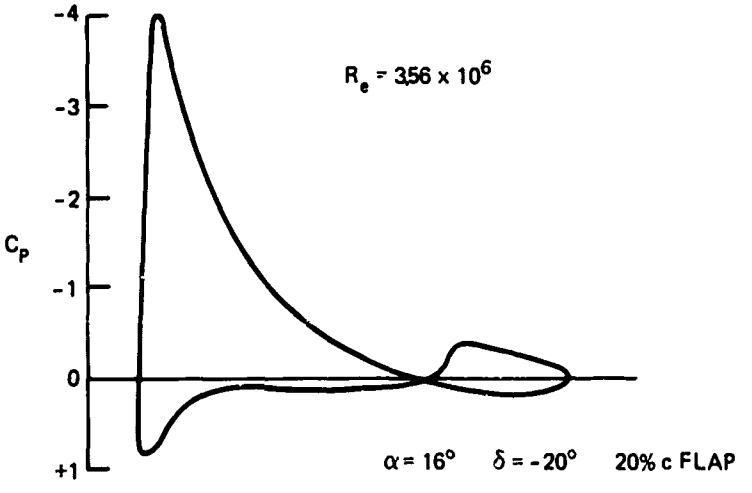

Figure 6 – Pressure Distribution on Flapped Symetric Foil[1]

[2]Jacobs, E.N. and R.M. Pinkerton, *"Pressure Distribution over a Symmetrical Airfoil Section with Trailing Edge Flap,"* Langley Memorial Aeronautical Laboratory Report No. 360 (April 1930).

[3]Rothblum, R.S., D.A. Mayer, and G.M. Wilburn, *"Ventilation, Cavitation, and Other Characteristics of High-Speed Surface-Piercing Struts,"* Naval Ship Research and Development Center Report 3023 (Oct 1972).

angle of attack, some sharp anomalies appear in the pressure distribution. This indicates the possiblity of separation or ventilation at the hinge line. The details of construction of the hinge line may also be important, since an abrupt break in the contour could provide an air path.

If flap ventilation should prove to be a problem, it could be alleviated by the use of fences as shown in Figure 7. If nose cavitation should trigger nose ventilation, nose fences as

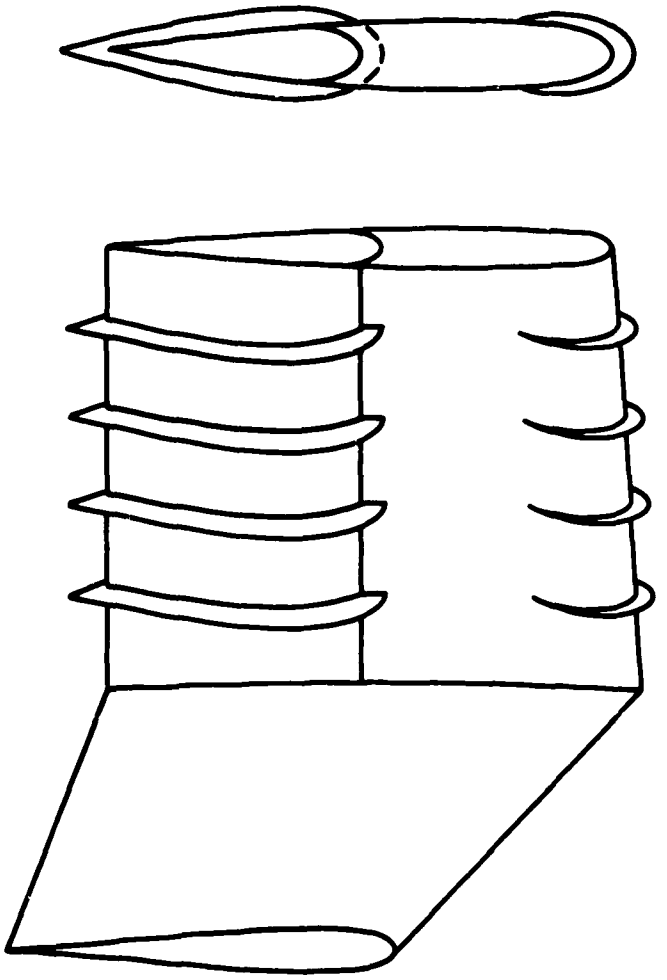

Figure 7 – Possible Use of Ventilation Fences to Prevent Flap or Nose Ventilation

shown in the Figure may also be required. Previous experience[4,5] with fences and fence-like appendages indicated that the use of fences might not add appreciably, if at all, to the total strut drag. The power consumption required to activate the flap depends on the control system and the two-dimensional hinge moment coefficient

$$C_h \equiv \frac{M_h}{\frac{1}{2}\rho V^2 c^2_{flap}}$$

as a function of flap angle and lift coefficient. For symetric wing sections, the theoretical hinge moment coefficient is

$$C_h = C_\ell \left(\frac{dC_h}{dC_\ell}\right) + \delta \left(\frac{dC_h}{d\delta}\right)$$

where $\frac{dC_h}{dC_\ell}$ and $\frac{dC_h}{d\delta}$ are given in Figure 8.[1] (δ is in radians)

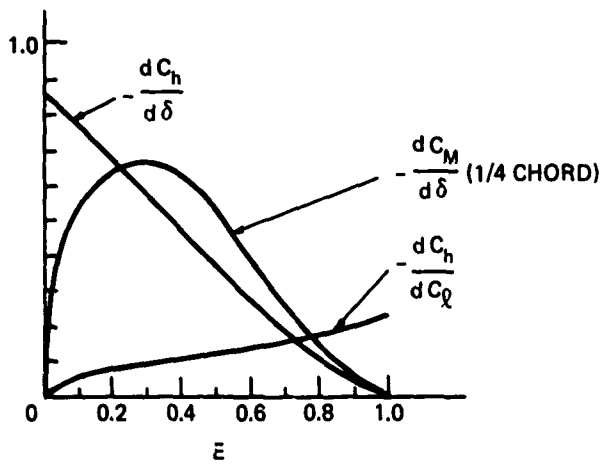

Figure 8 – Theoretical Hinge Moment and Pitching Moment of Plain Trailing Edge Flaps[1]

A rough correction for aspect ratio can be applied by multiplying the theoretical moment coefficient by the ratio of the empirically derived finite span sideforce coefficient slope to the infinite span slope. Figure 9 gives sideforce coefficient slopes for several experimental cases of finite aspect ratio and a theoretical curve.[3]

---

[4] Swales, P.D., R.C. McGregor, R.S. Rothblum, *"The Influence of Fences on Strut and Foil Ventilation,"* 10th ONR Symposium, Boston (1974).

[5] Layne, D.E., *"Effects of External Stiffeners on the Ventilation, Force and Cavitation Characteristics of a Surface-Piercing Hydrofoil Strut,"* Naval Ship Research and Development Center Report SPD-621-01 (Apr 1975).

As an example, consider a strut with a 50% flap, and an aspect ratio of 1. From Figure 9, $dC_s/d\beta \sim 0.02$. For a $C_s \sim 0.2$, $\beta \sim 10$ degrees. For a 50% flap/chord ratio, Figure 5 indicates the flap efficiency is about 0.8. To generate or counteract a sideforce coefficient of 0.2 would thus require a flap angle of about 13 degrees. The hinge moment coefficient formula then gives

$$C_h = 0.2 \left(\frac{dC_h}{dC_\ell}\right) + \frac{13}{57.3} \left(\frac{dC_h}{d\delta}\right)$$

From Figure 8, for E = 50%, $\frac{dC_h}{dC_\ell} \cong -0.13$ and $\frac{dC_h}{d\delta} \cong -0.36$.

Then $C_h = -0.2 \times 0.13 - \frac{0.36 \times 13}{57.3} = -0.11$

For a one foot chord strut at 50 kts,

$$-M_h = V^2 c^2_{flap} \frac{1}{2} \rho \times 0.11$$

$$-M_n = 190 \text{ ft lb/ft } (860 \text{ N} \cdot \text{m/m})$$

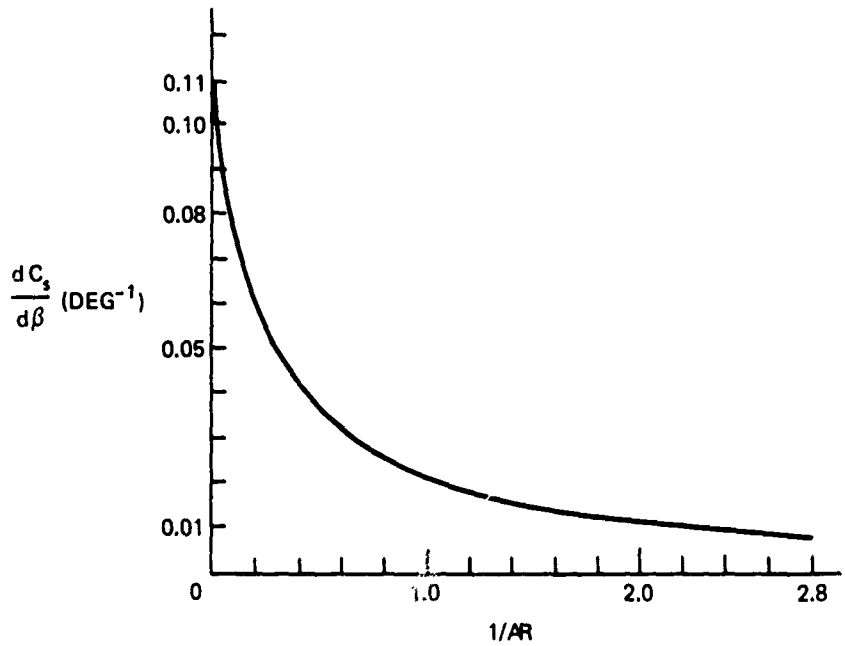

Figure 9 – Sideforce Coefficient Slope Versus Reciprocal of Aspect Ratio for Surface Piercing Struts Without Endplate
From Reference 3

For a one foot span

$$-M_n = 190 \text{ ft lb} \sim 200 \text{ ft lb } (270 \text{ N} \cdot \text{m})$$

For a 15 foot (4.5 m) chord strut of AR = 1, since the moment varies as the cube of the ratio of linear dimensions, $-M_n$ = 656000 ft lbs (890 k N · m).

Assuming that $\dot{\delta} \cong 10$ deg/s, the peak rate of work will be

$$10 \text{ deg} \times \frac{2\pi \text{ rad}}{360 \text{ deg}} \times \frac{6.5 \times 10^5 \text{ lb ft/sec}}{550 \text{ lb ft/sec}} \text{ HP}$$

$$= 210 \text{ HP } (150 \text{ kW})$$

The average power for a complete cycle (i.e. $\delta = 0, +13°, 0, -13°, 0$) would be just 1/4 the peak power, or about 50 HP, as can be seen from the geometry of Figure 10.

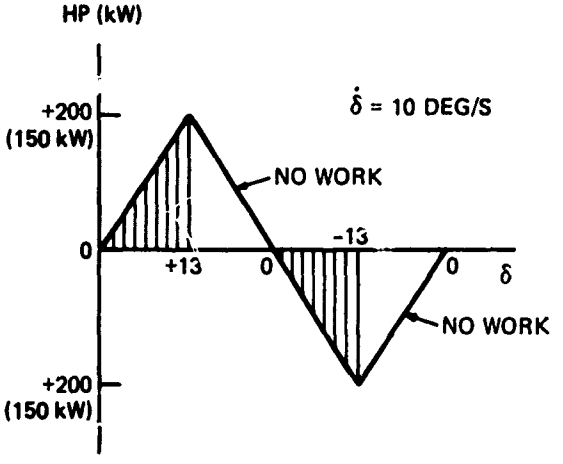

Figure 10 – Power Requirement as a Function of a Flap Angle, δ, for $\dot{\delta}$ = 10 deg/s

Several points in the foregoing calculations were unresolved with respect to the use of flaps on surface-piercing struts. The flap effectiveness would be influenced by cavitation and ventilation, for which there is no prediction method. The intersection between the strut and flap may create anomalous characteristics that override the beneficial influence of the flap on the pressure distribution.

Besides these unknowns, the effect of fences on these same factors cannot be predicted. Because of this, an experiment was necessary to establish a rational basis for applying flaps and fences to surface piercing struts. To this end, a model with flap was constructed and tested with and without fences, in the Rotating Arm facility of the Center.

THE FLAP AND FENCE EXPERIMENT

The Model. A NACA 16-012 section strut with a one-foot chord (c = 305 mm) and just over 4 chords of uniform span was modified to allow the 50 percent trailing section to function as a flap. The flap extended from the strut tip to a height of 3 chords. Figure 11 shows the model and experimental setup. The strut-flap hinge intersection was smoothed by gluing 0.010 inch (0.25 mm) spring brass to the strut sides, tangent to the section. Four removable ventilation fences, articulated to turn with the flap, were built to be attached to the strut at 0.25 c intervals from the tip. To the tip was affixed an endplate, 1/8 inch (3 mm) thick with beveled edges, parallel sided with half-breadth of 0.25 c, semi-circular leading and trailing section.

Test Conditions. The strut was towed vertically, piercing the water surface to a depth of one chord, from the six-component Aerojet Dynamometer, mounted at a radius of 120 c on the Rotating Arm, at angular velocities ranging from 0.14 to 0.7 rad/s. Linear velocities ranged from 10 to 50 kt. Flap angle, δ, was varied between -20 and 20 degrees.

Sign Conventions. As viewed from above, the Arm rotated clockwise; counterclockwise sideslip angle, β, was considered positive. Sideforce to port was positive. Flap angle which would ordinarily be expected to increase sideforce was positive. That is, for positive δ, the trailing edge of the flap would move to starboard.

Data Collection and Sources of Error. The lift and drag forces were digitized, analyzed, and recorded by an automatic data processing system, which also controlled sideslip angle and an underwater camera and strobe light. The data collection system is shown schematically in Figure 12. An analysis of the accuracy of the dynamometer and sideslip angle transducer can be found in Reference 3. Briefly, that analysis indicated that the forces were measured and recorded with an error of less than 1 or 2 percent, assuming the electronics were near-perfect for practical purposes. The sideslip angle was measured independently by three methods which agreed to within 1/3 degree, which is representative of the overall angular error range. The principal source of error arose from the imposition of unsteady forces which, at the lower speeds, created a signal many times as great as the mean signal of interest, in spite of the use of 10 Hz low pass filters.

The best judgement of the effect of this factor is obtained by examining the scatter of the points plotted on the resulting graphs of force coefficients versus sideslip angle presented here. Each point on the graphs represents 200 data points averaged over approximately 1/2 second for a particular value of sideslip angle.

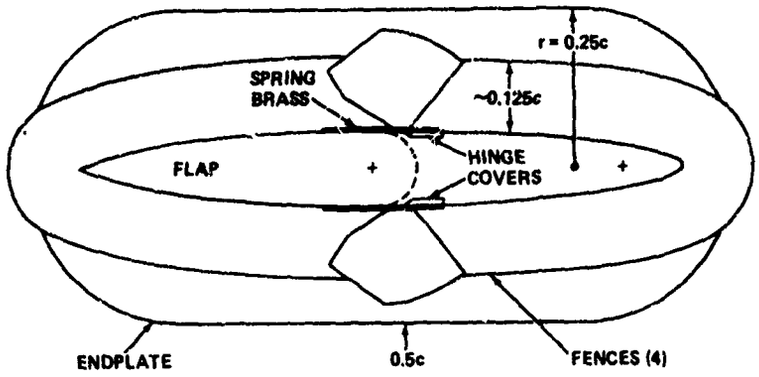

NACA 16-012

COORDINATES IN INCHES (mm)	
"X"	"Y"
0	0
.150 (3.81)	.155 (3.93)
.300 (7.62)	.217 (5.51)
.600 (15.24)	.301 (7.64)
.900 (22.9)	.364 (9.64)
1.200 (30.48)	.416 (10.54)
1.800 (45.72)	.496 (12.59)
2.400 (6[illegible]96)	.560 (14.22)
3.600 (91.44)	.650 (16.51)
4.800 (121.9)	.703 (17.86)
6.000 (152.9)	.720 (18.28)
7.200 (182.9)	.700 (17.78)
8.400 (213.4)	.632 (16.06)
9.600 (293.8)	.504 (12.80)
10.800 (274.3)	.302 (7.67)
11.400 (289.6)	.170 (4.31)
12.000 (304.8)	.014 (0.36)
NOSE RADIUS – .084" (2.13mm)	

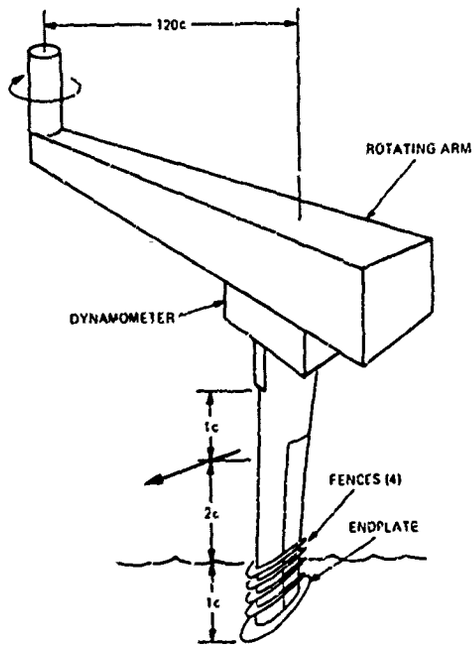

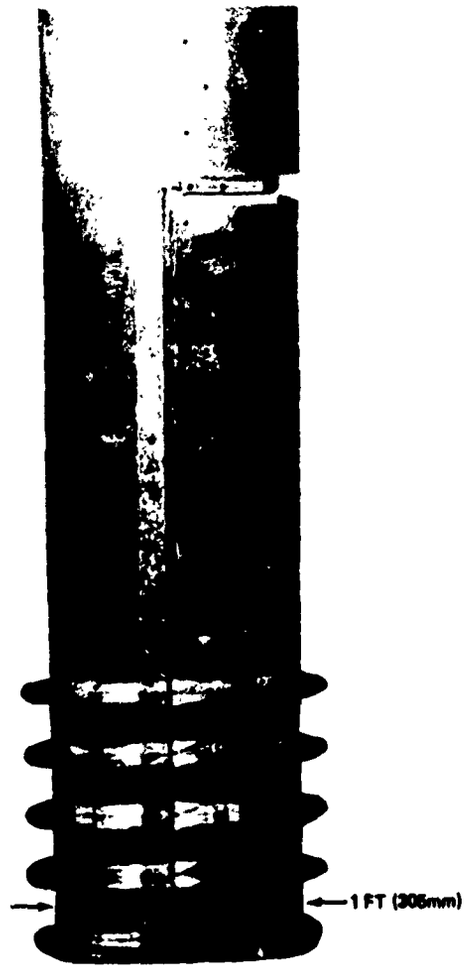

Figure 11 – Flapped Model with Fences, Mounting Arrangement, Section, Offsets, Photograph

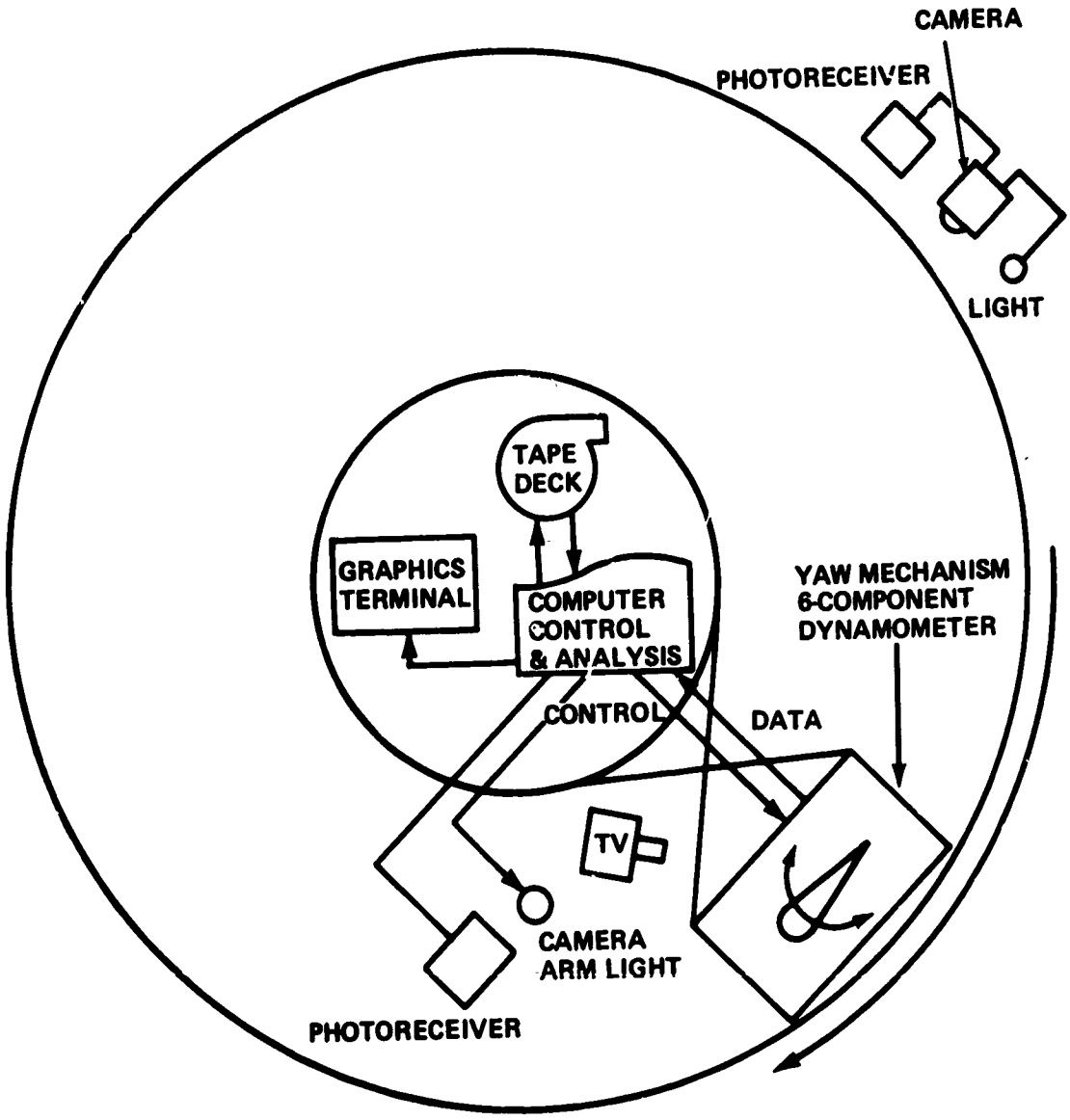

Figure 12 – Data Collection Schematic

Another factor affecting the reliability of the results was the technique of continuous running used on the Rotating Arm. The water surface became very disturbed after a few minutes of rotation. Nelka[7] found that this did not affect ventilation inception but did influence cavity washout. Because of the exploratory nature of this test, it was felt that the disturbed water surface would not be a serious detriment. In fact, it was undoubtedly more representative of actual prototype conditions than a smooth towing tank. Unfortunately, it did introduce a further undefined quantity.

Depth of submergence could be controlled only by raising and lowering the water level in the Rotating Arm Basin. This was not very satisfactory, as the water level tended to drop as much as an inch (25 mm) per day. An accurate estimate of the submergence during operations was difficult to obtain because the lowered water surface rendered the wave damping beaches ineffective. Thus, the disturbances created by the tests were very persistent. Therefore, a variation of ±0.08 c in depth of submergence from the nominal one chord submergence would not be surprising. The gross phenomena affecting the forces acting on the strut – ventilation, cavitation and separation – would not be measurably affected by such a small change in submergence. However, the mean values of the forces would be expected to be approximately proportional to the submergence, and could therefore be ±8% of their values at the proper submergence. The submergence would not change much from run-to-run, making most comparisons between adjacent runs free from this factor.

RESULTS OF THE FLAP AND FENCE EXPERIMENT

Figures 13 to 22 show the sideforce and drag coefficients, C_s and C_D, versus sideslip angle, β, for various values of flap angle, δ, over the range of velocities tested. The force coefficients are defined as follows:

$$C_x \equiv F_x \left(\frac{1}{2} \rho V^2 ch \right)^{-1}$$

where

F_x is force in the appropriate direction
ρ is density
V is linear velocity
c is chord length
h is submergence to strut tip from mean free surface

[7] Nelka, J.J., *"Effects of Mid-Chord Flaps on the Ventilation and Force Characteristics of a Surface-Piercing Hydrofoil Strut,"* Naval Ship Research and Development Center Report 4508 (Nov 1974).

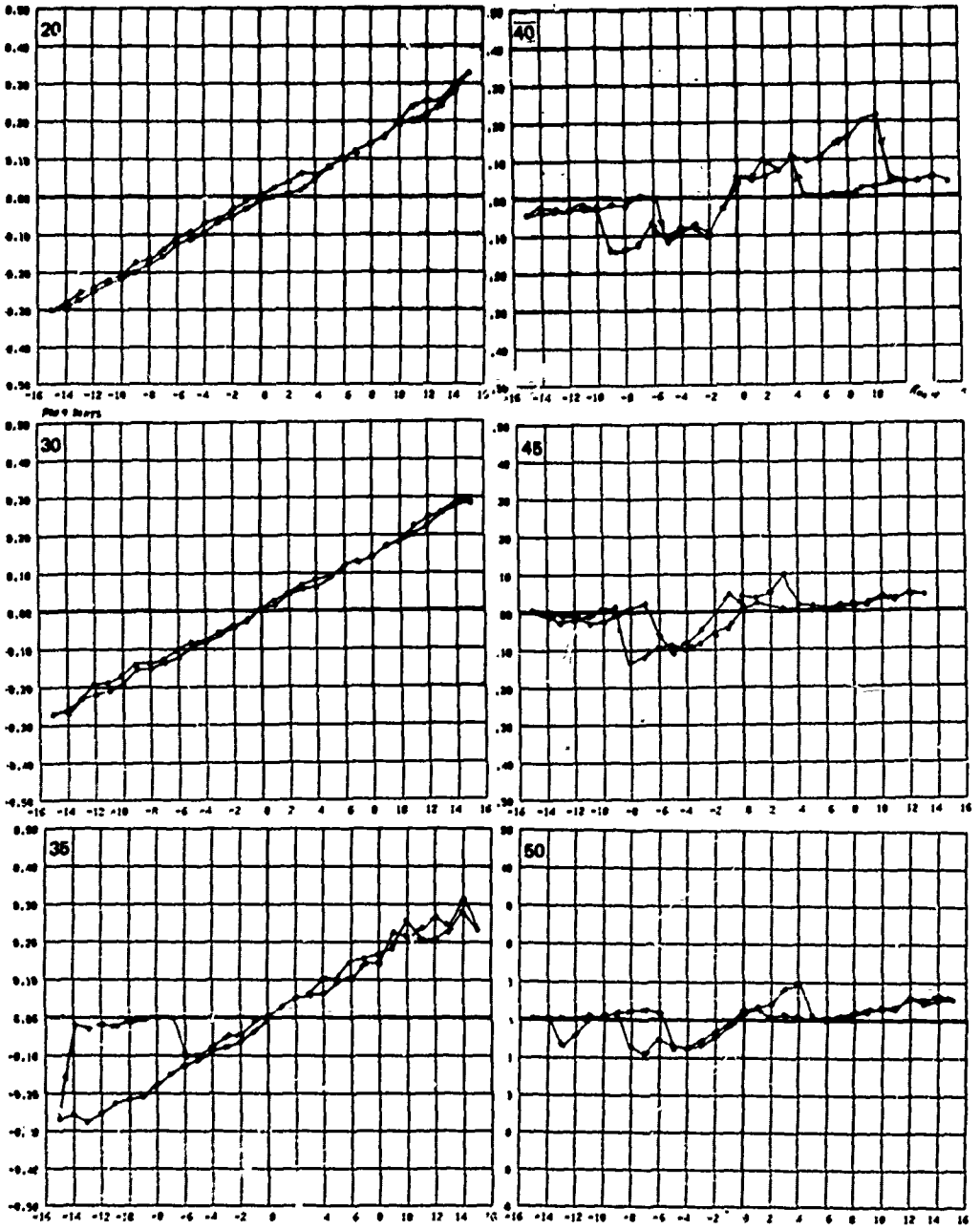

FIGURE 13a SIDEFORCE COEFFICIENT VS. SIDESLIP ANGLE, FLAPPED STRUT, WITHOUT FENCES, 0 DEGREES FLAP, 20, 30, 35, 40, 45, 50 KTS.

FIGURE 13b DRAG COEFFICIENT VS. SIDESLIP ANGLE, FLAPPED STRUT, WITHOUT FENCES, 0 DEGREES FLAP, 20, 30, 35, 40, 45, 50 KTS.

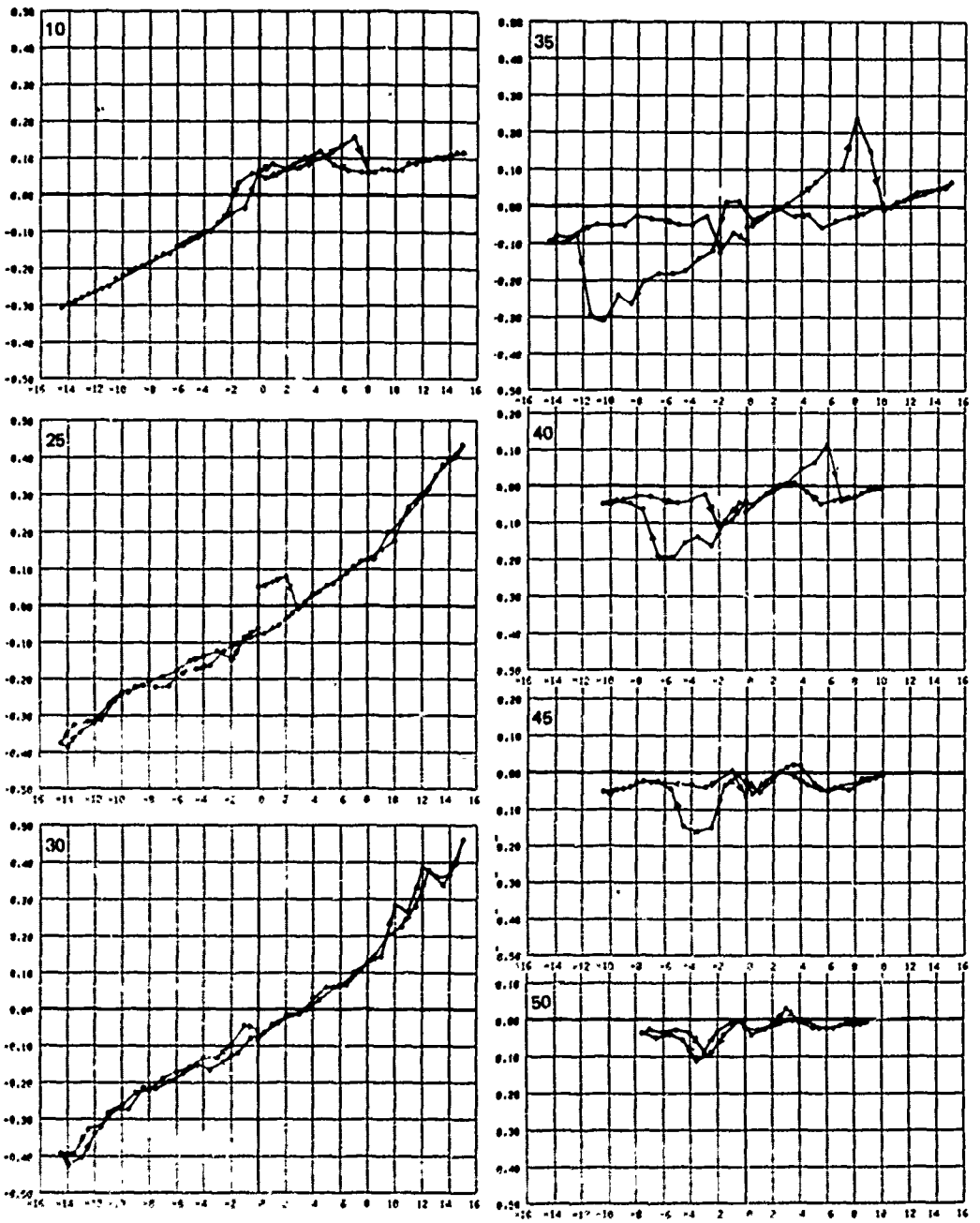

FIGURE 14a SIDEFORCE COEFFICIENT VS. SIDESLIP ANGLE, FLAPPED STRUT, WITHOUT FENCES, 5 DEGREES FLAP, 10, 25, 30, 35, 40, 45, 50 KTS.

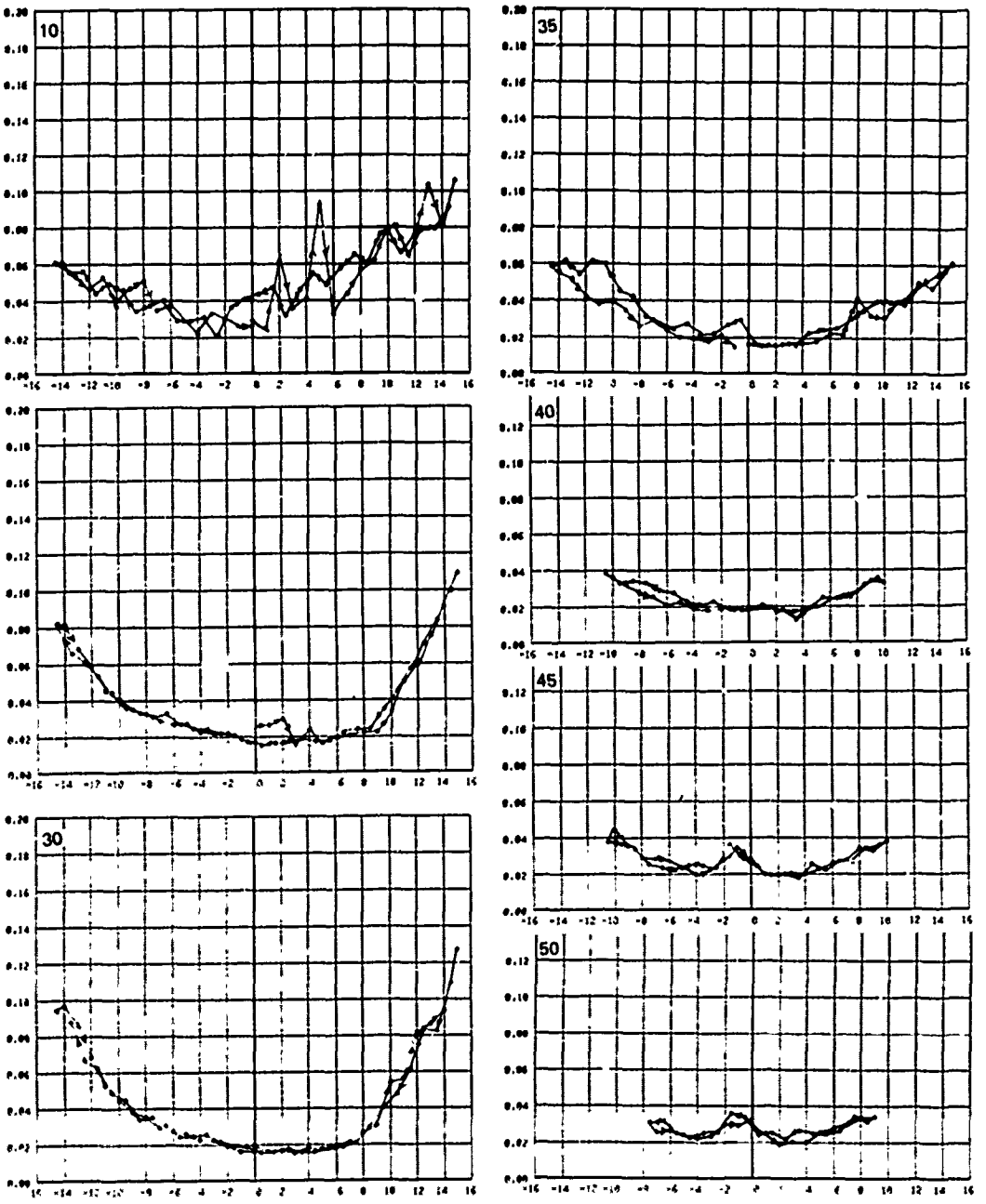

FIGURE 14b DRAG COEFFICIENT VS. SIDESLIP ANGLE, FLAPPED STRUT, WITHOUT FENCES, 5 DEGREES FLAP, 10, 25, 30, 35, 40, 45, 50 KTS.

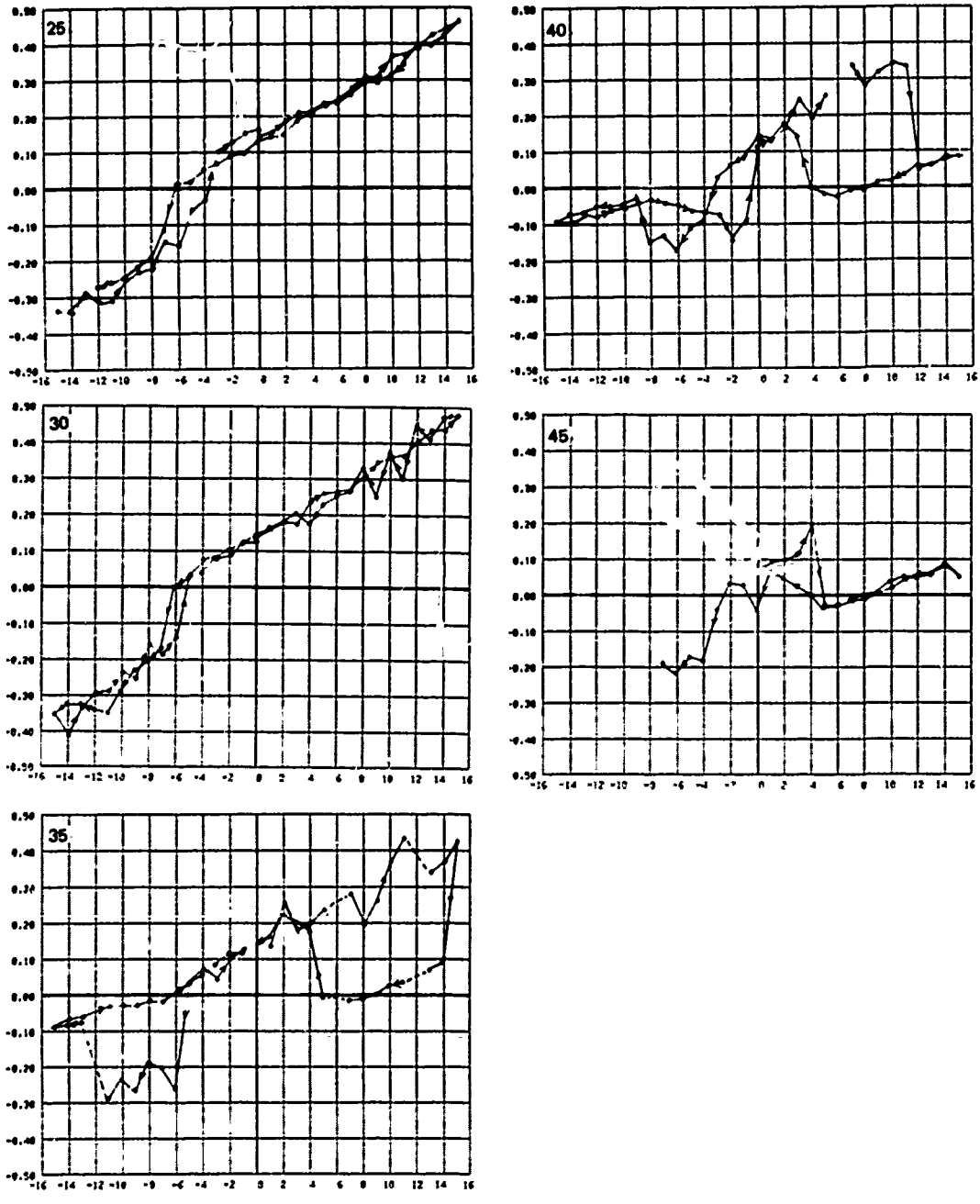

FIGURE 15a SIDEFORCE COEFFICIENT VS. SIDESLIP ANGLE, FLAPPED STRUT, WITHOUT FENCES, 7½ DEGREES FLAP, 25, 30, 35, 40, 45 KTS.

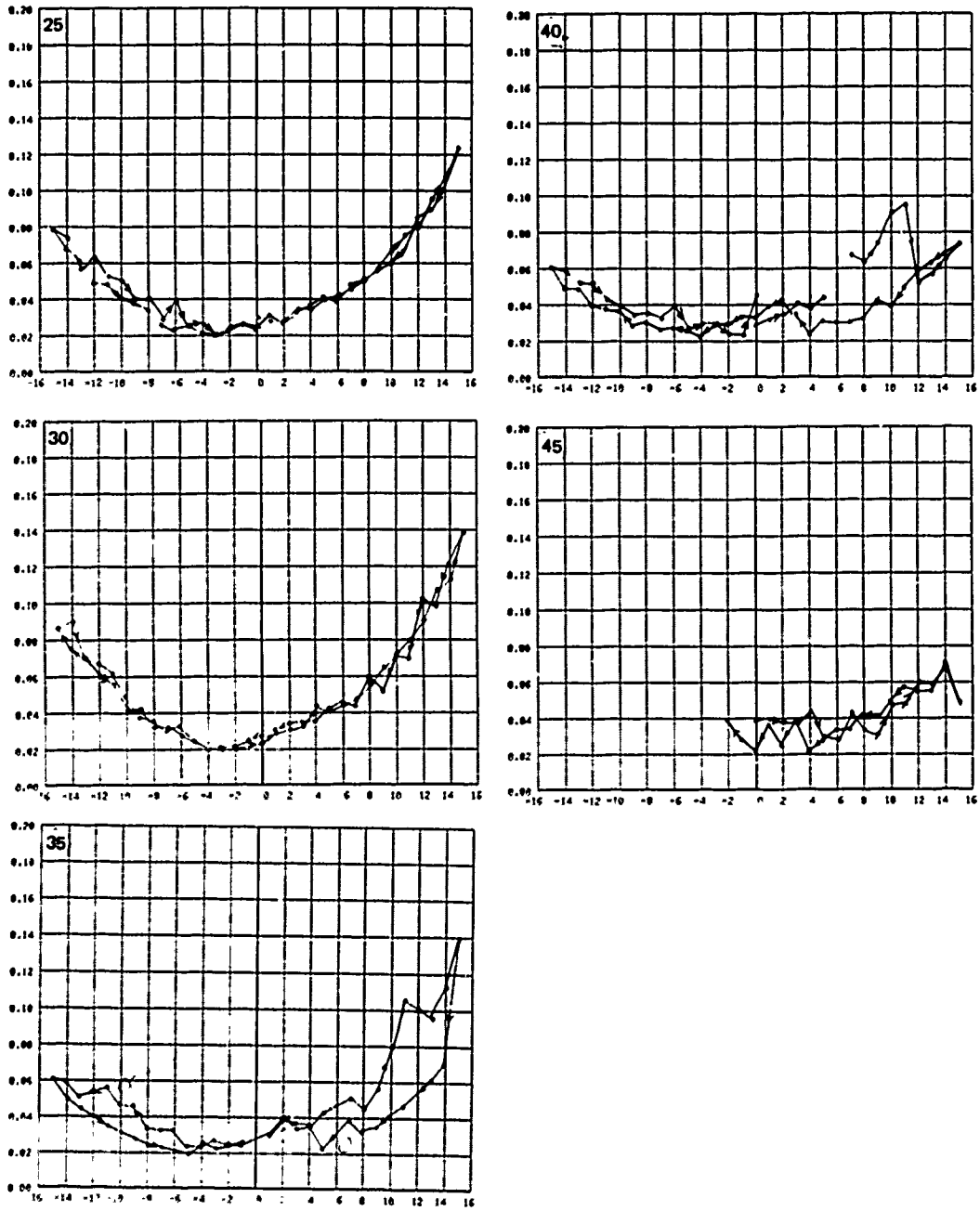

FIGURE 15b DRAG COEFFICIENT VS. SIDESLIP ANGLE, FLAPPED STRUT. WITHOUT FENCES, 7½ DEGREES FLAP, 25, 30, 35, 40, 45 KTS.

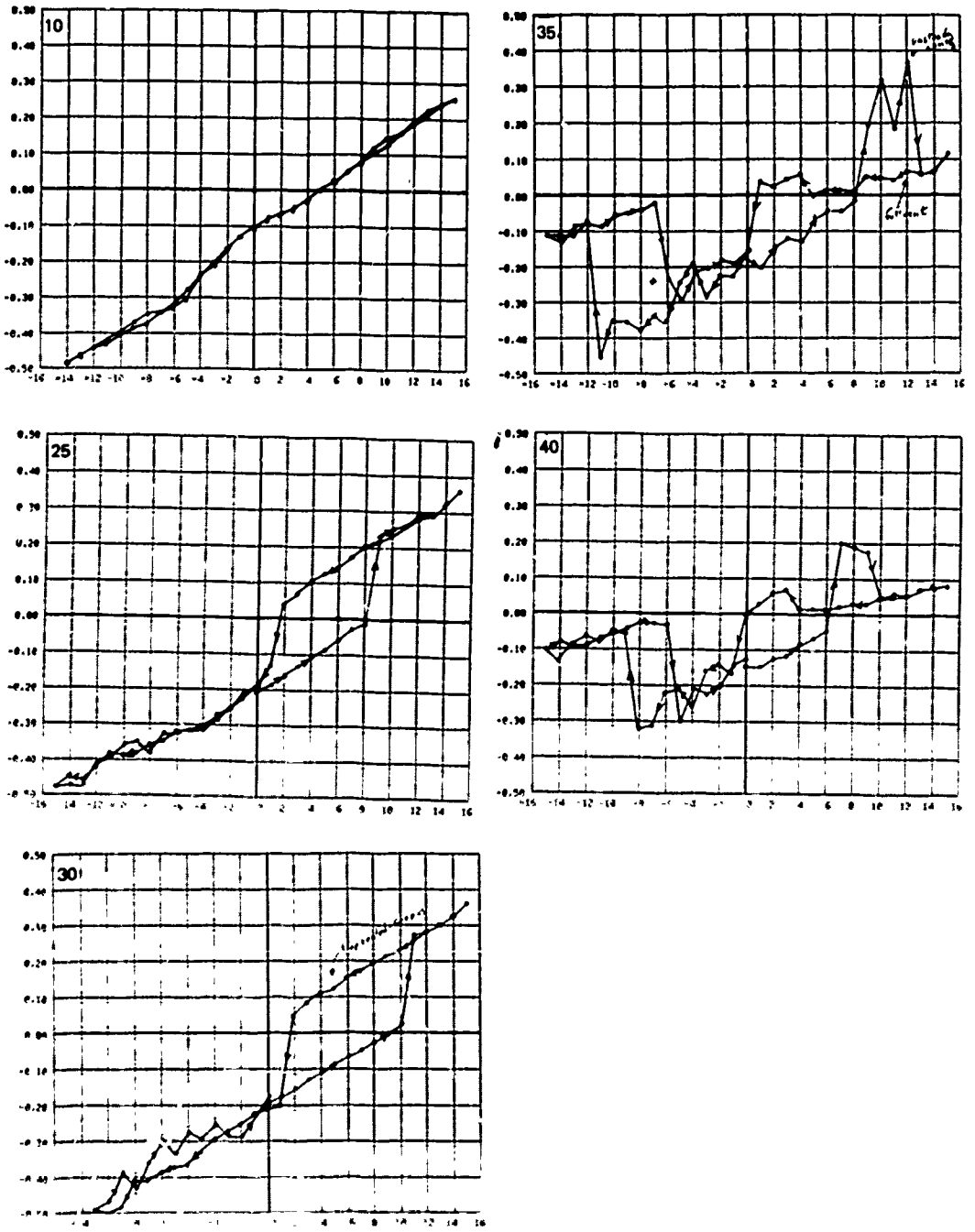

FIGURE 16a SIDEFORCE COEFFICIENT VS. SIDESLIP ANGLE, FLAPPED STRUT, WITHOUT FENCES, -10 DEGREES FLAP, 10, 25, 30, 35, 40 KTS.

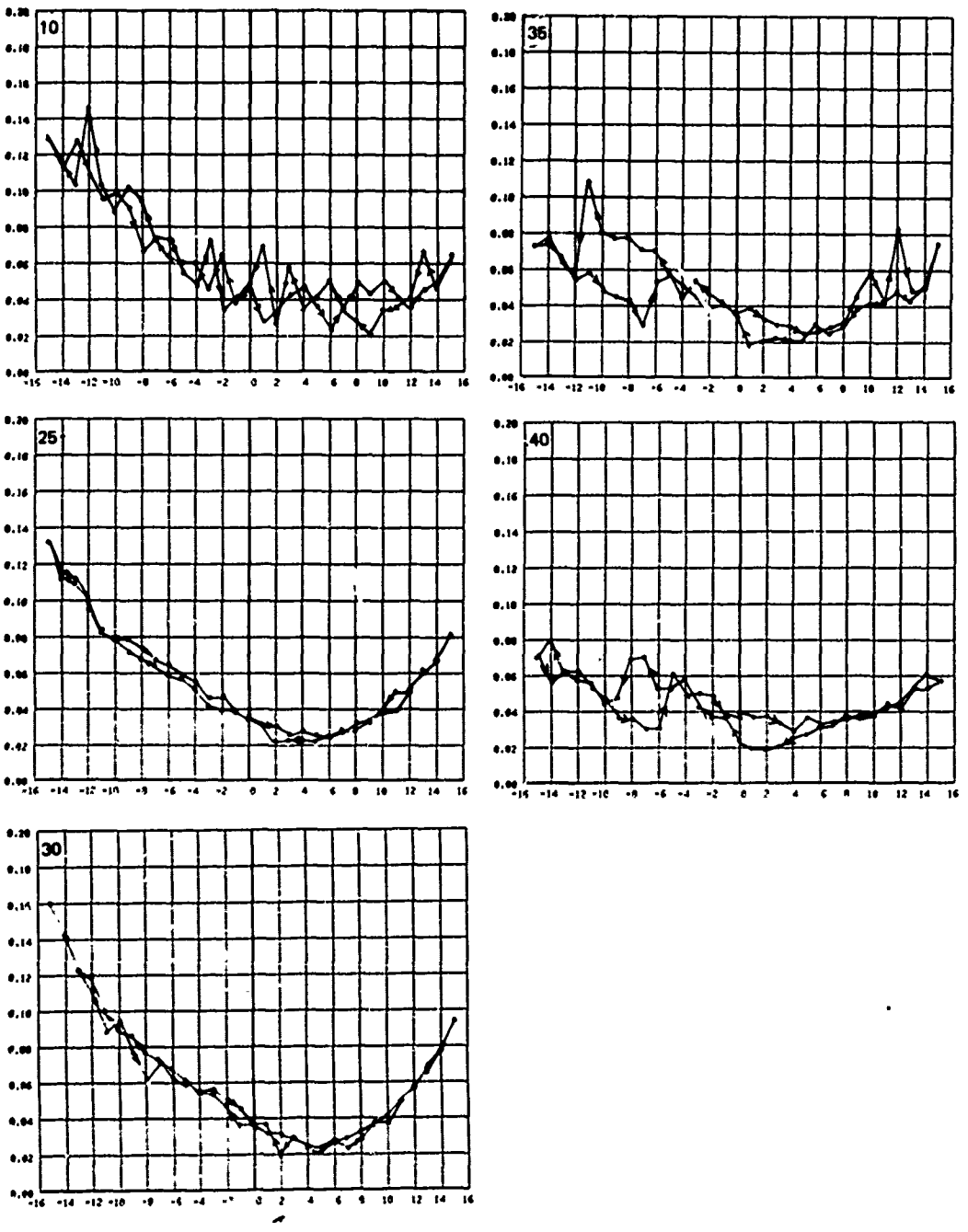

FIGURE 16b DRAG COEFFICIENT VS. SIDESLIP ANGLE, FLAPPED STRUT, WITHOUT FENCES, -10 DEGREES FLAP, 10, 25, 30, 35, 40 KTS.

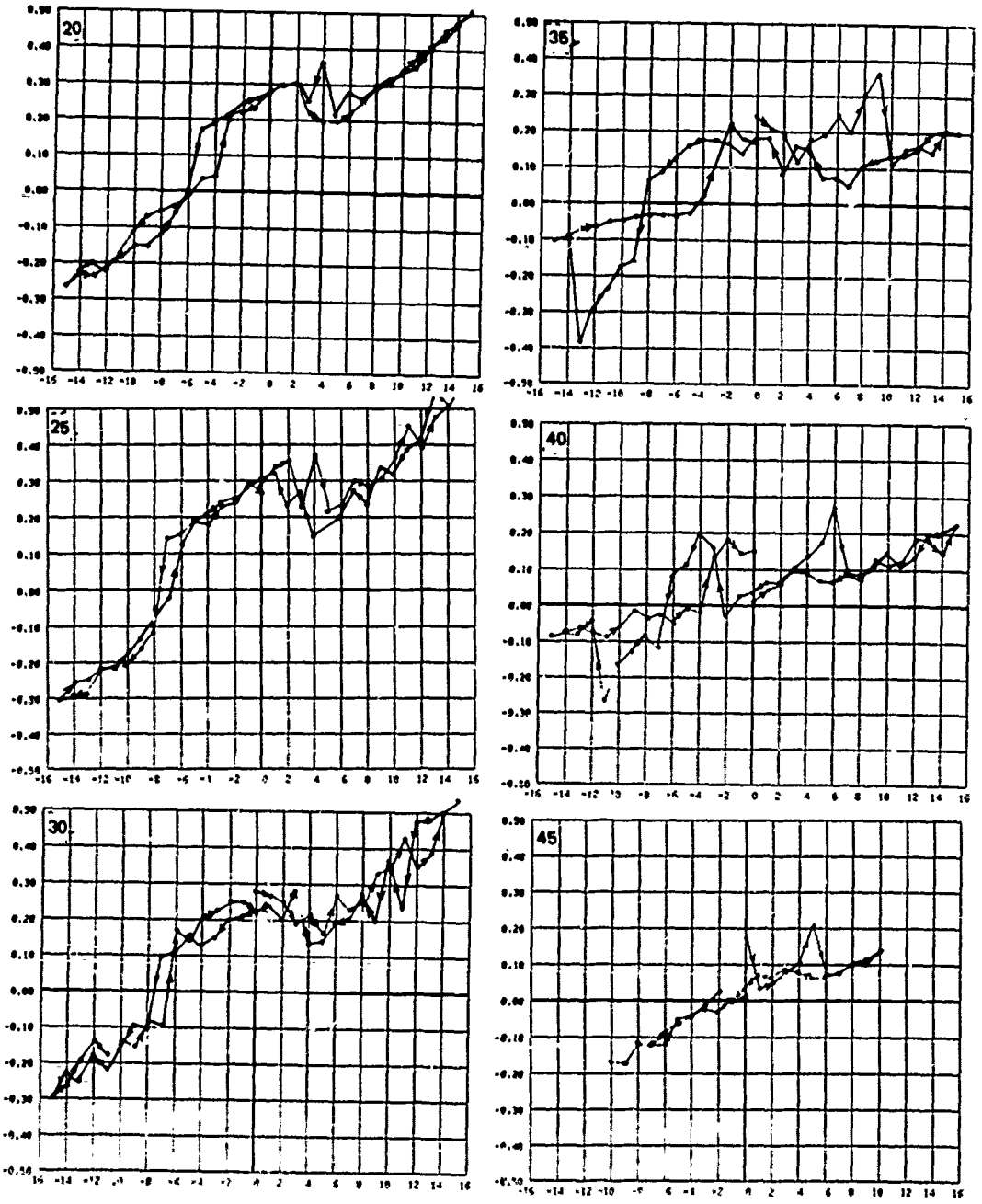

FIGURE 17a SIDEFORCE COEFFICIENT VS. SIDESLIP ANGLE, FLAPPED STRUT, WITHOUT FENCES, 15 DEGREES FLAP, 20, 25, 30, 35, 40, 45 KTS.

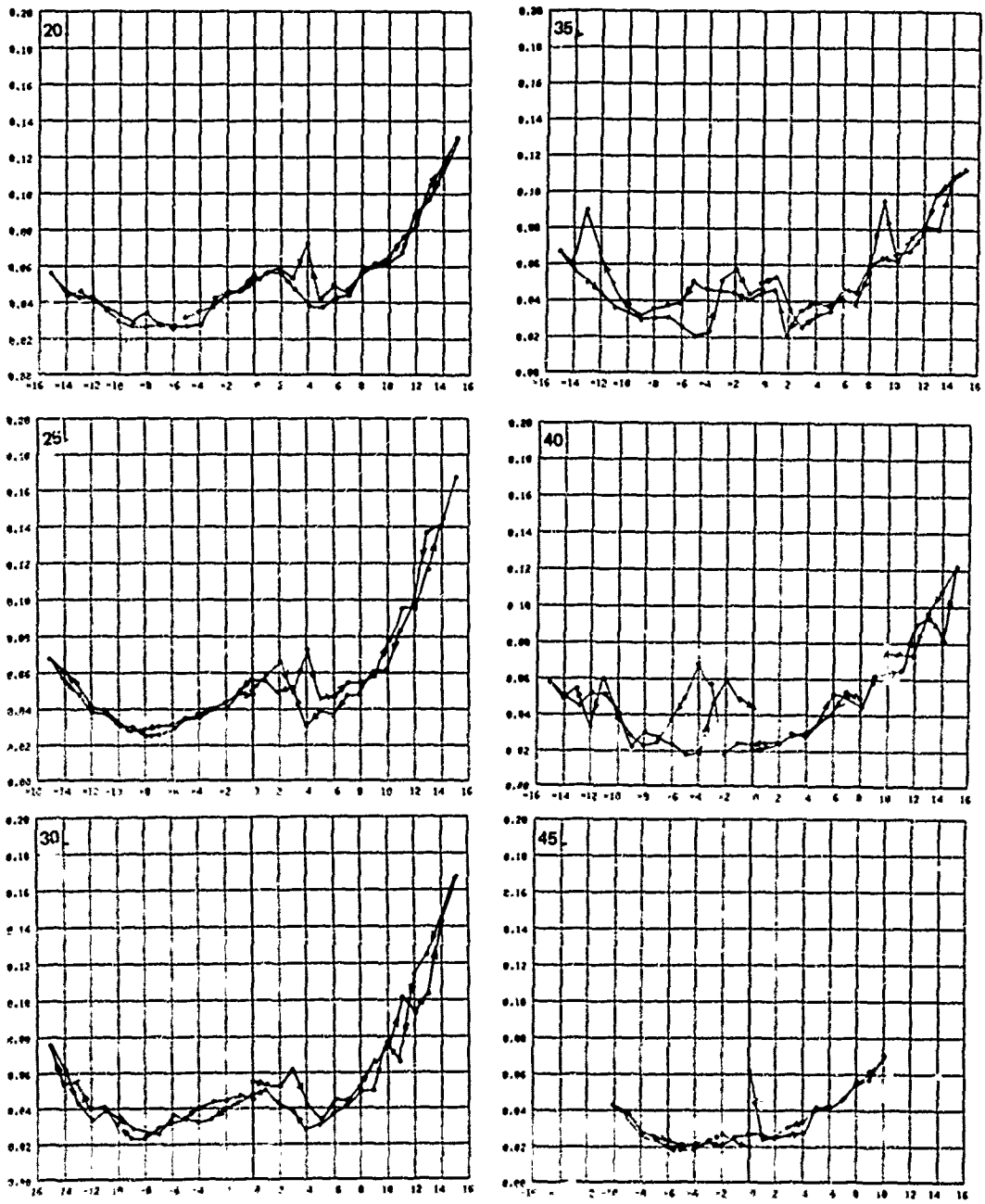

FIGURE 17b DRAG COEFFICIENT VS. SIDESLIP ANGLE, FLAPPED STRUT, WITHOUT FENCES, 15 DEGREES FLAP, 20, 25, 30, 35, 40, 45 KTS.

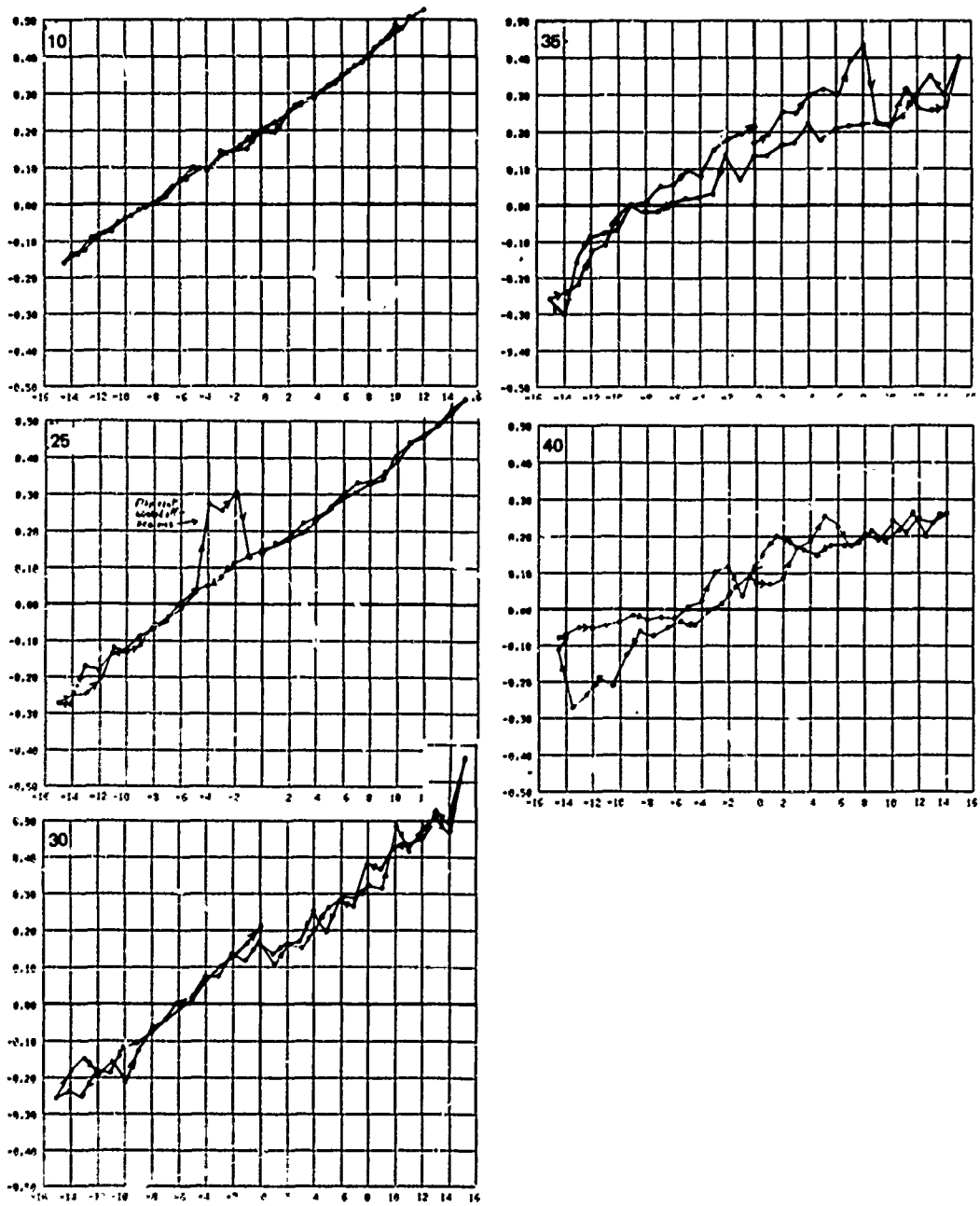

FIGURE 18a SIDEFORCE COEFFICIENT VS. SIDESLIP ANGLE, FLAPPED STRUT, WITHOUT FENCES, 20 DEGREES FLAP, 10, 25, 30, 35, 40 KTS.

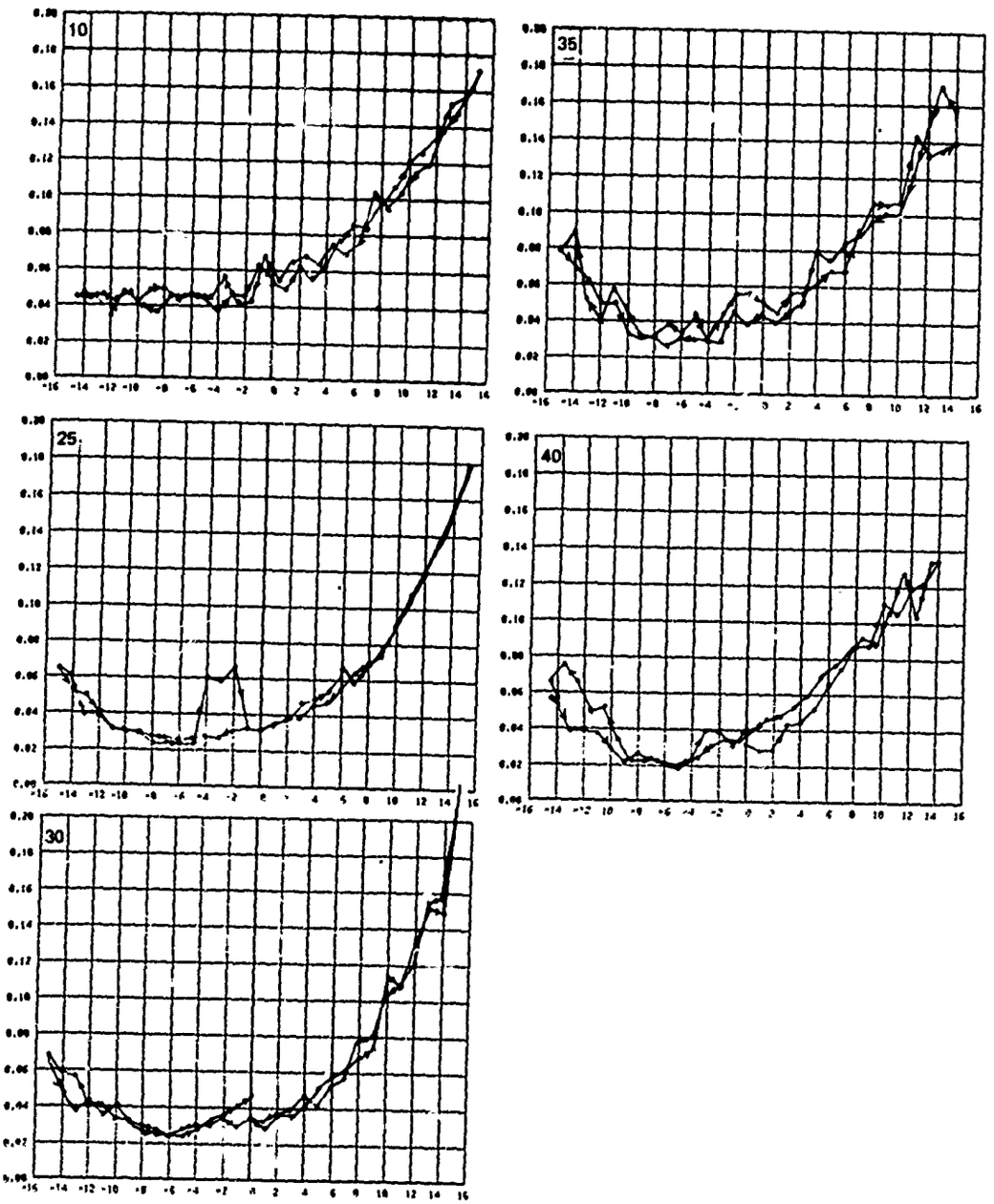

FIGURE 18b DRAG COEFFICIENT VS. SIDESLIP ANGLE, FLAPPED STRUT, WITHOUT FENCES, 20 DEGREES FLAP, 10, 25, 30, 35, 40 KTS.

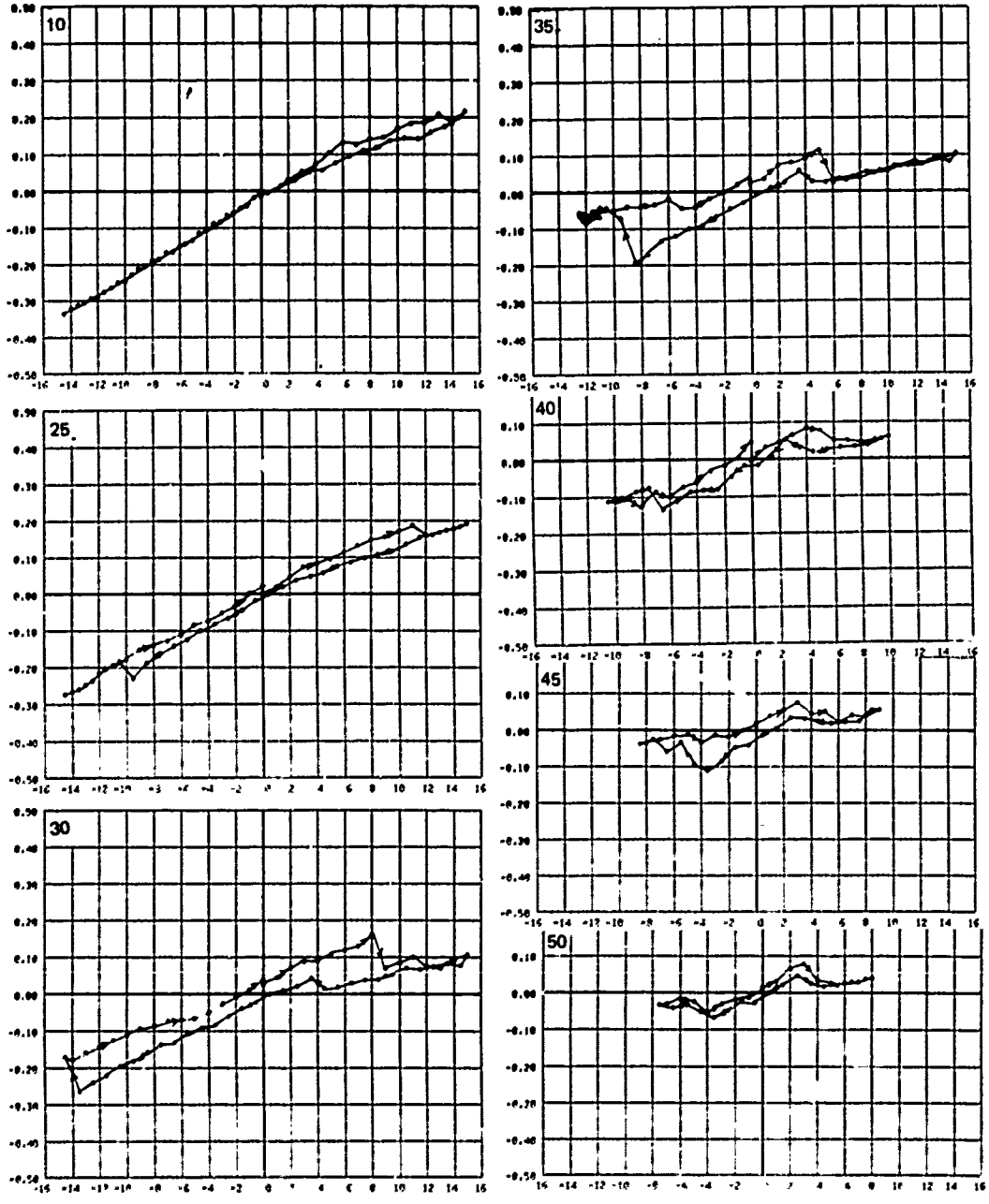

FIGURE 19a SIDEFORCE COEFFICIENT VS. SIDESLIP ANGLE, FLAPPED STRUT, WITH FENCES, 0 DEGREES FLAP, 10, 25, 30, 35, 40, 45, 50 KTS.

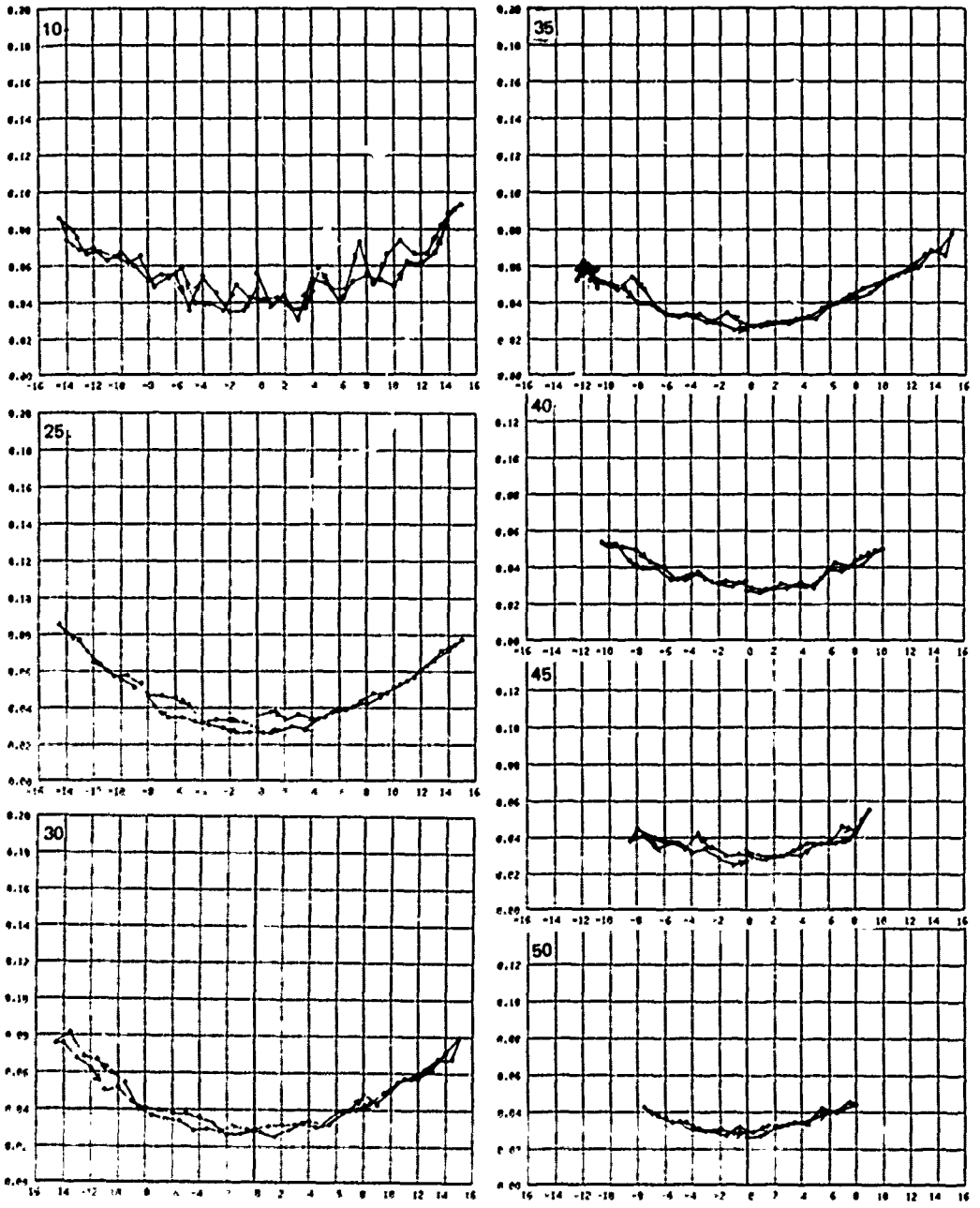

FIGURE 19b DRAG COEFFICIENT VS. SIDESLIP ANGLE, FLAPPED STRUT, WITH FENCES, 0 DEGREES FLAP, 10, 25, 30, 35, 40, 45, 50 KTS.

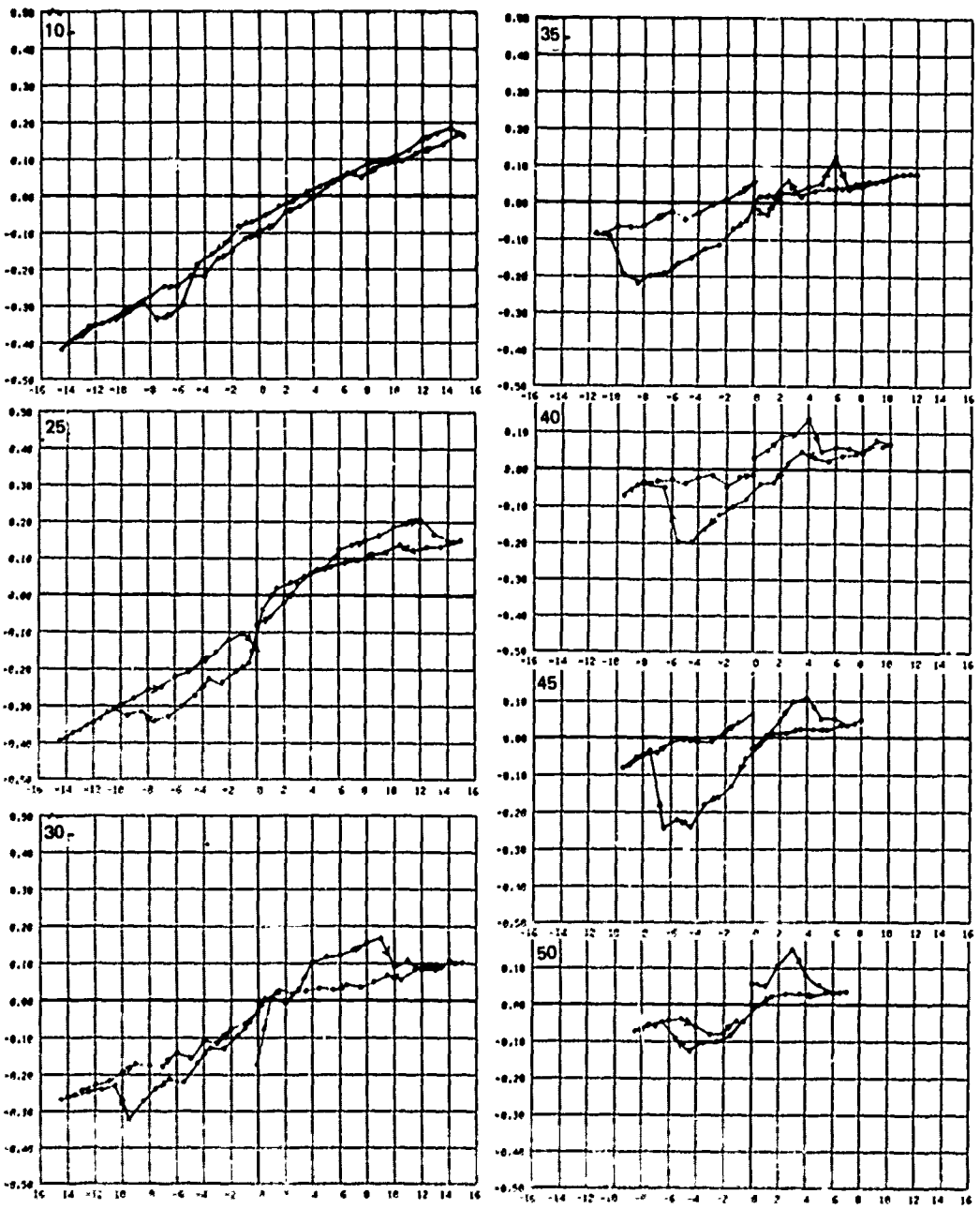

FIGURE 20a SIDEFORCE COEFFICIENT VS. SIDESLIP ANGLE, FLAPPED STRUT, WITH FENCES, -10 DEGREES FLAP, 10, 25, 30, 35, 40, 45, 50 KTS.

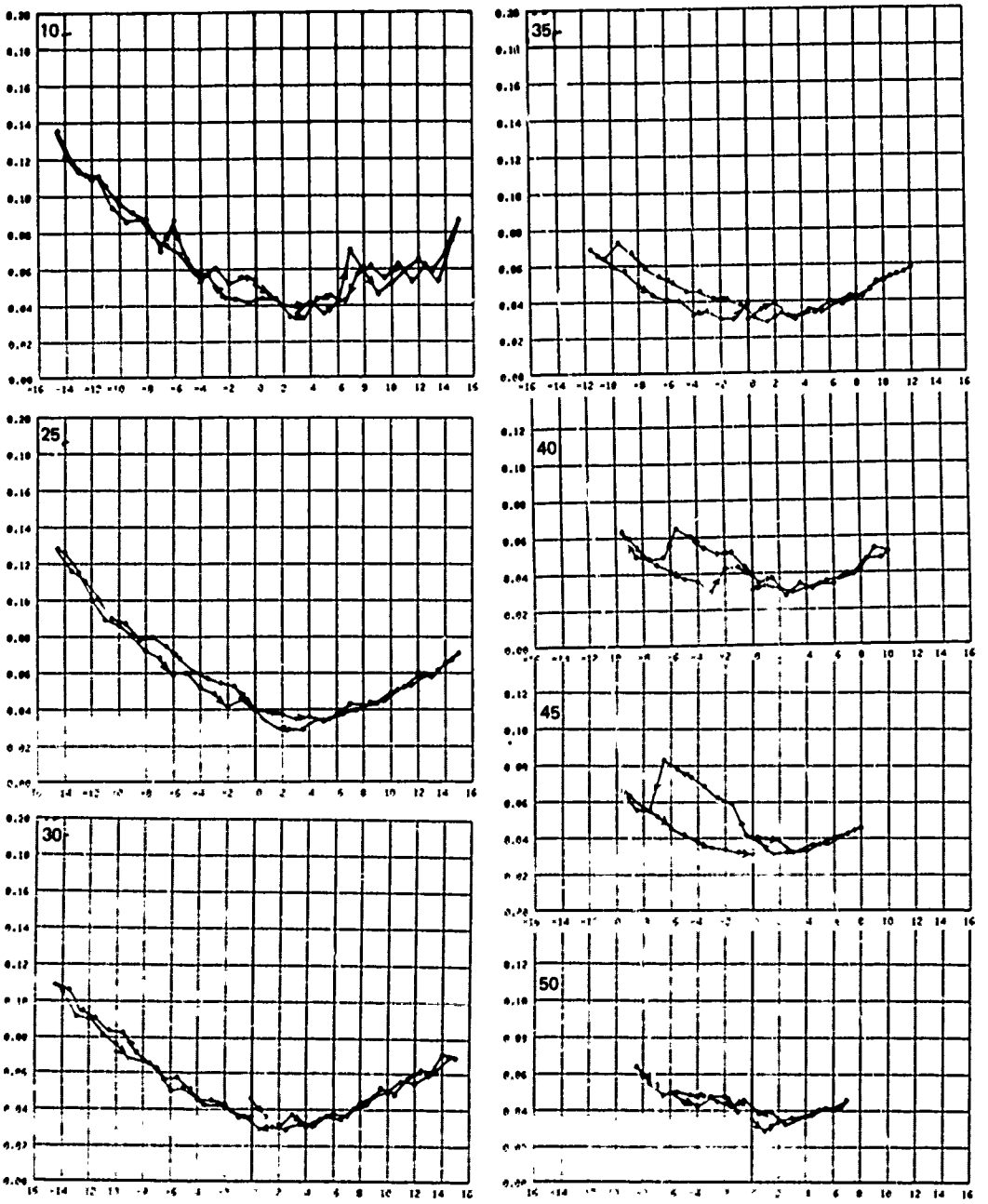

FIGURE 20b DRAG COEFFICIENT VS. SIDESLIP ANGLE, FLAPPED STRUT, WITH FENCES, -10 DEGREES FLAP, 10, 25, 30, 35, 40, 45, 50 KTS.

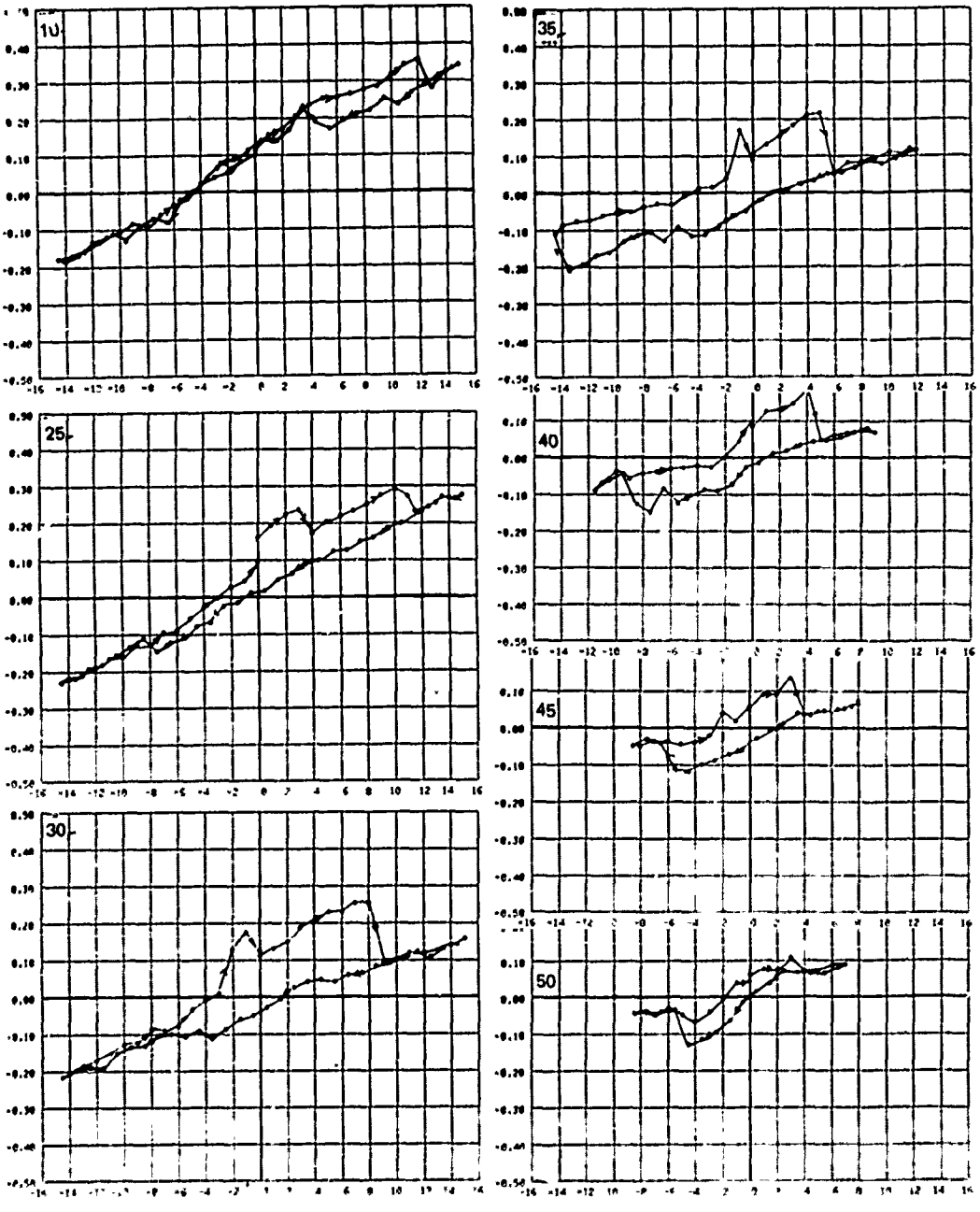

FIGURE 21a SIDEFORCE COEFFICIENT VS. SIDESLIP ANGLE, FLAPPED STRUT, WITH FENCES, 10 DEGREES FLAP, 10, 25, 30, 35, 40, 45, 50 KTS.

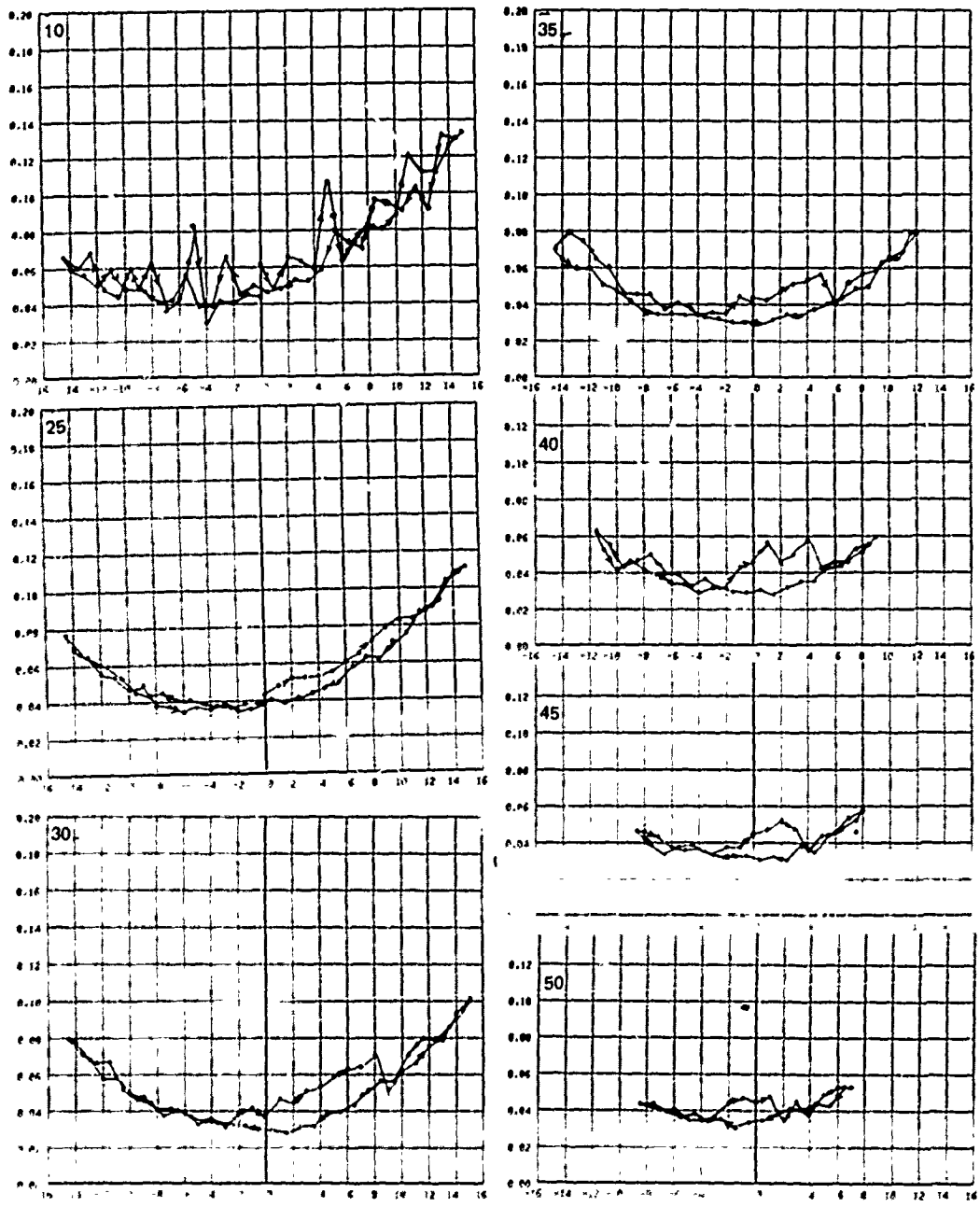

FIGURE 21b DRAG COEFFICIENT VS. SIDESLIP ANGLE, FLAPPED STRUT, WITH FENCES, 10 DEGREES FLAP, 10, 25, 30, 35, 40, 45, 50 KTS.

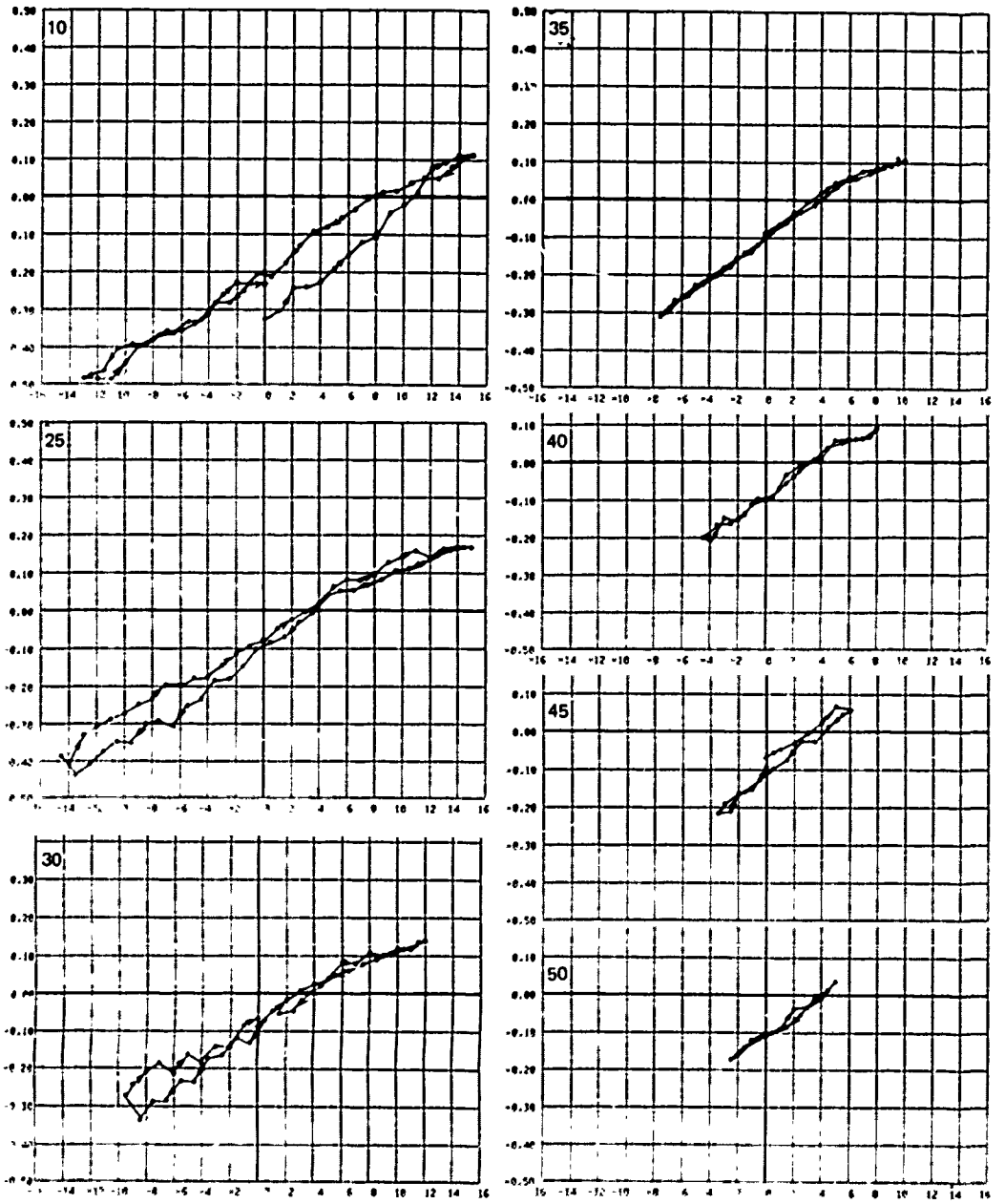

FIGURE 22a SIDEFORCE COEFFICIENT VS. SIDESLIP ANGLE, FLAPPED STRUT, WITH FENCES, -20 DEGREES FLAP, 10, 25, 30, 35, 40, 45, 50 KTS.

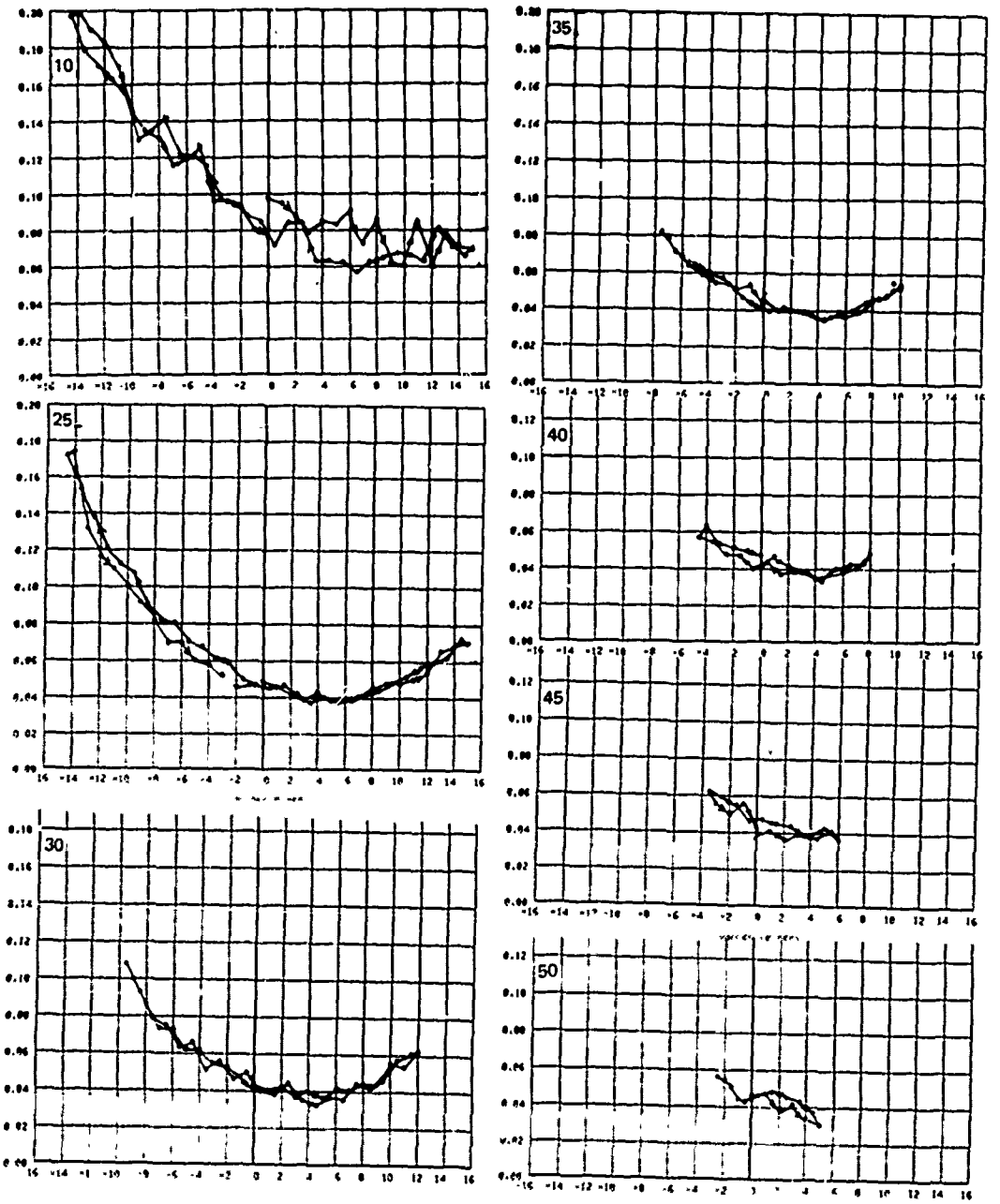

FIGURE 22b DRAG COEFFICIENT VS. SIDESLIP ANGLE, FLAPPED STRUT, WITH FENCES, -20 DEGREES FLAP, 10, 25, 30, 35, 40, 45, 50 KTS.

In Figure 13, for $\delta = 0$, the slope of the sideforce coefficient, $dC_s/d\beta$, for the lower velocities is $dC_s/d\beta \sim 0.2$. This is lower than Nelka's value of 0.25 to 0.29 for the same strut in the same test facility. The only major discrepancy between the two tests was the flap modification which allowed an air path down the hinge line. Photographs of the submerged strut underway confirmed that partial ventilated cavities fed by the hinge slot were occurring.

At the higher speeds, the sideforce coefficients were abruptly cut off, rather than decreased. This was also due to premature ventilation, undoubtedly caused by the hinge slot. The hysteresis loops were caused by the persistence of partial or fully vented cavities to lower sideslip angles than the inception angles. Usually, abrupt changes in forces indicate a change from one flow state to another, such as, flap wetted to flap vented, strut wetted to strut vented, and combinations of these states.

Figure 14 shows the effect of a small flap angle, $\delta = 5$ degrees. Note that for 10 and 25 knots, there is evidence that the flap was effective near $\beta = 0$ where the sideforce curve is raised. However, the flap quickly became vented with increasing β as shown by the sudden decrease of the sideforce curve to its zero flap value. At higher speeds, the flap had a negative effect, decreasing the entire C_s vs β curve to predominantly negative values. This asymmetry was due to the flap being completely within the ventilated cavity when the entire strut was ventilated on the starboard side.

The same trends can be seen in Figures 15, 16, and 17. In Figure 17, for $\delta = 15$ degrees, the hysteresis had become more pronounced, but for some reason the asymmetric effect was not so notable at high speed. The highest speeds were not tested because of spray problems associated with the larger flap angles.

For $\delta = 20$ degrees, shown in Figure 18, significant change had occurred. Although there was some hysteresis and uncertainty of flow states, the flap still had an effect on the lift curve at 40 kts, the highest speed tested in that series. The photographs of these runs reveal that the "spike" in the 25 kt coefficient curve was caused by the momentary washout of the flap cavity. Evidently, at higher flap angles, the flap was always ventilated, which reduced the possible number of flow states and therefore lessened the hysteresis.

In Figures 19 - 22 are shown the results of re-testing certain values of flap angle with ventilation fences added to the strut.

Figure 19, for $\delta = 0$, is about the same as Figure 13, for the same flap angle without fences. The sideforce coefficient slope was virtually unchanged at all velocities tested.

Figures 20 and 21 show the results of a test to determine whether the experiment was symmetric with respect to positive and negative flap angles, considering the curved path of the

towing carriage. The flap angle was tested at -10 and 10 degrees. Except for some variation in the hysteresis loops, the results were symmetric. Comparison with the unfenced strut results for the same flap angle, Figure 15, reveals only insignificant differences.

Generally, the behavior of the strut with flap probably would be unsatisfactory for prototype application for the cases examined thus far, especially for $\delta \leq 15$ degrees, because of the erratic jumping form one flow state to another as reflected by the force coefficients. However, for $\delta = -20$ degrees, with fences, the results are promising as demonstrated by Figure 22. Except at 10 kts, there was almost no hysteresis. The flap was consistently about 20 percent effective, (as defined previously) and the sideforce versus sideslip angle curve is smooth, at least to the maximum values of $|\beta|$ tested. Unfortunately, the values of $|\beta|$ had to be restricted due to spray problems, wnich were bad enough with the large flap angle and worse with the fences. In this case, as in the unfenced case with $\delta = 20$ degrees, the flap was probably fully ventilated under all conditions of velocity and sideslip angle. Because this limited the number of possible flow states, the erratic behavior associated with smaller flap angles was eliminated.

No doubt the same would have been true of larger flap angles, although none were tested. The implication for craft control is that a "Bang! Bang!" approach would have to be used with surface-piercing flaps, with flap angles less than 20 degrees or so not permitted. Above 20 degrees, proportional control would again become possible. Although no flap angles between 15 and 20 degrees were tested, the momentary washout of the flap vent in the unfenced case, $\delta = 20$ degrees, (Figure 18) indicates that 20 degrees is probably close to a lower bound for proportional control.

The effect of flaps and fences on drag can be seen by comparing the drag coefficient presented in Figures 13, 18, 19 and 22. The zero sideforce drag coefficient for no flap angle and no fences (Figure 13b) ranged from 0.02 to 0.025, depending on velocity. With fences, the drag coefficient increased to 0.03 or slightly less. Therefore, the addition of fences alone caused a drag increase of 50 to 100 percent.

For a flap angle of 20 degrees and no fences (Figure 18b), and ignoring anomalous 10 and 35 kt cases, the zero sideforce drag coefficient ranged from 0.02 to 0.025. Thus flap angle alone did not significantly increase the zero sideforce drag.

However, when flap angle was applied with fences (Figure 22b), the zero sideforce drag increased to just below 0.04, an increase of 50 to 100 percent. Thus the drag increase due to flap angle depended upon whether or not fences were present.

To summarize, flap angle caused a relatively slight increase in zero sideforce drag. Fences created somewhat more, and the combination of fences and flap angle caused the greatest increase - about double the baseline case.

It is unfortunate that the baseline case was somewhat dubious. Dailey et al[8] found that the drag coefficient for the NACA 16-012 strut without endplate for the same submergence aspect ratio was only 0.01, and for aspect ratio 2 and 3 was 0.005 or less. Even adding endplate drag to the Dailey et al results would not be sufficient to explain the higher drag in the present tests. The explanation must therefore be that the drag increase was induced by the air flow from the flap hinge intersection.

CONCLUSIONS OF THE FLAP AND FENCE EXPERIMENT

- Flap and fence combinations were effective in changing sideforce reliably only for flap angles of 20 degrees, and in the presence of ventilation fences.
- Flap effectiveness, defined as the ratio of flap angle to sideslip angle at zero sideforce, was much less than predicted by airfoil data.
- Unless air is prevented from feeding down the flap hinge intersection, there will be a drag penalty associated with flaps even at zero flap angle.

[8] Dailey, N.L., M.F. Jeffers, R.S. Rothblum, *"Ventilation and Force Characteristics of the NACA 16-012 Surface-Piercing Strut in Cavitating Flow,"* Naval Ship Research and Development Center Ship Performance Department Report 479-H-03 (Aug 1972).

AIRBLEED

Baron Hanns von Schertel[9,10] was the first to apply the technique of deliberate introduction of air in controlled quantities to the otherwise fully wetted flow around a hydrofoil in order to influence the hydrodynamic forces acting on it. Other investigators have also examined the process, notably Lang, Daybell and Smith,[11] who published what is probably the most extensive information correlating the forces generated by air injection with the chordwise location of the supply holes and the air flow rate.

The airbleed literature indicates that it is possible to change the lift coefficient on a hydrofoil by quite large values, of the order of 0.6.

There are some potential disadvantages to the use of an airbleed system to compensate for turn-induced sideslip angles on surface piercing hydrofoil struts. Generally, there is a drag penalty, although Lang et al found that the lift:drag ratio did not change with air injection. There is also a hysteresis effect associated even with fully submerged, two-dimensional hydrofoils, whereby once airbleed is increased, a subsequent decrease in air flowrate does not cause the forces to return to their former strengths. This hysteresis effect would be expected to be even more pronounced in the case of a surface piercing strut, where it could become ventilated to the atmosphere. Possibly to prevent this, Von Schertel's hydrofoils have fences on their surface-piercing elements.[12] There is also the possibility of large unsteady forces due to the collapse and regeneration of partial cavities, as observed by Lang et al. A final possible disadvantage of an airbleed system is the power, if any, required to drive the air, and the ducting and controls to direct the proper amount of air to the desired location. This potential disadvantage must, of course, be weighed against the disadvantages of alternative measures for accomplishing the same result.

In order to more clearly define the problems involved in an airbleed system for a surface-piercing strut, and to clarify the ambiguities arising from the surface-piercing factor, the experiment in the Center's Rotating Arm facility concerning the flapped strut described previously was extended to include a test of an airbleed strut.

---

[9]Von Schertel, Hanns, *"Comparative Tests Between an Air Stabilizer and a Conventional Supramar PT50,"* Supramar, Ltd (1967).

[10]Von Schertel, Hanns, *"Experimental Investigation of Air-Fed Hydrofoils,"* Supramar, Ltd (Aug 1964).

[11]Lang, T.G., D.A. Daybell, and K.E. Smith, *"Water-Tunnel Tests of Hydrofoils with Forced Ventilation,"* NAVORD Report NOTS TP 2363 (Nov 1959).

[12]Von Schertel, Hanns, *"Hydrofoil Boats as a New Means of Transportation,"* paper presented to New York Metropolitan Section of SNAME, (30 Oct 1958).

ESTIMATE OF REQUIRED AIR FLOW RATE

Lang et al reported that for airbleed on hydrofoils, there is a certain airflow rate above which the forces are further affected only negligibly. This was called the critical volume flow rate, Q_{CR}, and was characterized by the formation of a stable, aerated cavity which enclosed the entire side of the foil over which the air was being ejected, from the ejection point to somewhat beyond the trailing edge. Lang et al presented an empirical formula for Q_{CR}, which encompassed their data. Referring to Figure 23 for definition of geometric terms,

$$Q'_{CR} \cong 0.09 - 0.05 \frac{a}{c}$$

where

$$Q'_{CR} \equiv \frac{Q_{CR}}{U_\infty t' b'},$$

where U_∞ was the upstream water tunnel velocity, and

$t' \cong y_p + (c - a) \tan \alpha$, $t' > 0$,

and b' was the *measured* gas-covered span.

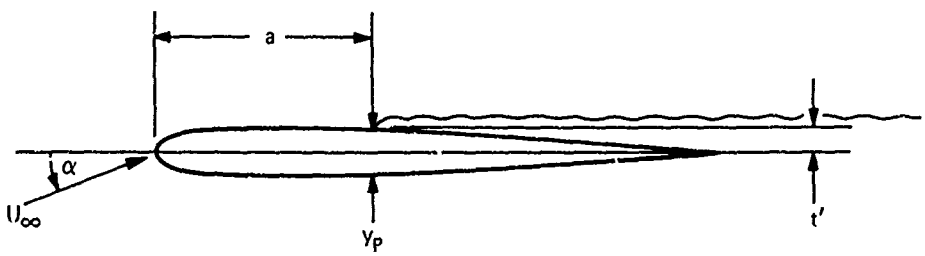

Figure 23 – Nomenclature for Lang, Daybell and Smith Formula

The maximum Q'_{CR} for their experiment was about 0.1.

For an aspect ratio 1 strut such as the NACA 16-012 section strut used in the flap experiment, assuming that natural ventilation would occur at about 8 degrees of sideslip angle,[3,7,8] then correcting the geometric angle of 8 degrees by the ratio of measured sideforce at subcavitating speed to ideal two dimensional,[3,7,8] the critical air flow rate required at 50 kts was predicted to be about 28 ft^3/min (13 x 10^{-3} m^3/s). In actual fact, it would be surprising if this airflow rate were required to trigger full ventilation for a strut on the verge of natural ventilation. However, this conservative figure was used to select the air supply for the airbleed experiment.

THE AIRBLEED AND FENCE EXPERIMENT

The Model. A strut was chosen nearly identical to the one used in the flap experiment, except that the section was somewhat thicker at the nose. Figure 24 shows the model and gives the offsets. Air could be supplied from a common manifold to any one or combination of 5 vertical rows of 1/32 inch (8 mm) diameter holes, each spaced 1/8 inch apart (16 mm) and extending vertically from the strut tip for one and one-half chord. The rows were located at 5, 10, 25, 50 and 75 percent of chord aft of the leading edge, on the port side of the strut. A sixth row of holes was added on the starboard side at the 5 percent chord location after the initial tests of this model. Four removable ventilation fences were built to be attached to the strut at 0.25 c intervals from the tip. An endplate similar to the one used for the flapped model was affixed to the tip.

Air Supply. Air was supplied from a compressor continuously charging an accumulator. The coupling to the strut was vertical, through the strut and dynamometer axis, using a rotating coupling and flexible hose to ensure that the air pressure did not affect the measurement of hydrodynamic forces. Zero velocity runs verified this.

Test Conditions. The strut was towed as before, vertically, piercing the water surface to a depth of one chord, at a radius of 120 c on the Rotating Arm. Angular velocities ranged from 0.14 to 0.7 rad/s, corresponding to linear velocities of 10 to 50 kts. Airflow rate was varied between 10 and 35 ft^3/min (4.7×10^{-3} and 16.5×10^{-3} m^3/s), corrected to standard (dry air) conditions of 20 degrees Celcius and 101 kPa (standard atmosphere). Bursts of air as high as 100 SCFM were also included in the tests. Air was supplied through each row of holes separately, except for the port side 0.75 c holes, which were not tested individually, and the starboard side 0.05 c holes, which could not be controlled independently of the port 0.05 c holes. All port side holes were fed simultaneously, and all port and starboard holes were simultaneously supplied. Sideslip angles were varied between ± 15 degrees.

Data Collection. Airflow was monitored using a National Bureau of Standards calibrated venturi throat instrumented with a differential and an absolute pressure gage, and a platinum wire thermometer. The computer continuously performed the calculation of airflow rate, assuming adiabatic expansion, and recorded this information with the force, sideslip angle and velocity data.

Otherwise, the data collection system was identical to that described for the flapped strut experiment.

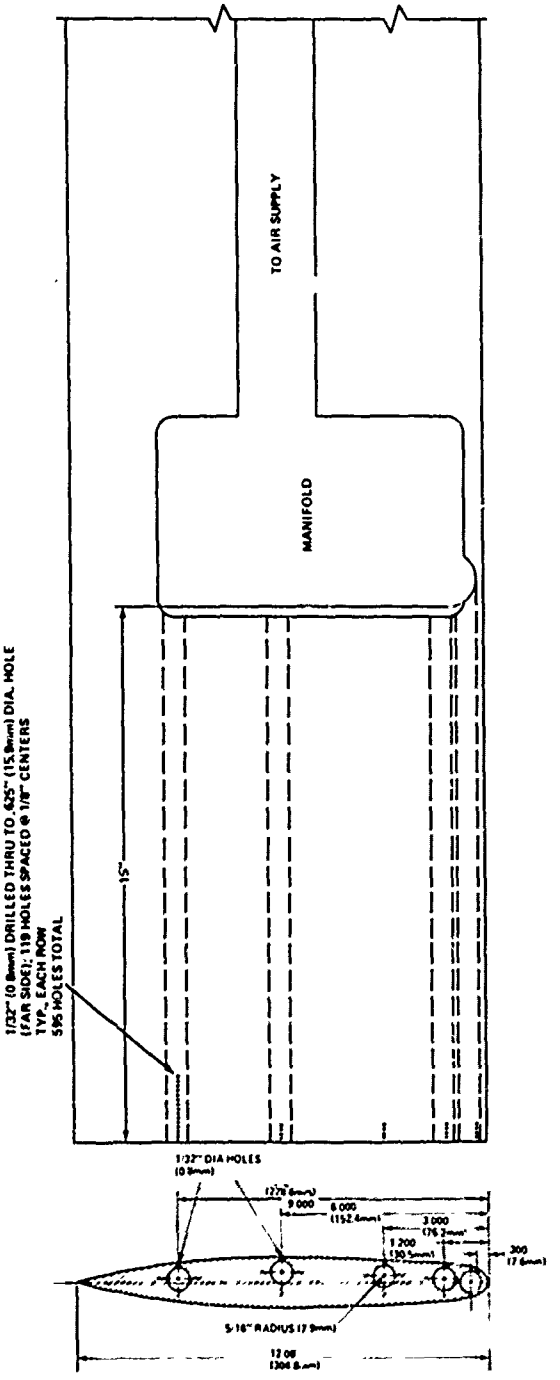

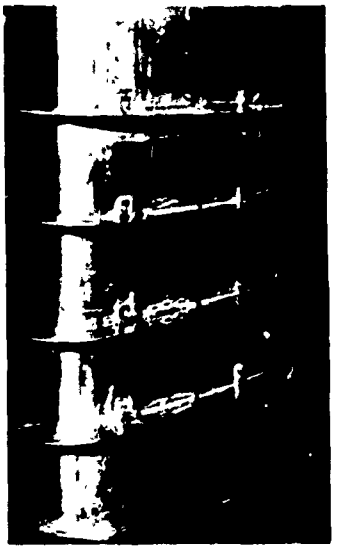

COORDINATES IN INCHES (mm)	
"X"	"Y"
0	0
.030 (.76)	.140 (3.55)
.060 (1.52)	.191 (4.85)
.090 (2.28)	.227 (5.76)
.120 (3.04)	.255 (6.47)
.180 (4.57)	.299 (7.59)
.240 (6.09)	.332 (8.43)
.300 (7.62)	.359 (9.11)
.360 (9.14)	.381 (9.67)
.480 (12.19)	.416 (10.56)
.600 (15.24)	.443 (11.25)
.720 (18.28)	.464 (11.78)
.840 (21.33)	.482 (12.24)
.960 (24.38)	.496 (12.59)
1.080 (27.43)	.508 (12.90)
1.200 (30.98)	.519 (13.10)
1.320 (33.52)	.529 (13.43)
1.440 (36.54)	.537 (13.63)
1.560 (39.62)	.545 (13.84)
1.680 (42.67)	.552 (14.02)
1.800 (45.72)	.559 (14.19)
1.920 (48.76)	.565 (14.35)
2.100 (53.34)	.574 (14.57)
2.400 (60.96)	.589 (19.96)
2.700 (68.58)	.603 (15.31)
3.000 (76.20)	.618 (15.69)
3.300 (83.82)	.632 (16.05)
3.600 (91.44)	.646 (16.40)
3.900 (99.06)	.660 (16.76)
4.200 (106.68)	.673 (17.09)
4.500 (114.30)	.686 (17.42)
4.800 (121.92)	.697 (17.70)
5.100 (129.54)	.706 (17.93)
5.400 (137.16)	.714 (18.13)
5.700 (144.78)	.718 (18.23)
6.000 (152.40)	.720 (18.28)
↓ 12.000	CIRCULAR ARC, 25.36 INCH (644mm) RADIUS
NOSE RADIUS – .392 (9.95mm)	

Figure 24 – Airbleed Model with Fences

RESULTS AND DISCUSSION OF THE AIRBLEED AND FENCE EXPERIMENT

Figures 25 through 50 show the sideforce and drag coefficients, as previously defined, versus sideslip angle over the range of velocities, hole locations and airflow rates tested. Figure 25 shows the results of testing the airbleed strut with the main feed holes for each row plugged by the insertion of snug-fitting metal rods. This was the technique used to block rows of holes so that airbleed from individual rows could be tested separately.

Because this was not a positive method of sealing air from the ejection holes, some air still leaked into the flow around the strut. This is probably why $dC_s/d\beta$ decreased from 0.021/degree to 0.017/deg when velocity was increased from 10 to 25 and 30 kts, as shown in Figure 25.

There was no previously published force coefficients for the airbleed strut section with endplate. The 10 kt values of C_s and $dC_s/d\beta$ are in very close agreement with the results of Rothblum, et al,[3] for a similar test of the same method, but without endplate. Correcting for the endplate effects by adding the half-breadth of the endplate to the depth of the airbleed strut, (for purpose of calculating aspect ratio) and extrapolating between aspect ratio 2.0 and 1.0 in Reference 3, the expected value of $dC_s/d\beta$ was 0.023/degree. Compared with the measured value at 10 kts, $dC_s/d\beta$ = 0.021/degree, this was about 8 percent too low.

The ventilation inception angles for the airbleed strut with plugged holes were between 8 and 9 degrees at 45 kts and 5 and 6 degrees at 50 kts, lower then 9 1/2 degrees at 45 kts and 8 degrees at 50 kts as given in Reference 3. While this is not a very significant difference, it supports the contention that the results for the plugged airbleed model may have been affected by some air injection.

The drag coefficient at zero sideslip angle for the plugged airbleed strut was about 0.02 for the 25 and 30 kt runs. The 10 kt runs are not considered reliable for drag measurements because of the small magnitude of the forces at low speeds. There was also a substantial unsteady signal from the drag force transducer at low speeds which may have been due to towing accelerations - the mass of the strut and "floating frame" of the dynamometer was approximately a tonne, compared to measured forces of the order of a few pounds (30 to 40 newtons).

According to Hoerner,[13] the drag of an endplate can be estimated by the formula

$$C_D \text{ (endplate)} = 0.008\ (A_E/A) + 0.004/AR$$

[13]Hoerner, S.F., *"Fluid-Dynamic Drag,"* published by author (1965).

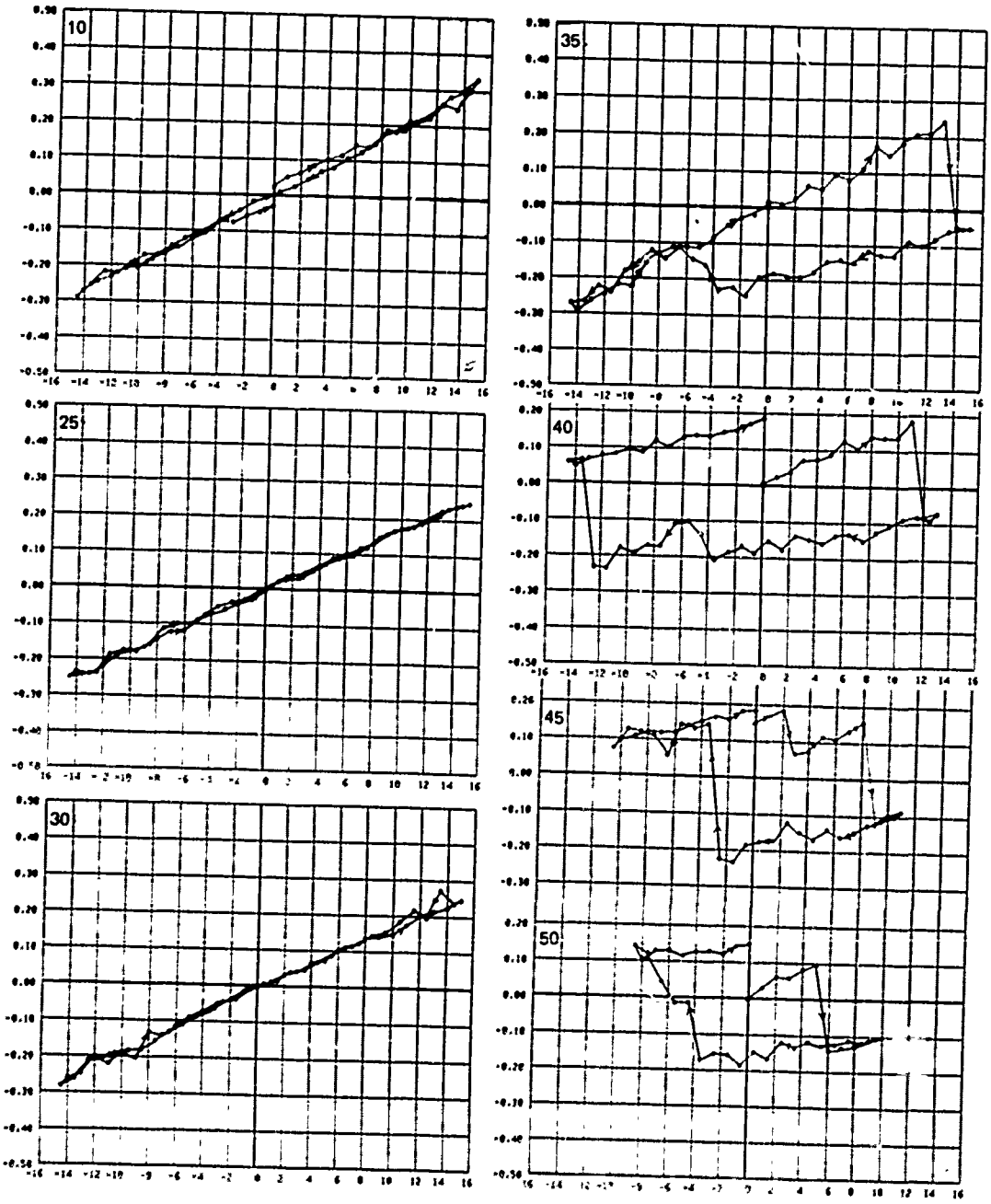

FIGURE 25a SIDEFORCE COEFFICIENT VS. SIDESLIP ANGLE, AIRBLEED STRUT, OFF, PLUGGED, WITHOUT FENCES, 10, 25, 30, 40, 50 KTS.

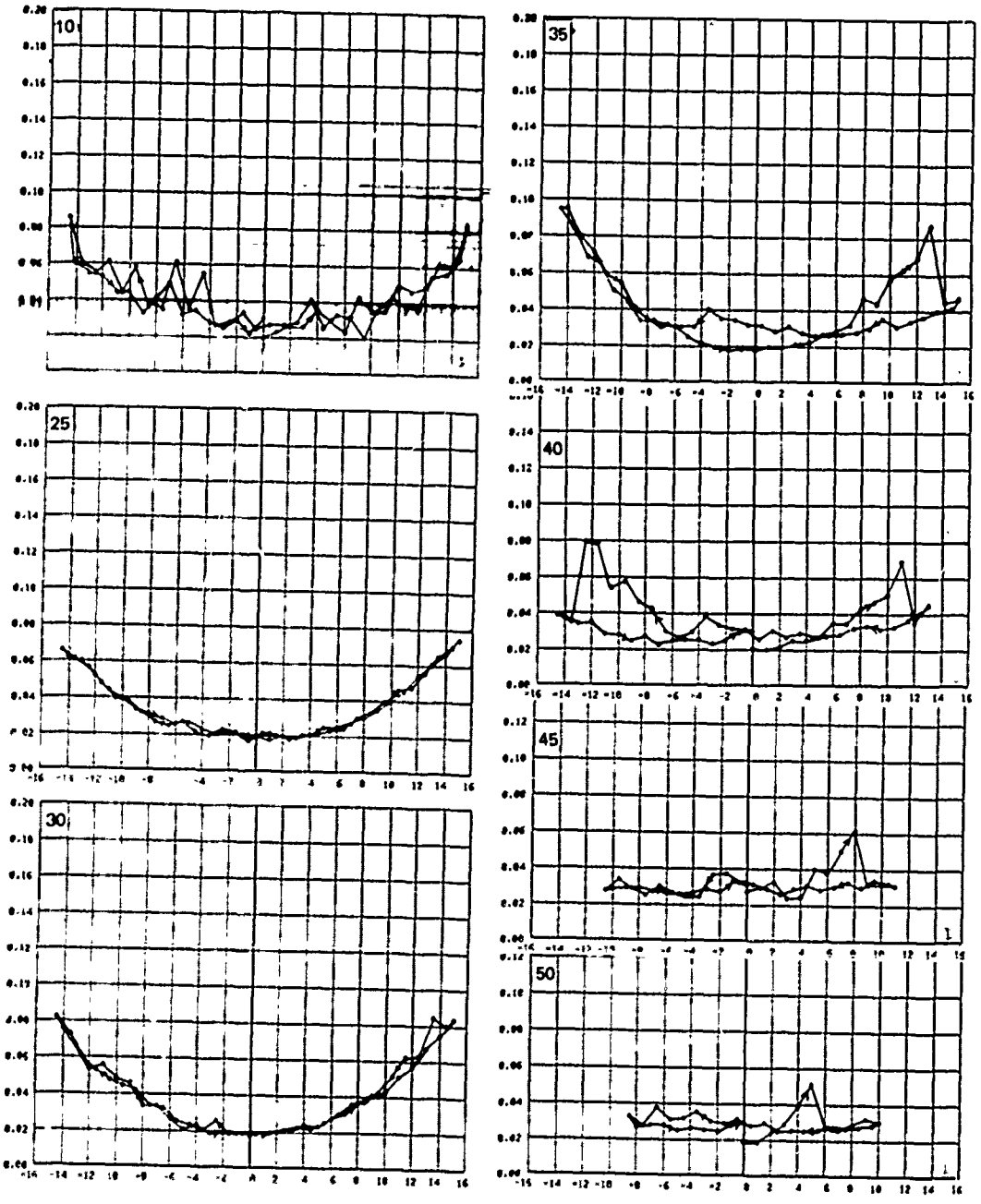

FIGURE 25b DRAG COEFFICIENT VS. SIDESLIF ANGLE, AIRBLEED STRUT, OFF, PLUGGED, WITHOUT FENCES, 10, 25, 30, 40, 50 KTS.

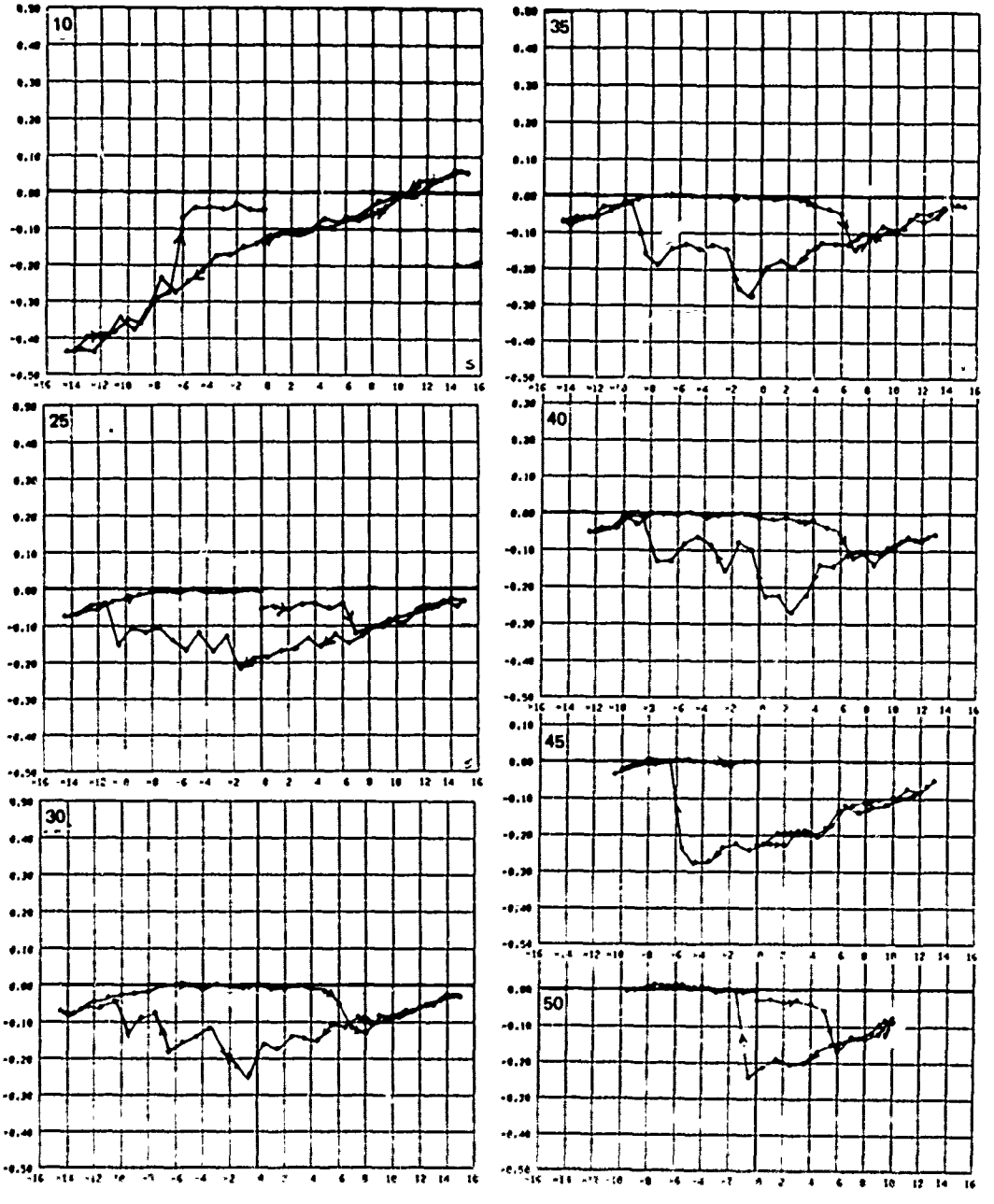

FIGURE 28a SIDEFORCE COEFFICIENT VS. SIDESLIP ANGLE, AIRBLEED STRUT, 35 SCFM (16.5 X $10^{-3}m^3/s$), WITHOUT FENCES, ALL HOLES, PORT SIDE, 10, 25, 30, 35, 40, 45, 50 KTS.

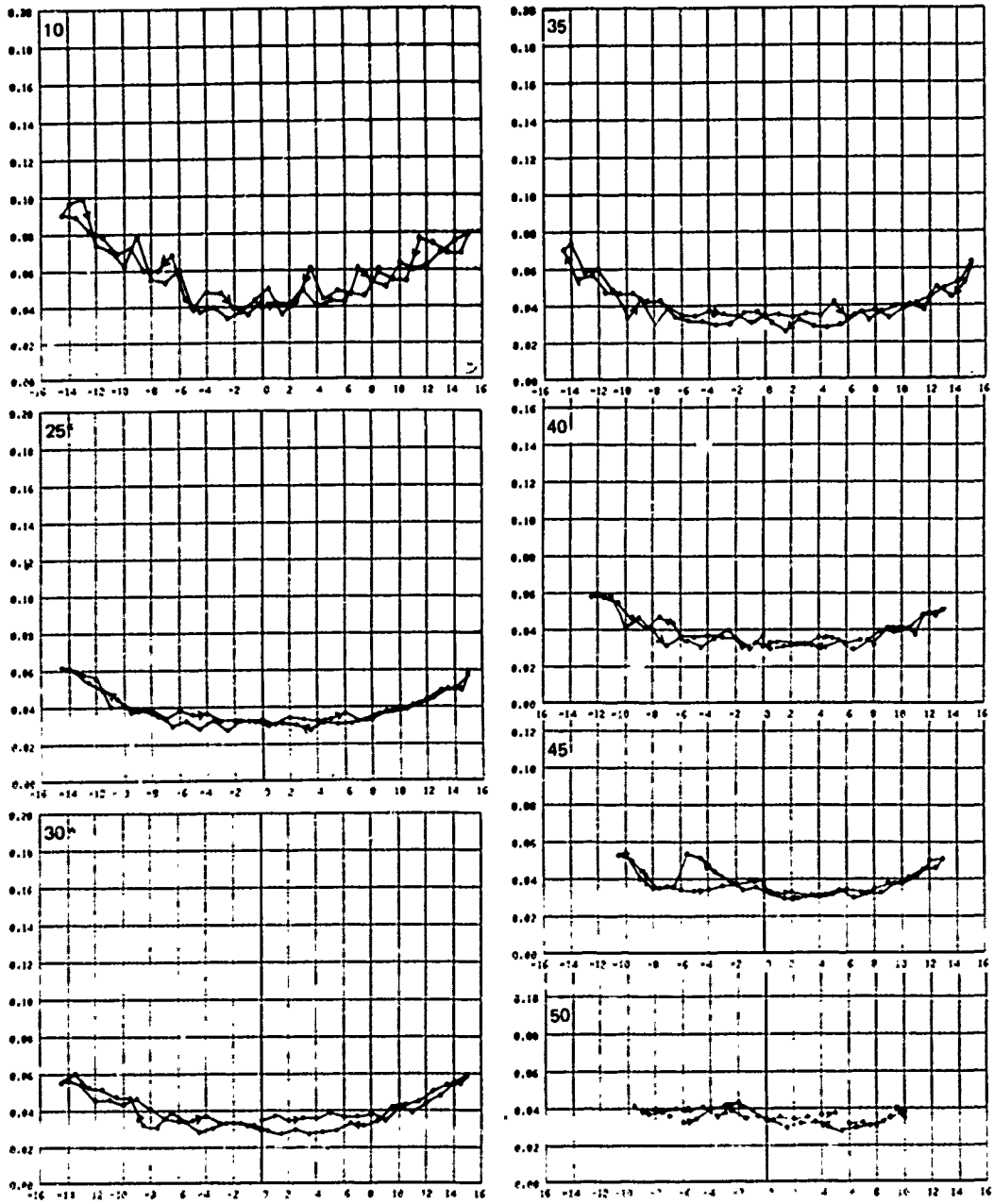

FIGURE 26b DRAG COEFFICIENT VS. SIDESLIP ANGLE, AIRBLEED STRUT, 35 SCFM (16.5 X $10^{-3}m^3/s$), WITHOUT FENCES, ALL HOLES, PORT SIDE, 10, 25, 30, 35, 40, 45, 50 KTS.

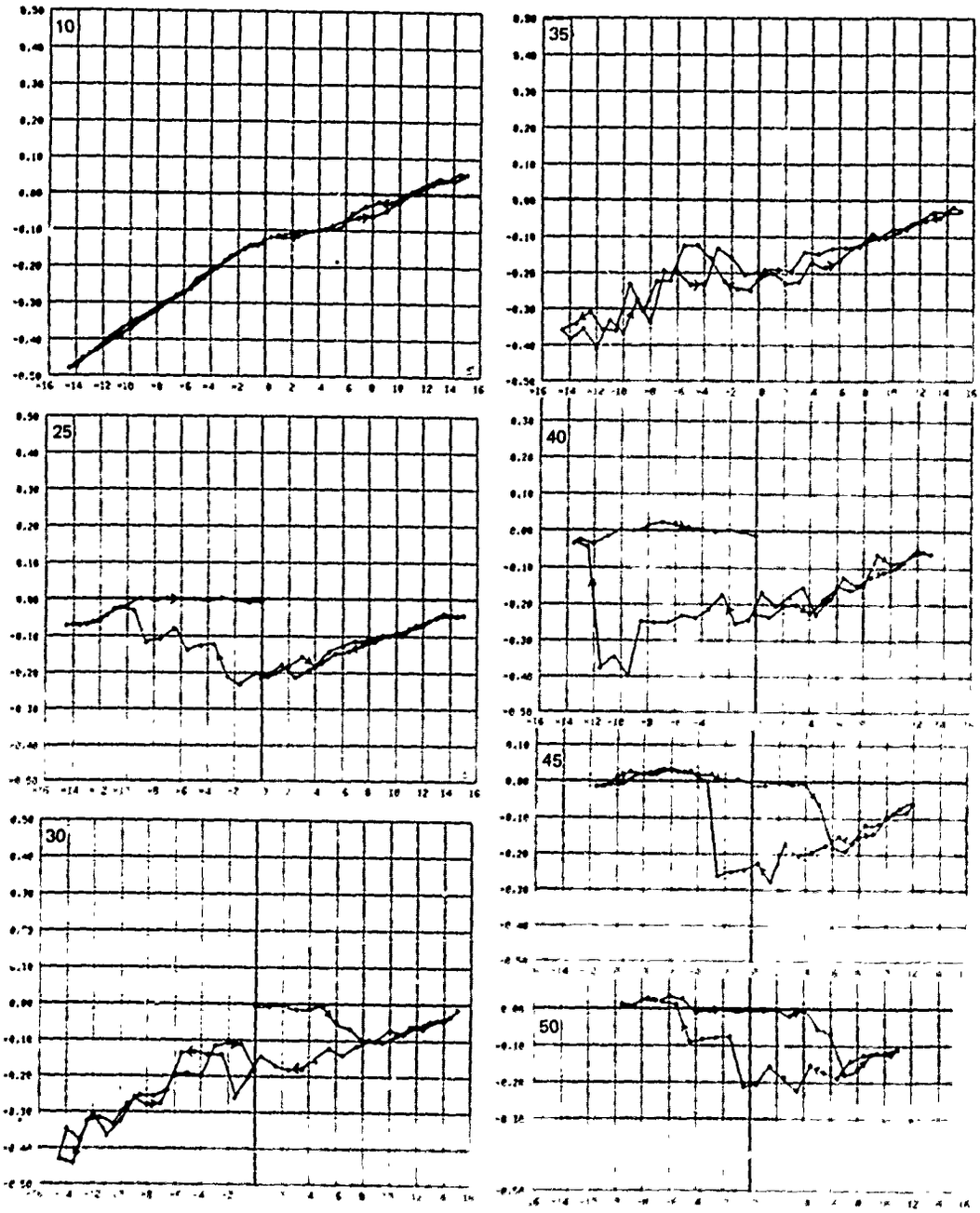

FIGURE 27a SIDEFORCE COEFFICIENT VS. SIDESLIP ANGLE, AIRBLEED STRUT, 20 SCFM (9.4 X $10^{-3}m^3/s$), WITHOUT FENCES, ALL HOLES, PORT SIDE ONLY, 10, 25, 30, 35, 40, 45, 50 KTS.

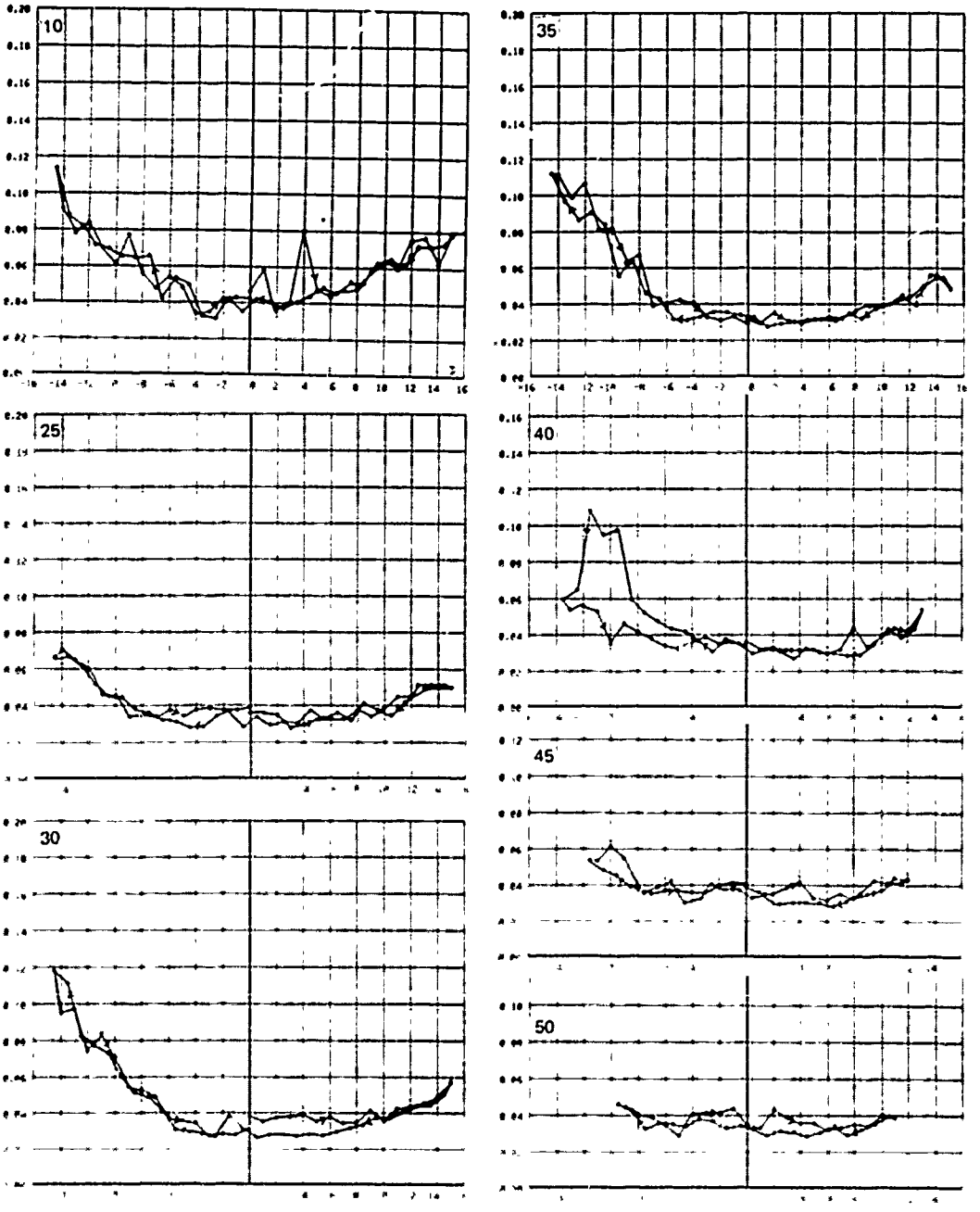

FIGURE 27b DRAG COEFFICIENT VS. SIDESLIP ANGLE, AIRBLEED STRUT, 20 SCFM (9.4 X $10^{-3}m^3/s$), WITHOUT FENCES, ALL HOLES, PORT SIDE ONLY, 10, 25, 30, 35, 40, 45, 50 KTS.

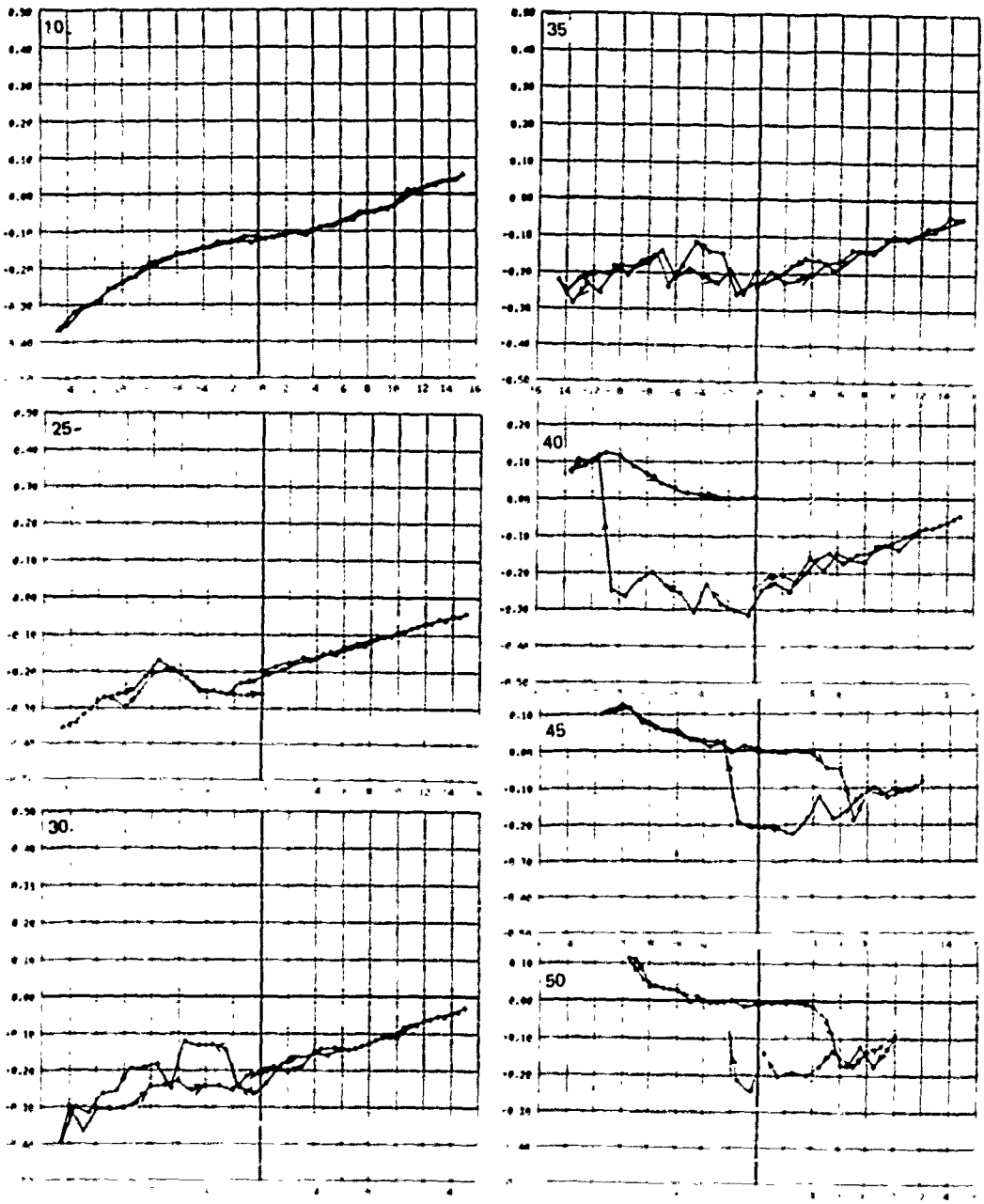

FIGURE 28a SIDEFORCE COEFFICIENT VS. SIDESLIP ANGLE, AIRBLEED STRUT, ATMOSPHERIC, WITHOUT FENCES, ALL HOLES, PORT SIDE, 10, 25, 30, 35, 40, 45, 50 KTS.

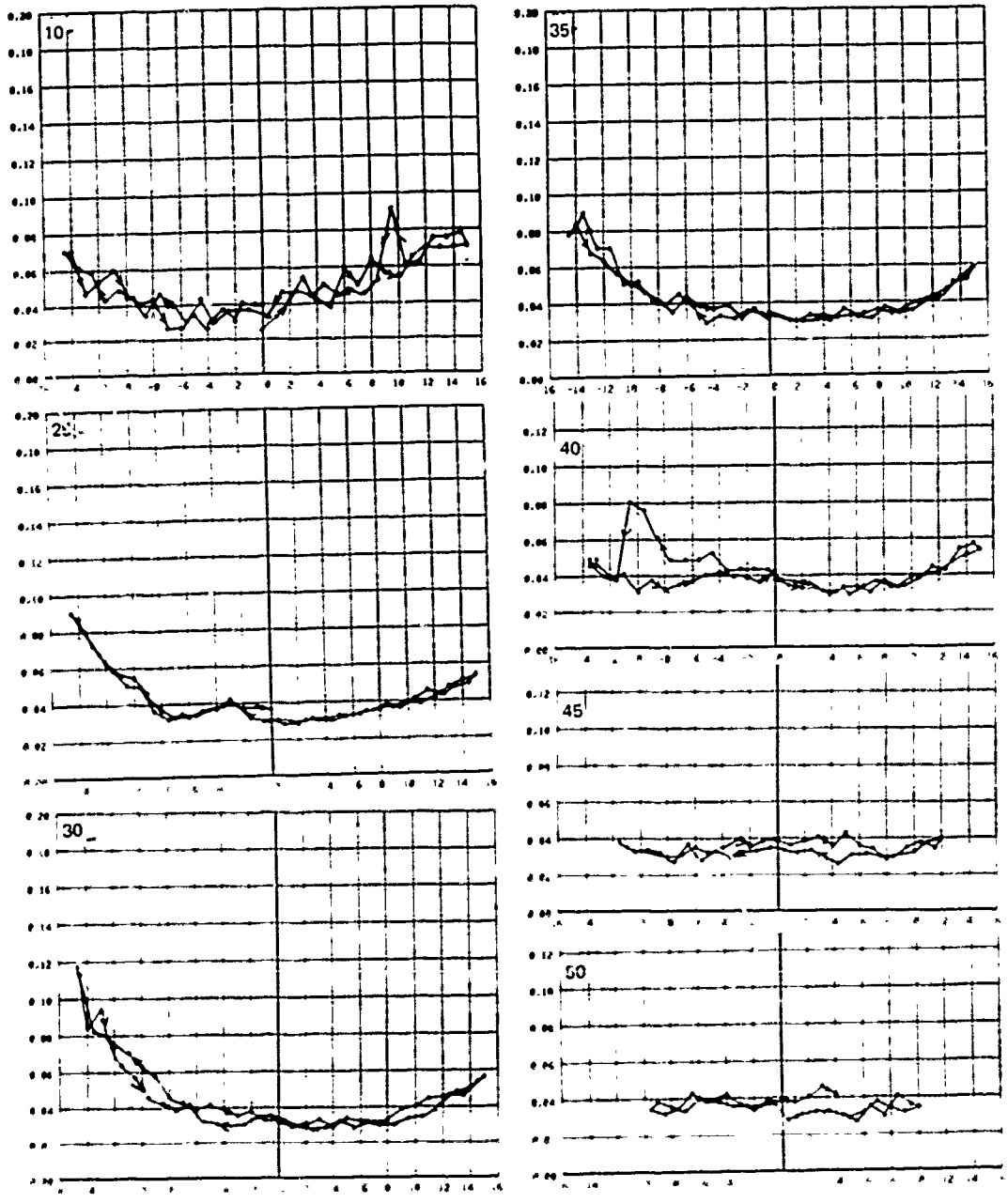

FIGURE 28b DRAG COEFFICIENT VS. SIDESLIP ANGLE, AIRBLEED STRUT, ATMOSPHERIC, WITHOUT FENCES, ALL HOLES, PORT SIDE, 10, 25, 30, 35, 40, 45, 50 KTS.

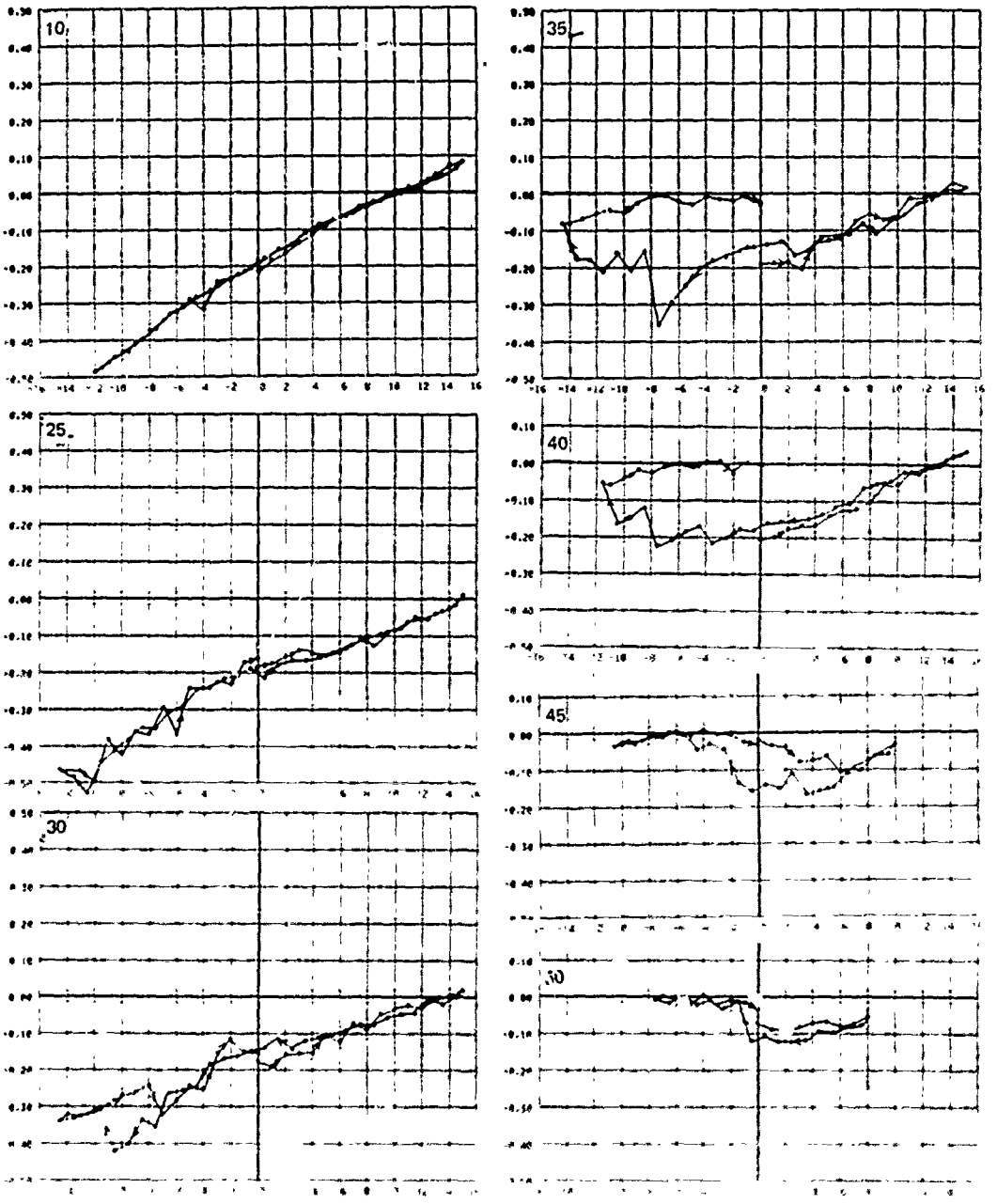

FIGURE 29a SIDEFORCE COEFFICIENT VS. SIDESLIP ANGLE, AIRBLEED STRUT, 35 SCFM (16.5 X 10^{-3} m^3/s), WITH FENCES, ALL HOLES, PORT SIDE, 10, 25, 30, 35, 40, 45, 50 KTS.

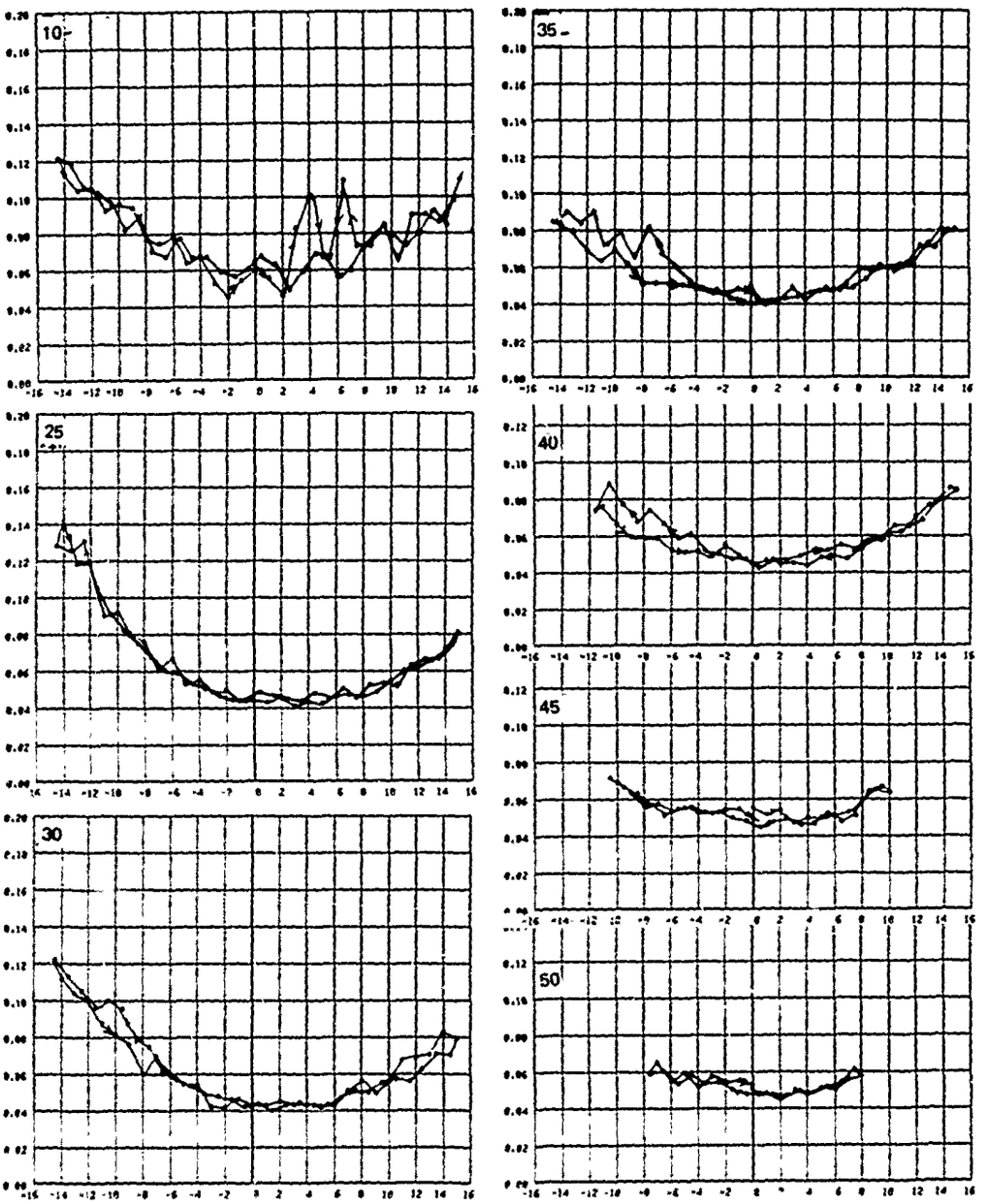

FIGURE 29b DRAG COEFFICIENT VS. SIDESLIP ANGLE, AIRBLEED STRUT, 35 SCFM (16.5 X $10^{-3}m^3/s$), WITH FENCES, ALL HOLES, PORT SIDE, 10, 25, 30, 35, 40, 45, 50 KTS.

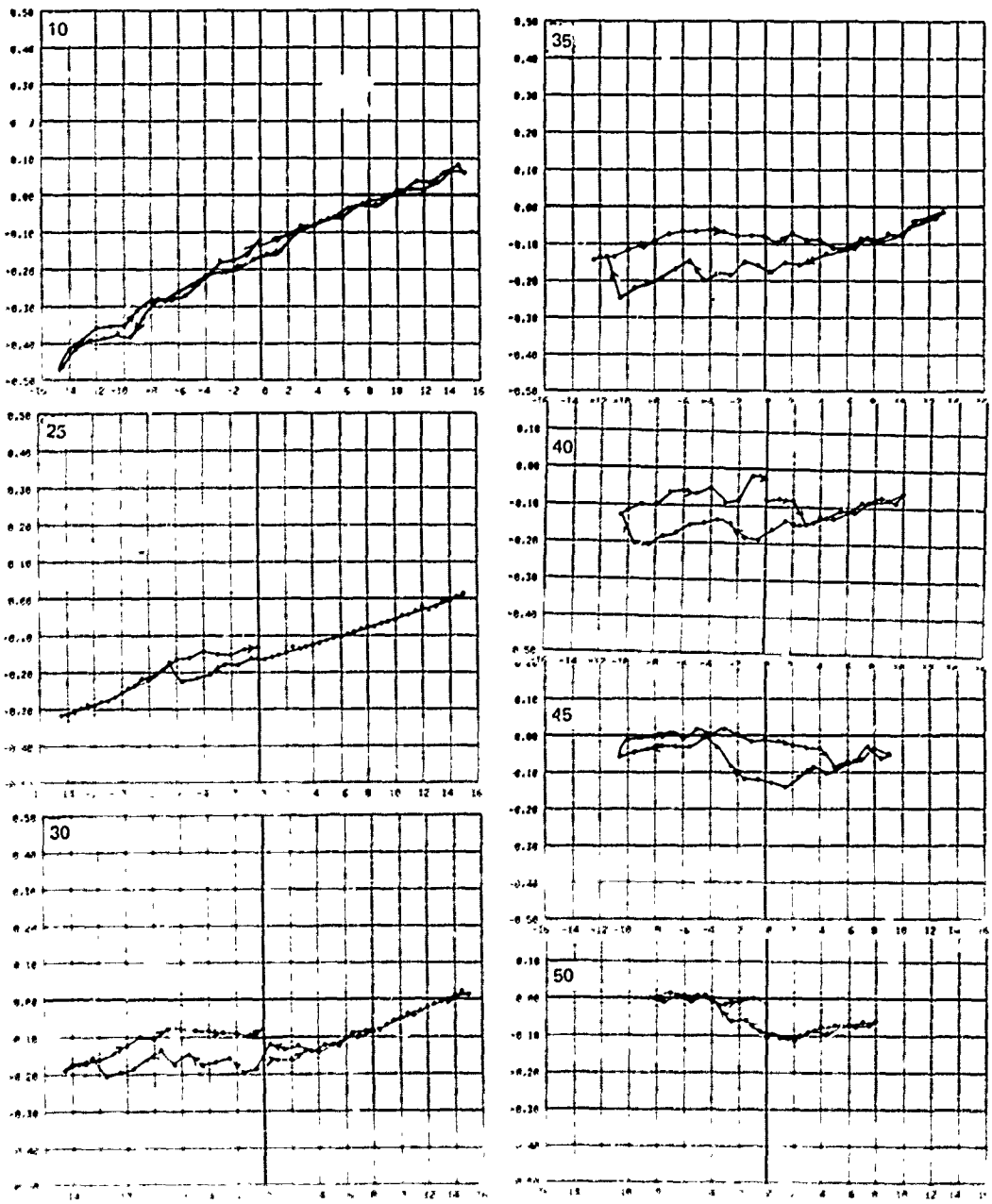

FIGURE 30a SIDEFORCE COEFFICIENT VS SIDESLIP ANGLE, AIRBLEED STRUT, 20 SCFM (9.4 X 10^{-3} m^3/s), WITH FENCES, ALL HOLES, PORT SIDE ONLY, 10, 25, 30, 35, 40, 45, 50 KTS.

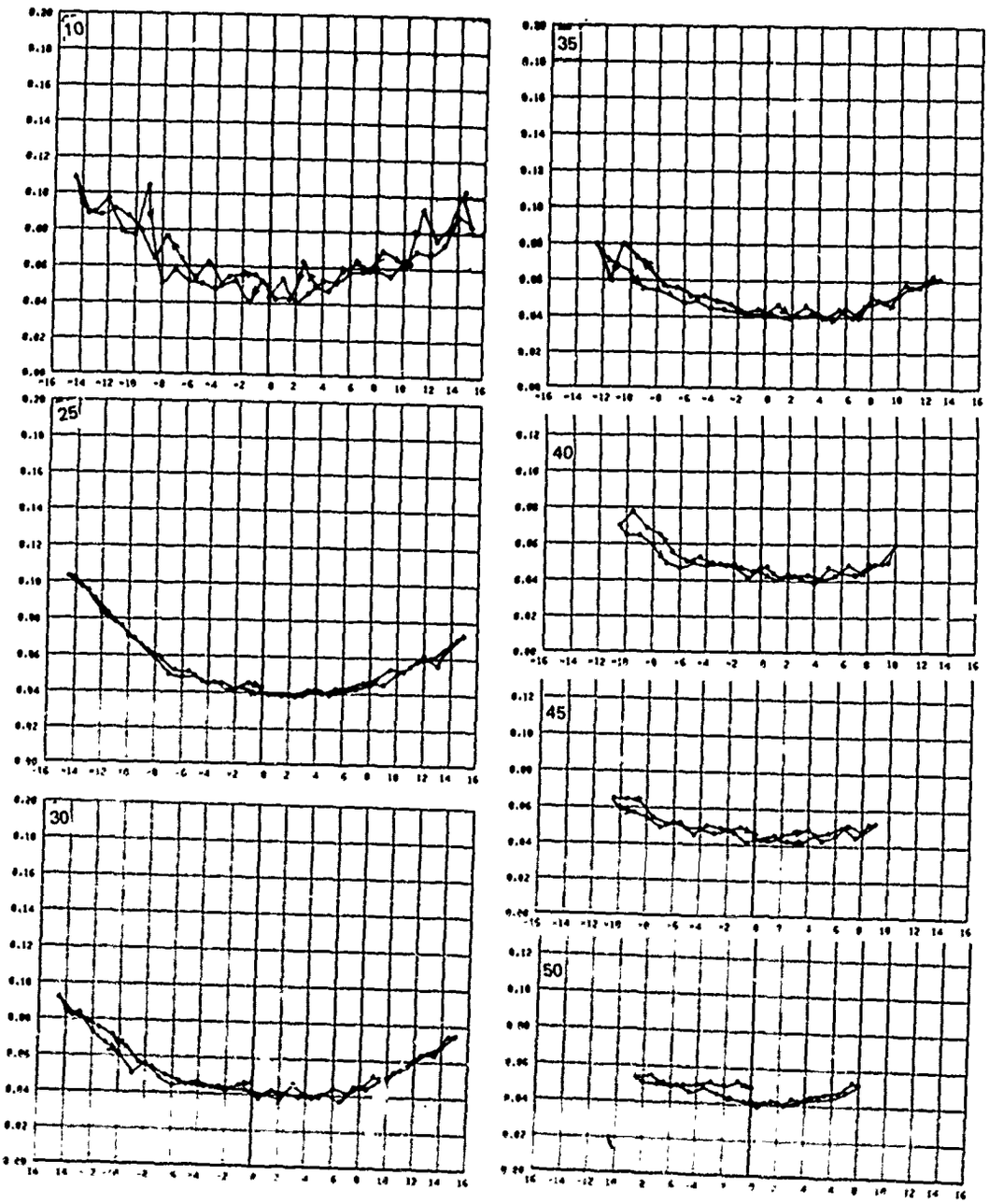

FIGURE 30b DRAG COEFFICIENT VS. SIDESLIP ANGLE, AIRBLEED STRUT, 20 SCFM (9.4 X 10^{-3} m^3/s), WITH FENCES, ALL HOLES, PORT SIDE ONLY, 10, 25, 30, 35, 40, 45, 50 KTS.

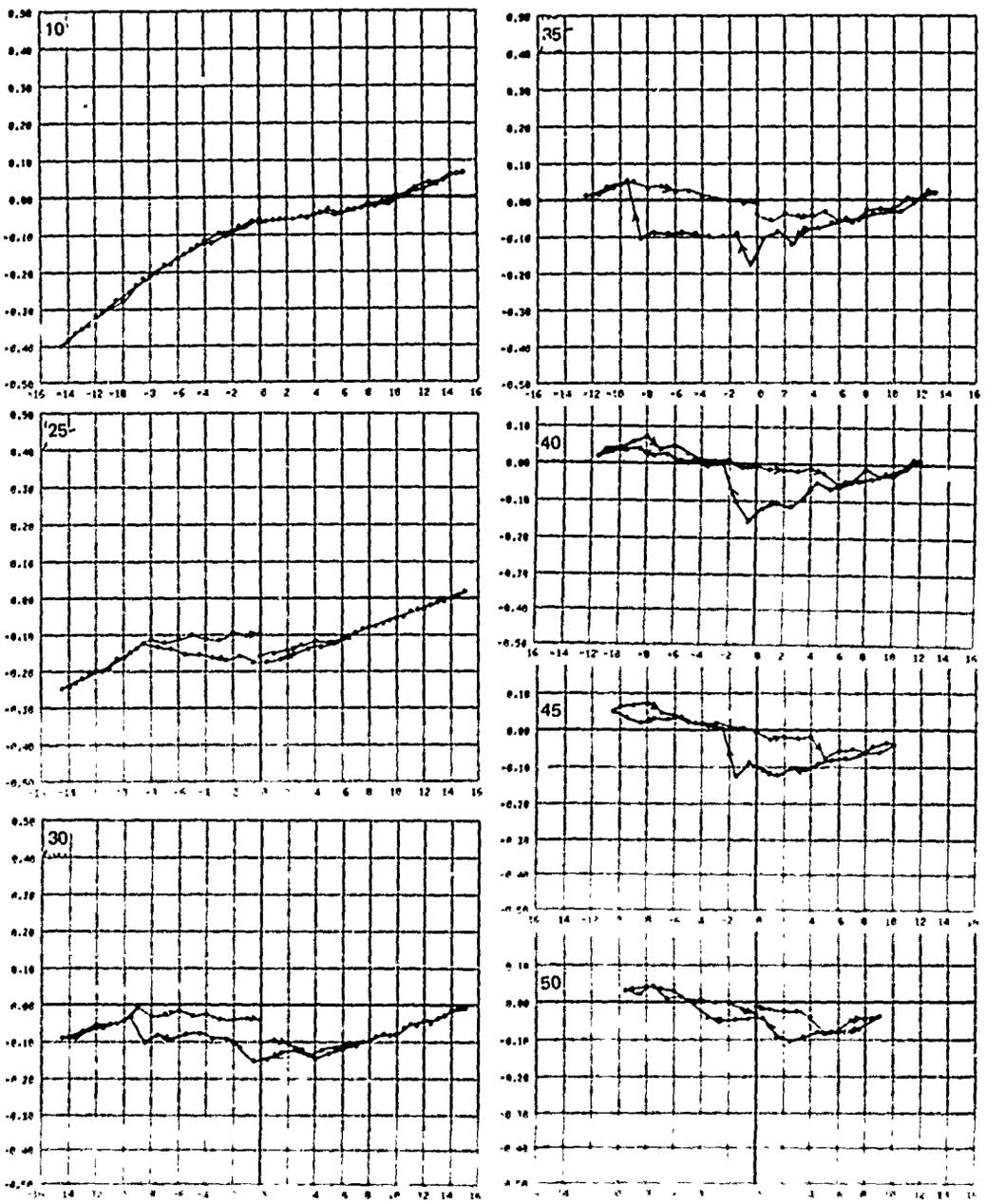

FIGURE 31a SIDEFORCE COEFFICIENT VS. SIDESLIP ANGLE, AIRBLEED STRUT, ATMOSPHERIC, WITH FENCES, ALL HOLES, PORT SIDE, 10, 25, 30, 35, 40, 45, 50 KTS.

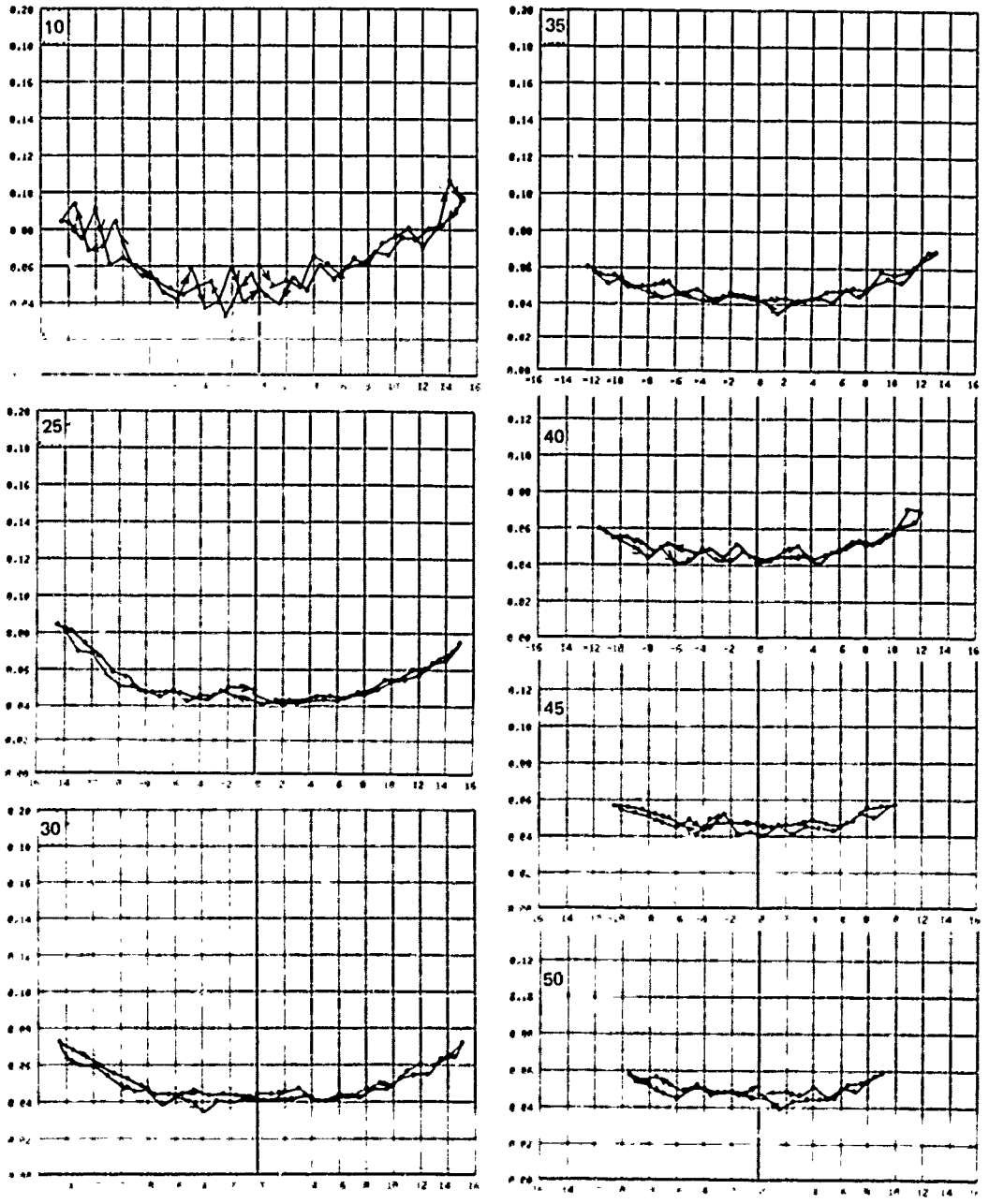

FIGURE 31b DRAG COEFFICIENT VS. SIDESLIP ANGLE, AIRBLEED STRUT, ATMOSPHERIC, WITH FENCES, ALL HOLES, PORT SIDE, 10, 25, 30, 35, 40, 45, 50 KTS.

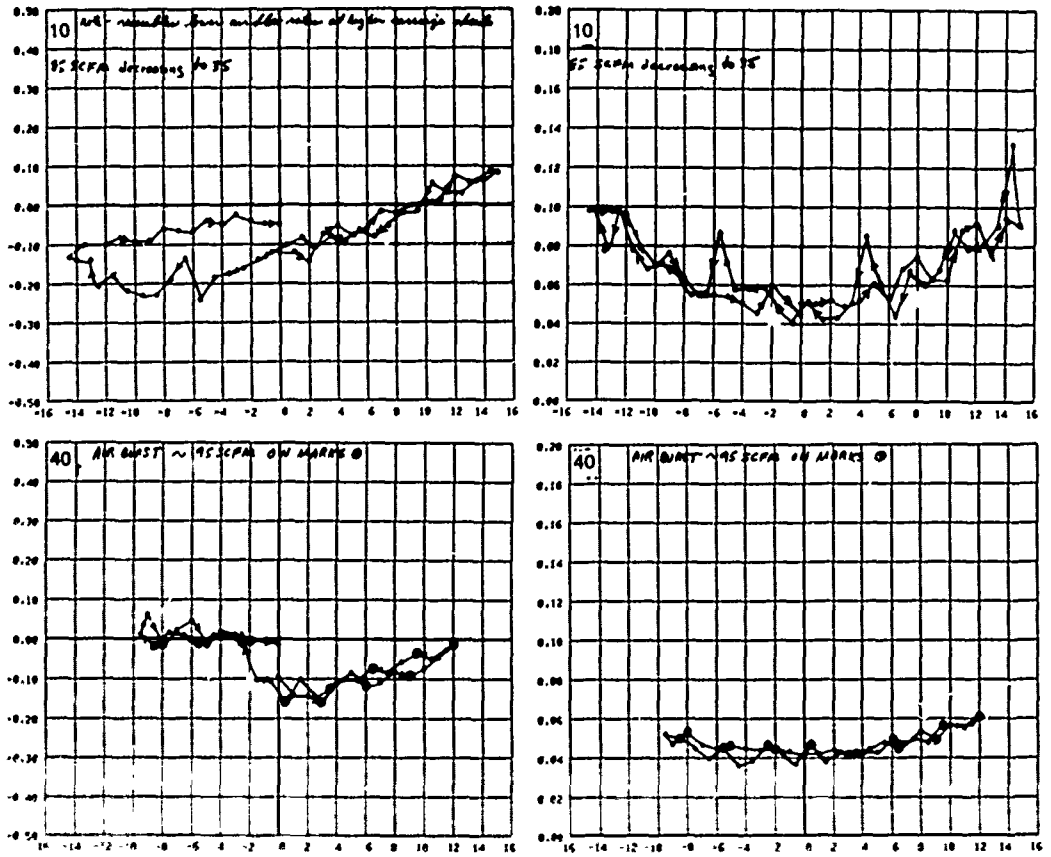

Figure 32 Max Air Runs — All Holes Open on Port Side — Fences on
Upper — Lift & Drag Coefficient vs. Sideslip Angle. Air Flow Started at ~85 SCFM at Beginning of Run, Decreasing to 35 SCFM Towards End of Run
Lower — Lift & Drag Coefficient vs. Sideslip Angle Burst of Air at ~95 SCFM During Data Collection Where Indicated by O Circle Around Graph Points, 10 & 40 kts.

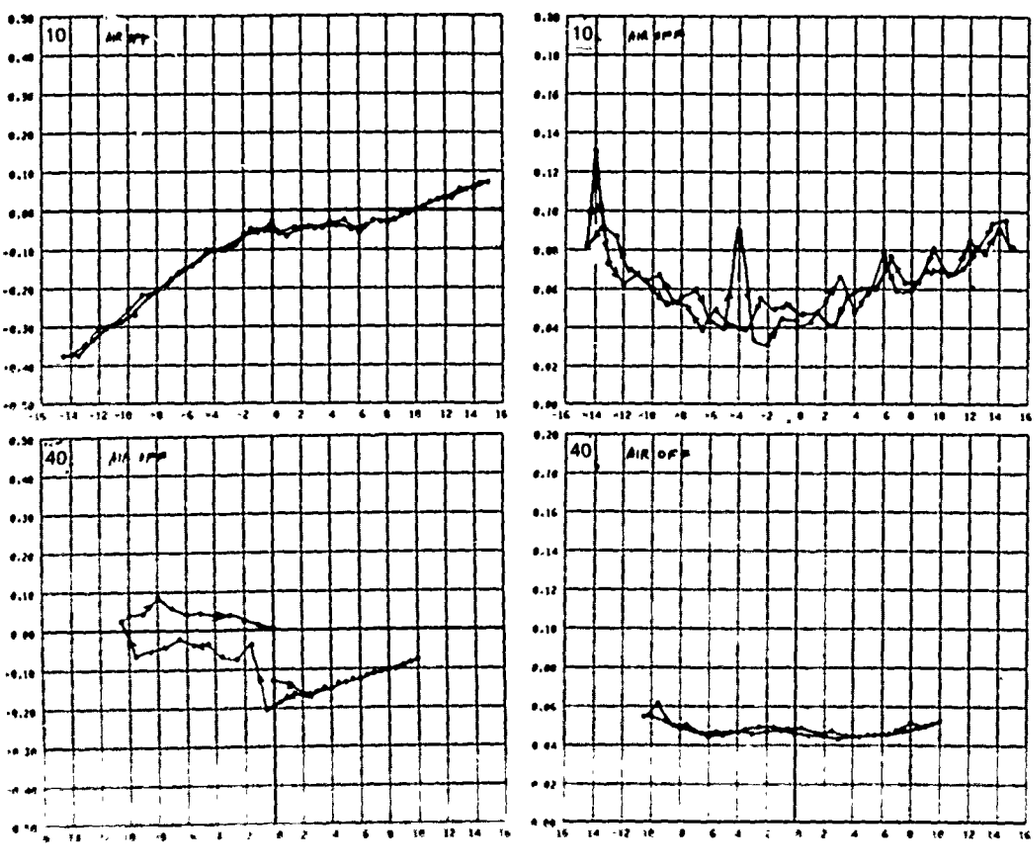

Figure 33 Air Off Runs — Lift and Drag Coefficient vs. Sideslip Angle with Air Flow Shut Off at Supply. Holes in Strut All Open, Port Side, Fences On, 10 & 40 kts.

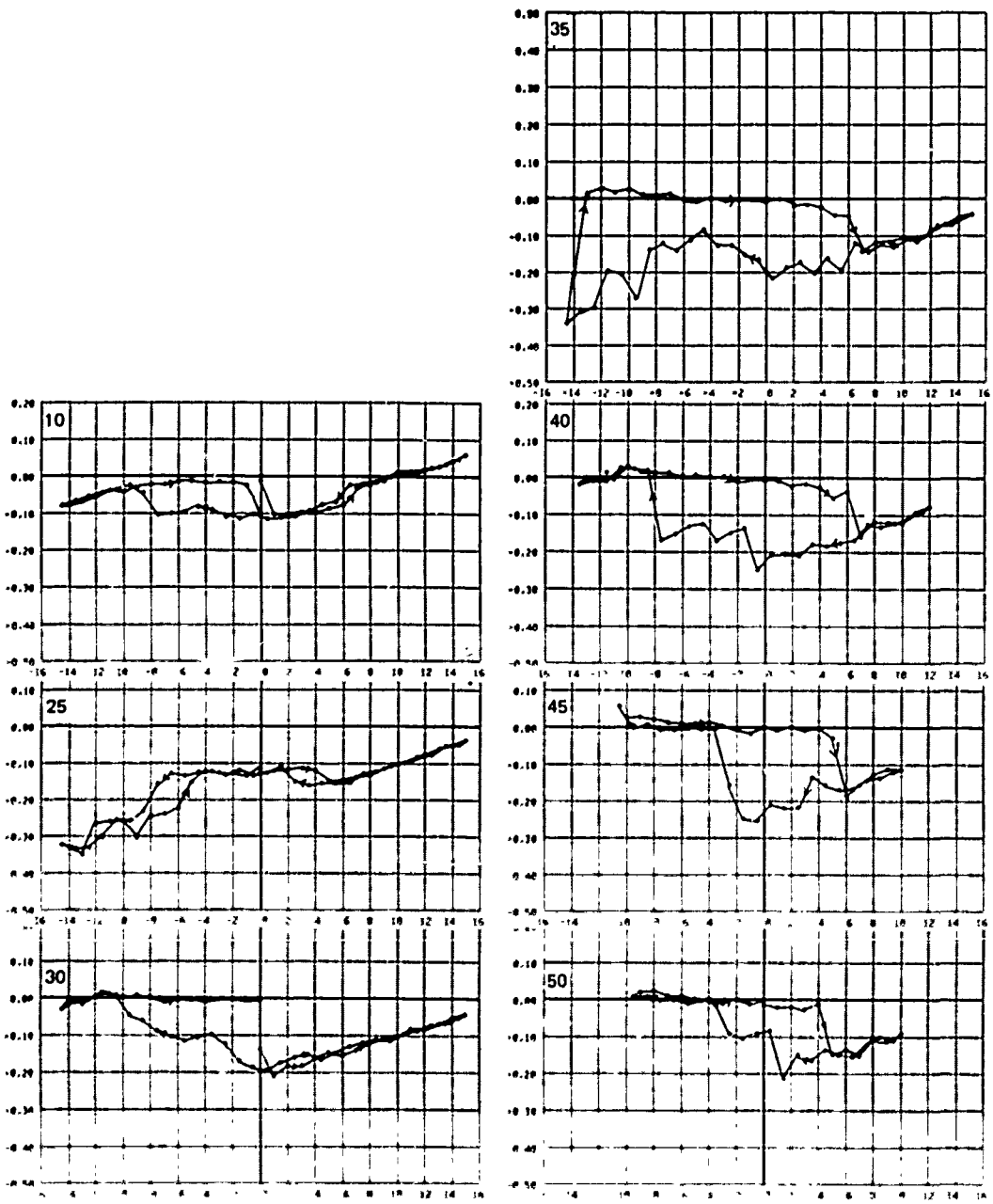

FIGURE 34a SIDEFORCE COEFFICIENT VS. SIDESLIP ANGLE, AIRBLEED STRUT, 20 SCFM (9.4 X 10^{-3} m^3 / s), WITHOUT FENCES, LEADING EDGE HOLES, PORT SIDE, 0, 10, 25, 30, 35, 40, 45, 50 KTS.

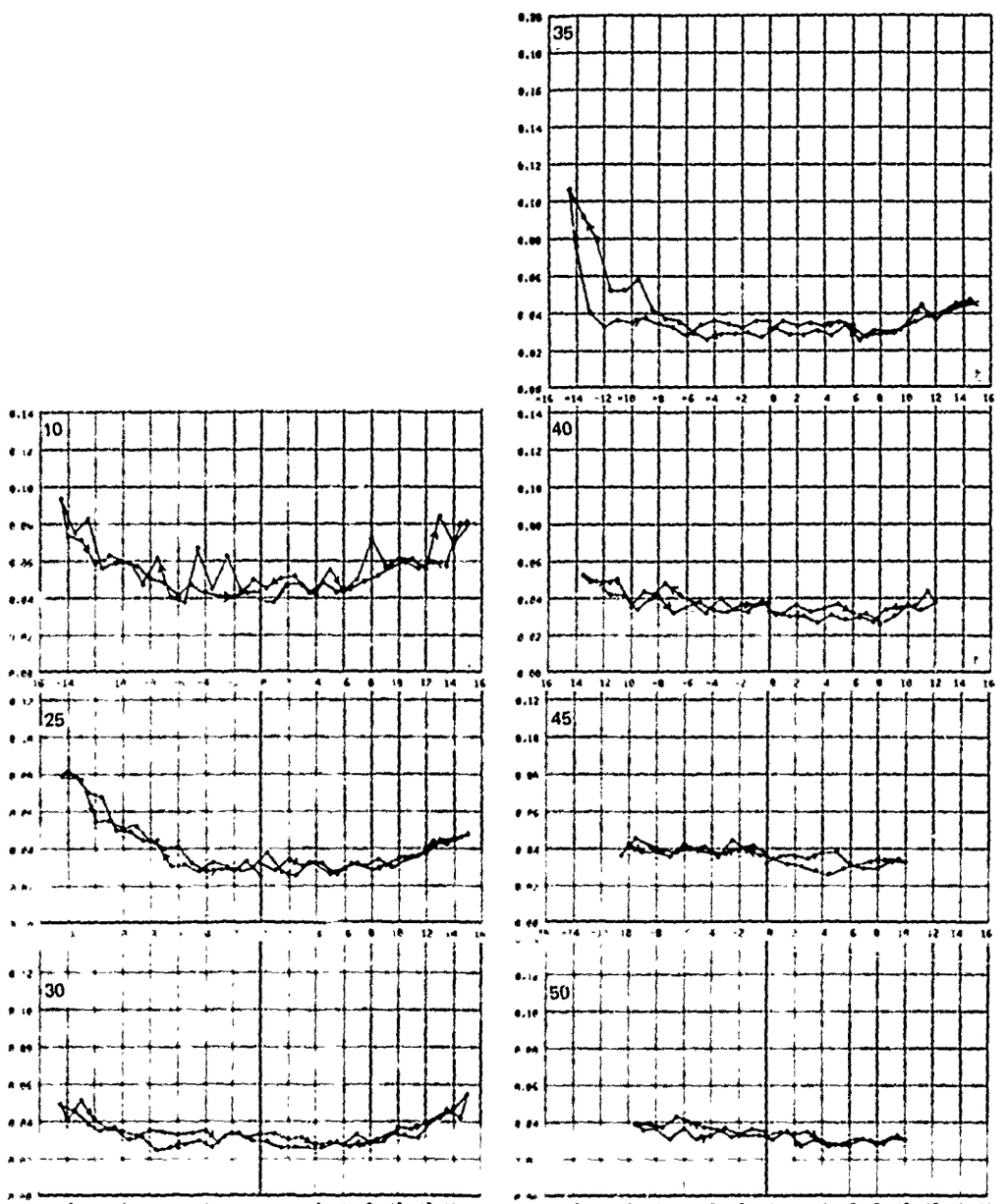

FIGURE 34b DRAG COEFFICIENT VS. SIDESLIP ANGLE, AIRBLEED STRUT, 20 SCFM (9.4 X $10^{-3}m^3/s$), WITHOUT FENCES, LEADING EDGE HOLES, PORT SIDE, 0, 10, 25, 30, 35, 40, 45, 50 KTS.

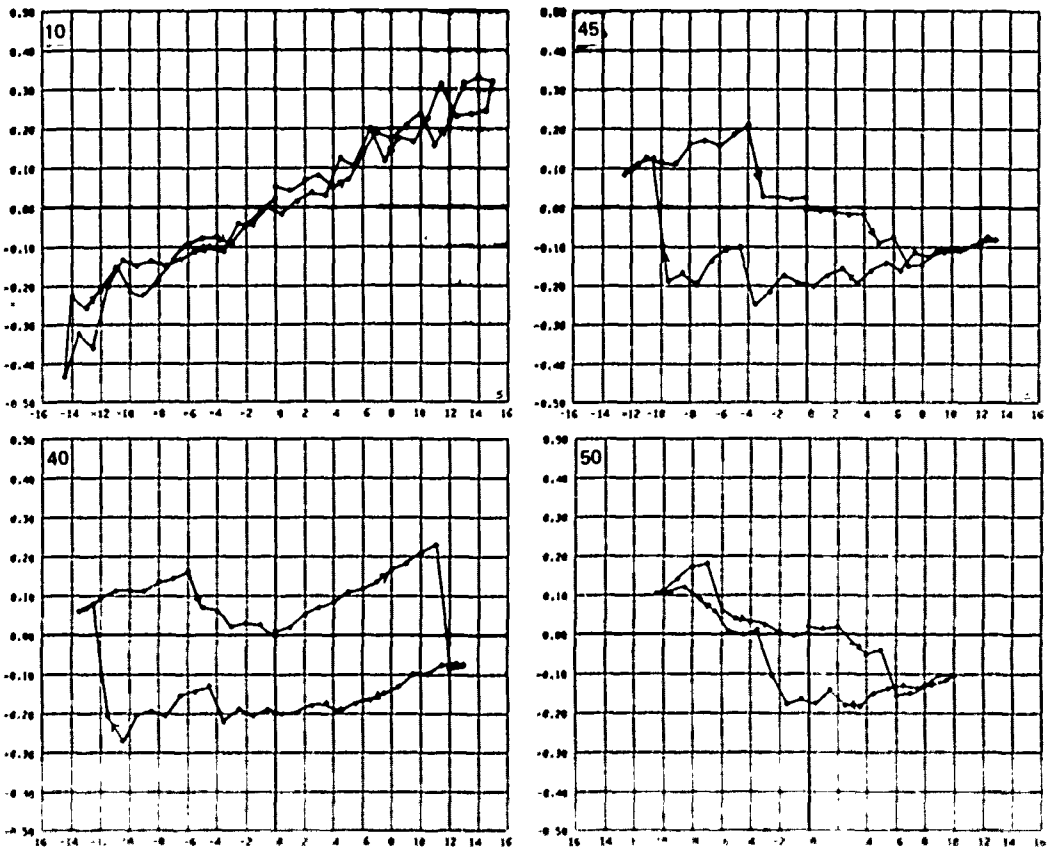

FIGURE 35a SIDEFORCE COEFFICIENT VS. SIDESLIP ANGLE, AIRBLEED STRUT, ATMOSPHERIC, WITHOUT FENCES, LEADING EDGE HOLES, PORT SIDE, 10, 40, 45, 50 KTS.

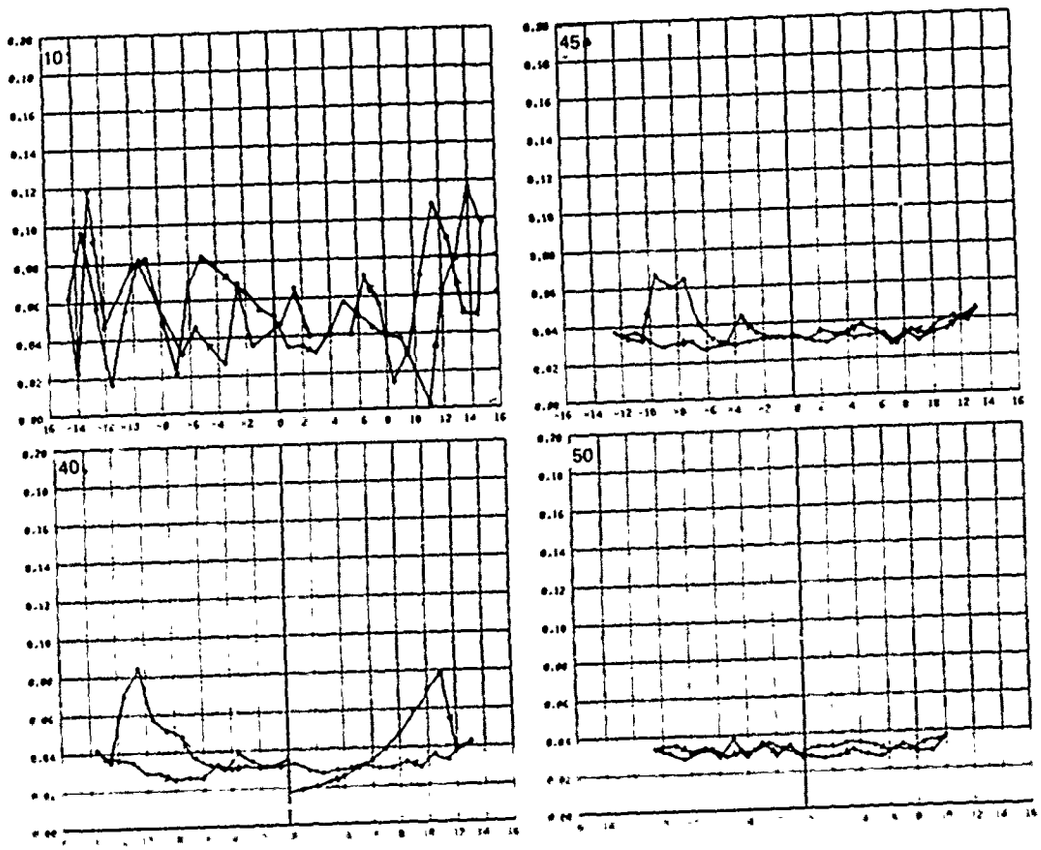

FIGURE 35b DRAG COEFFICIENT VS. SIDESLIP ANGLE, AIRBLEED STRUT, ATMOSPHERIC, WITHOUT FENCES, LEADING EDGE HOLES, PORT SIDE, 10, 40, 45, 50 KTS.

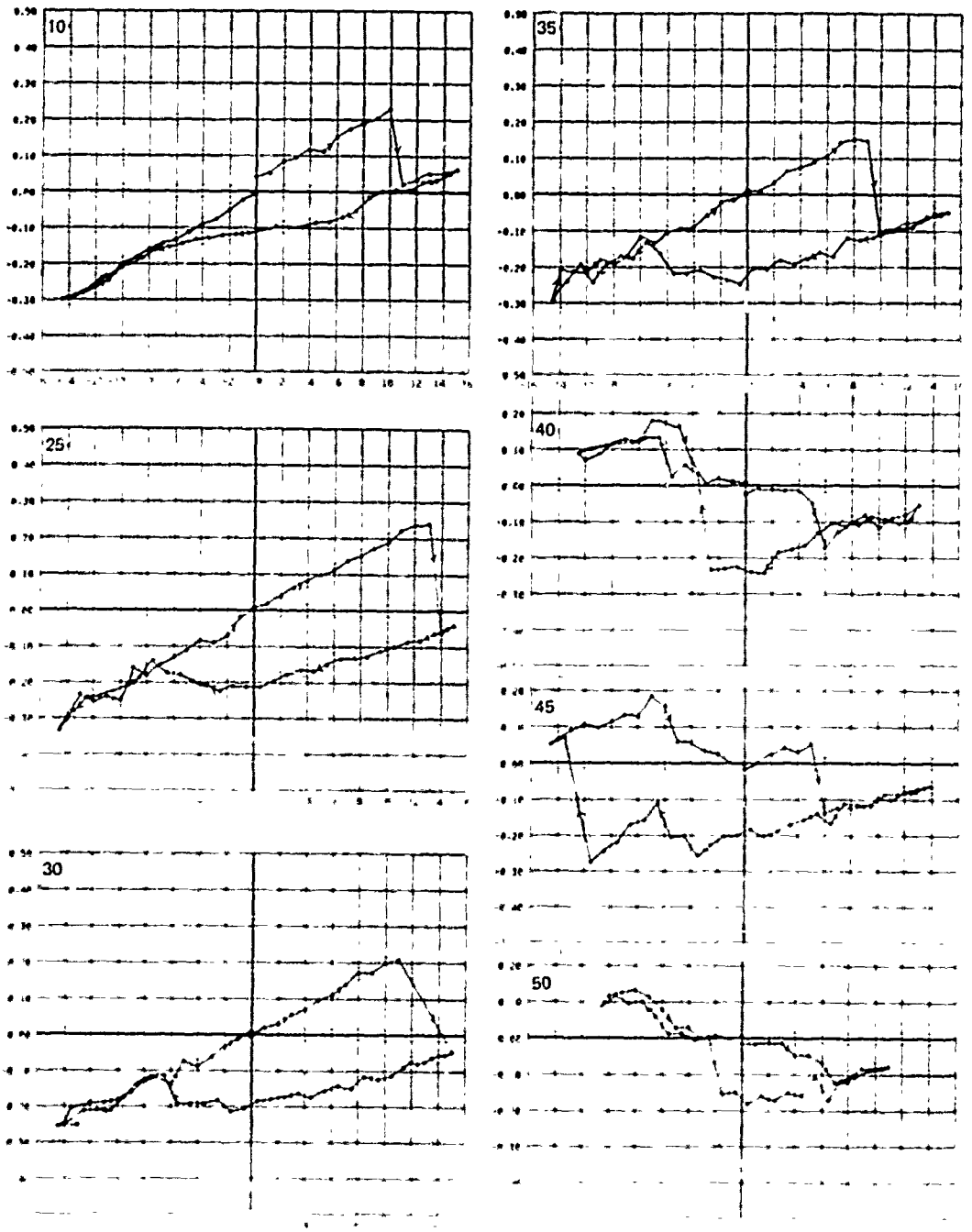

FIGURE 36a SIDEFORCE COEFFICIENT VS. SIDESLIP ANGLE, AIRBLEED STRUT, ATMOSPHERIC, WITHOUT FENCES, LEADING EDGE HOLES, PORT SIDE, 10, 25, 30, 35, 40, 45, 50 KTS.

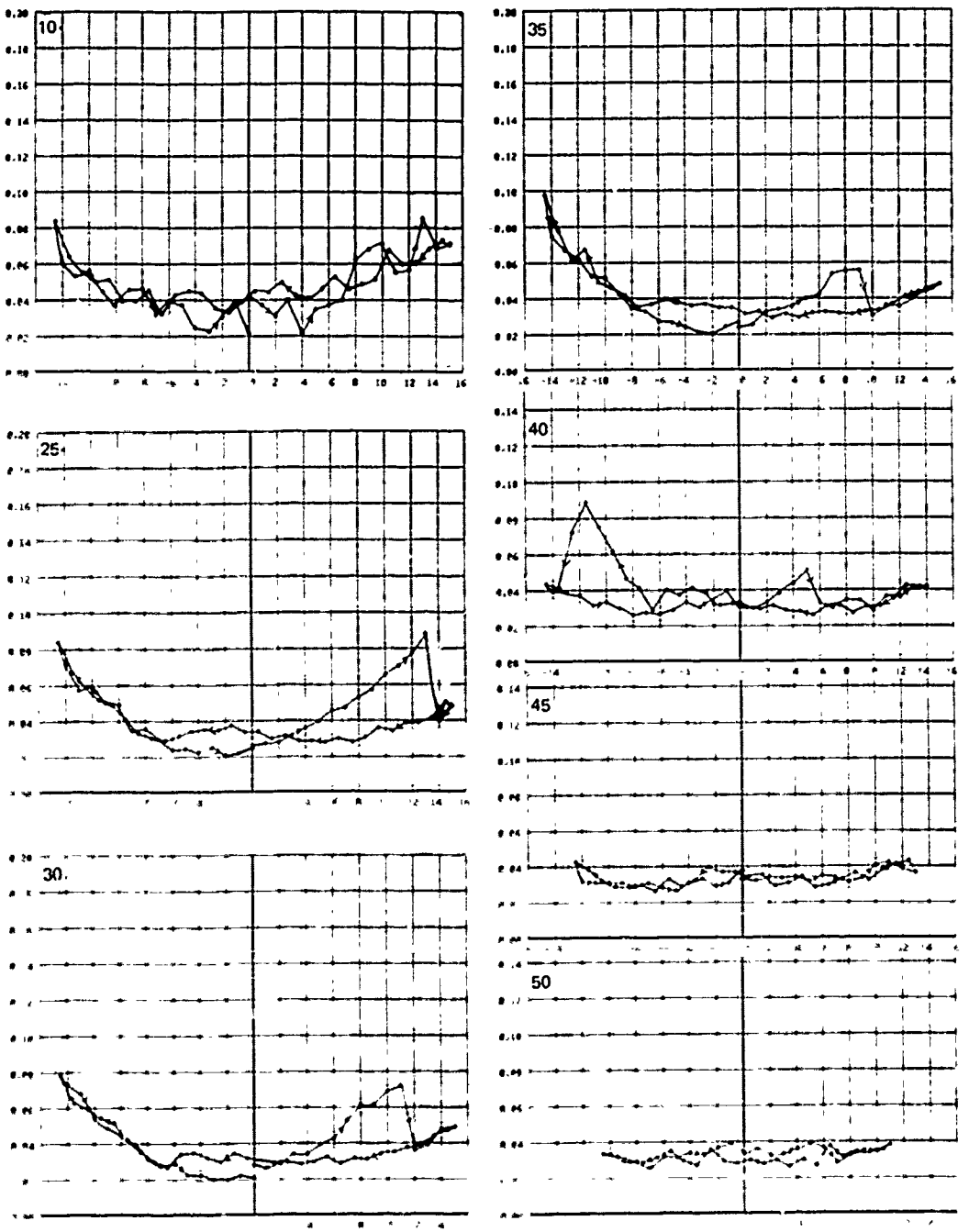

FIGURE 36b DRAG COEFFICIENT VS. SIDESLIP ANGLE, AIRBLEED STRUT, ATMOSPHERIC, WITHOUT FENCES, LEADING EDGE HOLES, PORT SIDE, 10, 25, 30, 35, 40, 45, 50 KTS

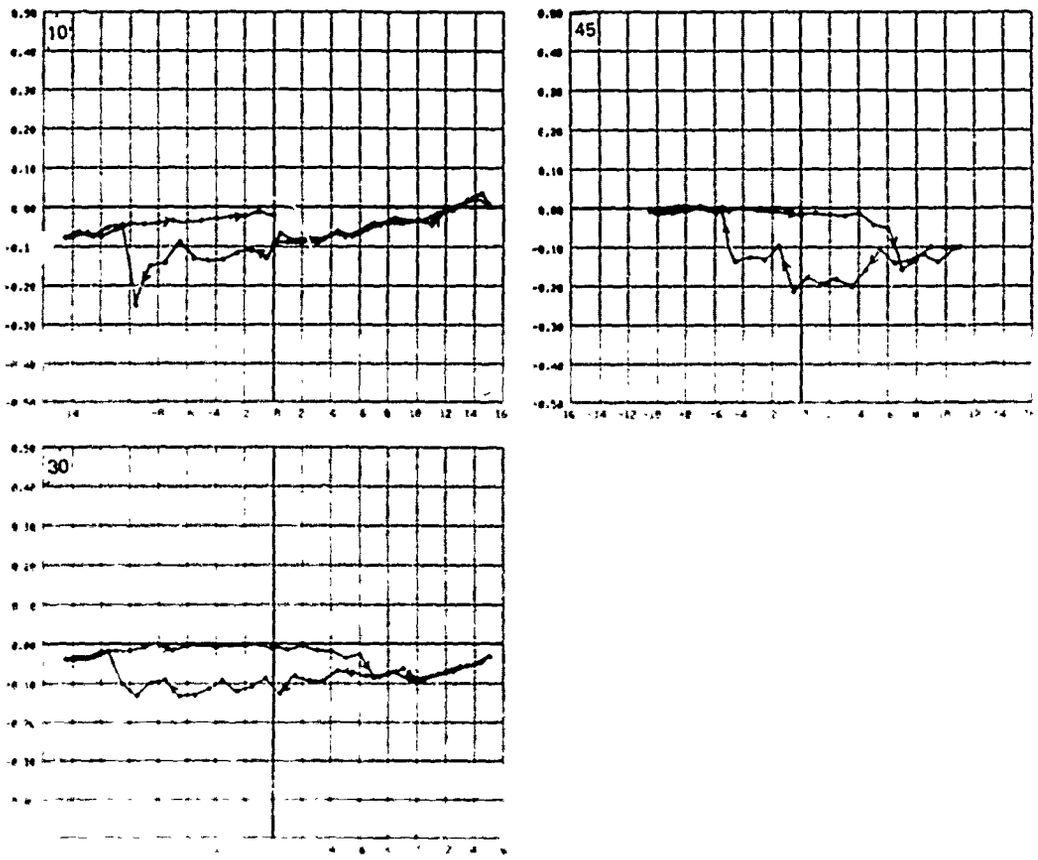

FIGURE 37a SIDEFORCE COEFFICIENT VS. SIDESLIP ANGLE, AIRBLEED STRUT, 35 SCFM (16.5 X 10^{-4} m^3/s), WITHOUT FENCES, 10% C HOLES, PORT SIDE, 10, 30, 45 KTS.

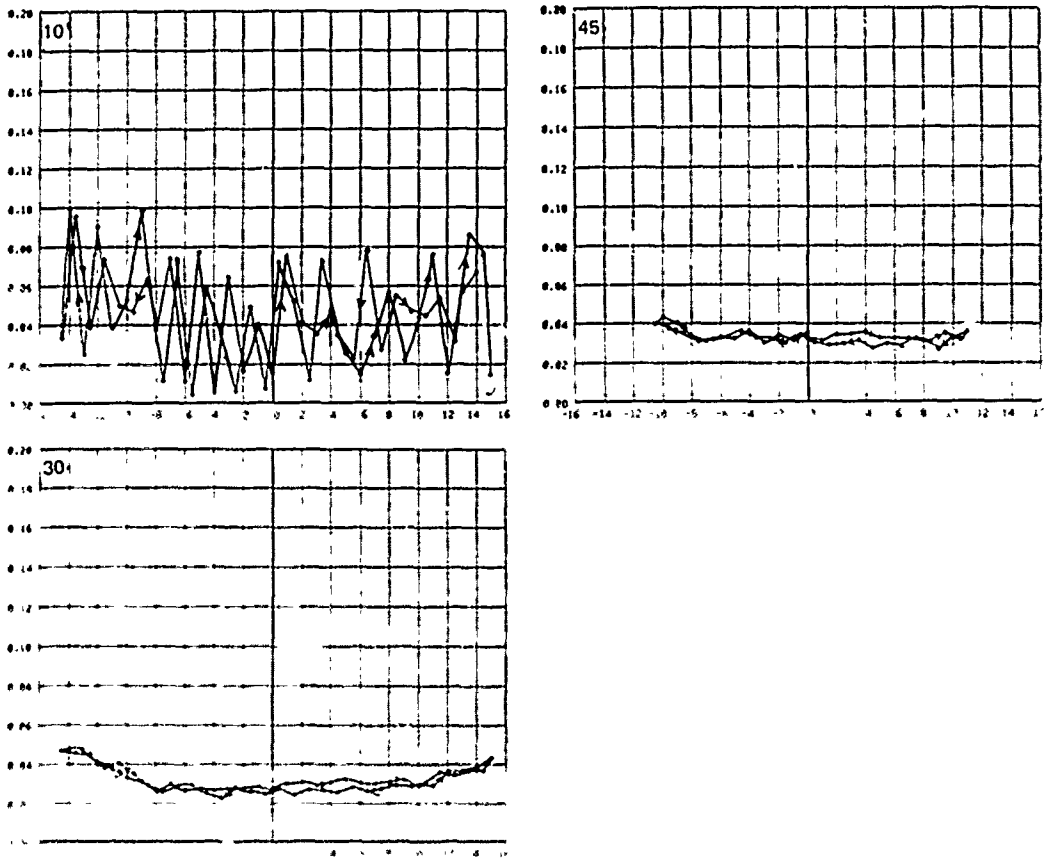

FIGURE 37b DRAG COEFFICIENT VS. SIDESLIP ANGLE, AIRBLEED STRUT, 35 SCFM (16.5 X 10^{-3} m^3/s), WITHOUT FENCES, 10% C HOLES, PORT SIDE, 10, 30, 45 KTS.

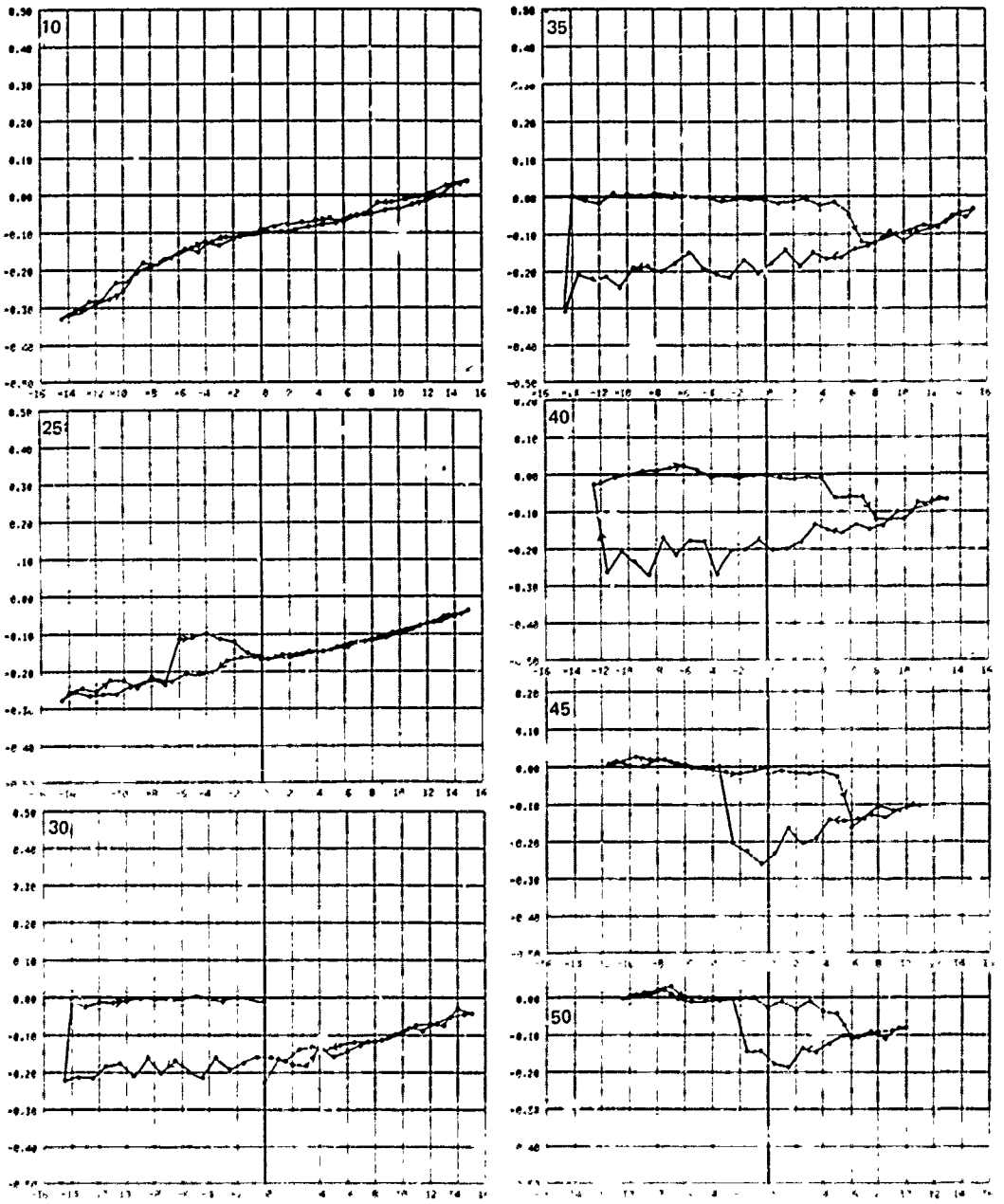

FIGURE 38a SIDEFORCE COEFFICIENT VS. SIDESLIP ANGLE, AIRBLEED STRUT 20 SCFM (9.4 X $10^{-3}m^3/s$), WITHOUT FENCES, 10% C HOLES, PORT SIDE, 10, 25, 30, 35, 40, 45, 50 KTS.

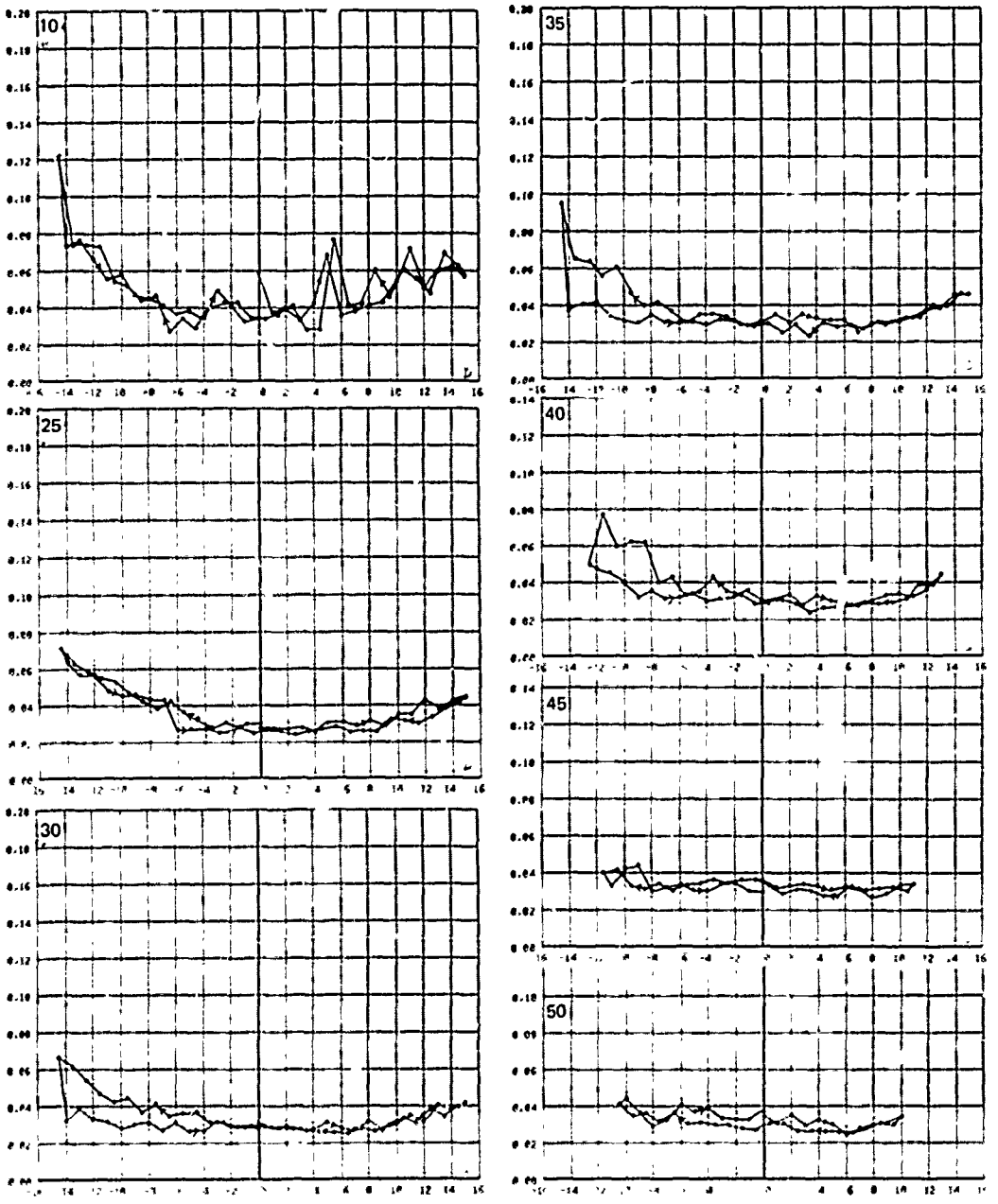

FIGURE 38b DRAG COEFFICIENT VS. SIDESLIP ANGLE, AIRBLEED STRUT, 20 SCFM (9.4 X 10^{-3} m^3/s), WITHOUT FENCES, 10% C HOLES, PORT SIDE, 10, 25, 30, 35, 40, 45, 50 KTS.

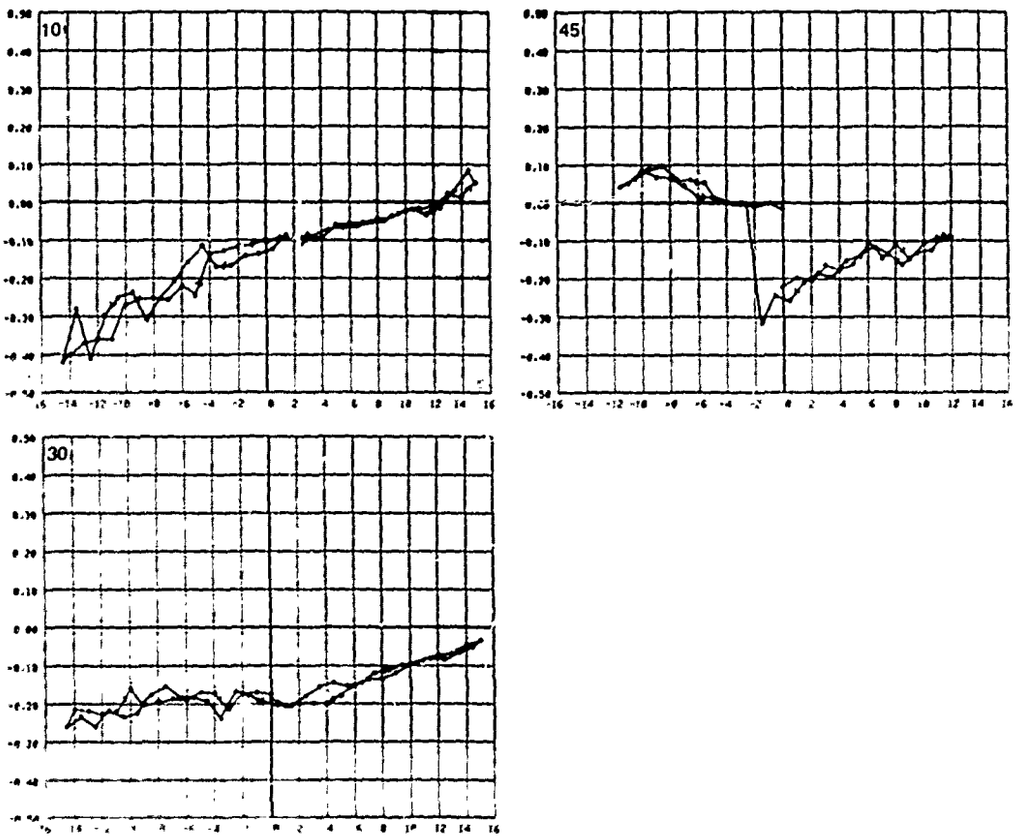

FIGURE 39a SIDEFORCE COEFFICIENT VS. SIDESLIP ANGLE, AIRBLEED STRUT, 10 SCFM (4.7 X $10^{-3}m^3/s$), WITHOUT FENCES, 10% C HOLES, PORT SIDE, 10, 30, 45 KTS.

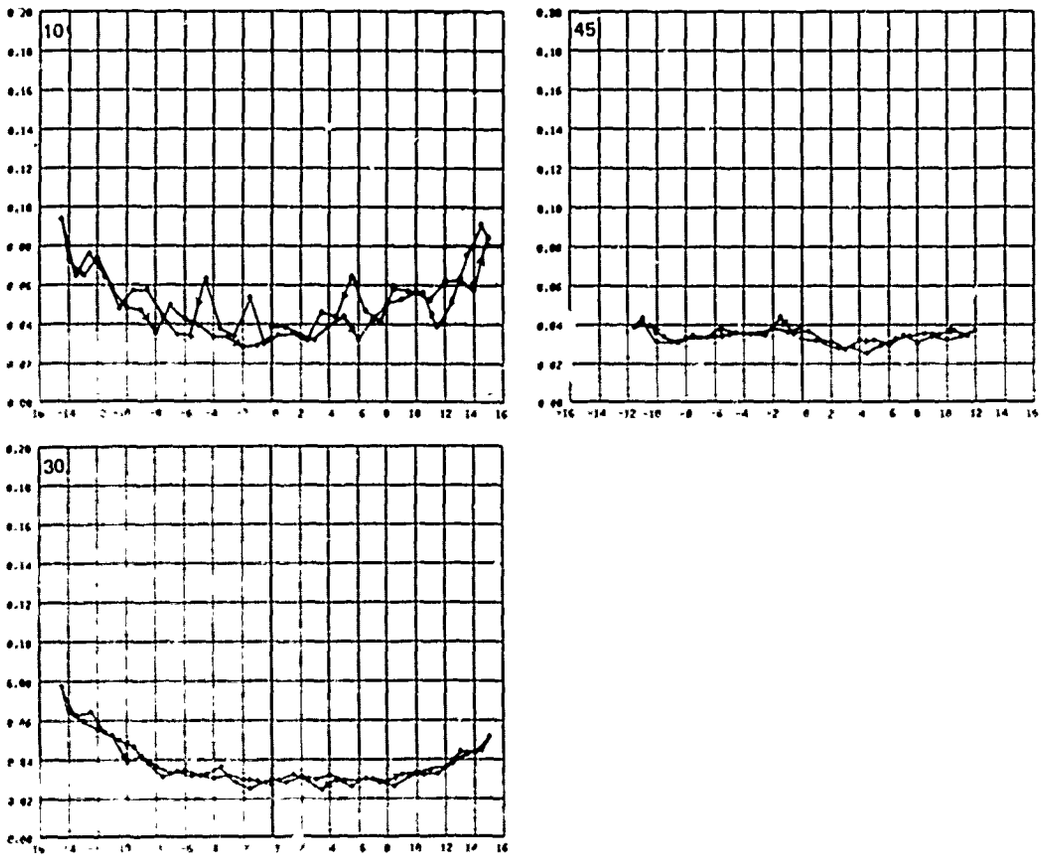

FIGURE 39b DRAG COEFFICIENT VS. SIDESLIP ANGLE, AIRBLEED STRUT, 10 SCFM (4.7 X 10^{-3} m^3/s), WITHOUT FENCES, 10% C HOLES, PORT SIDE, 10, 30, 45 KTS.

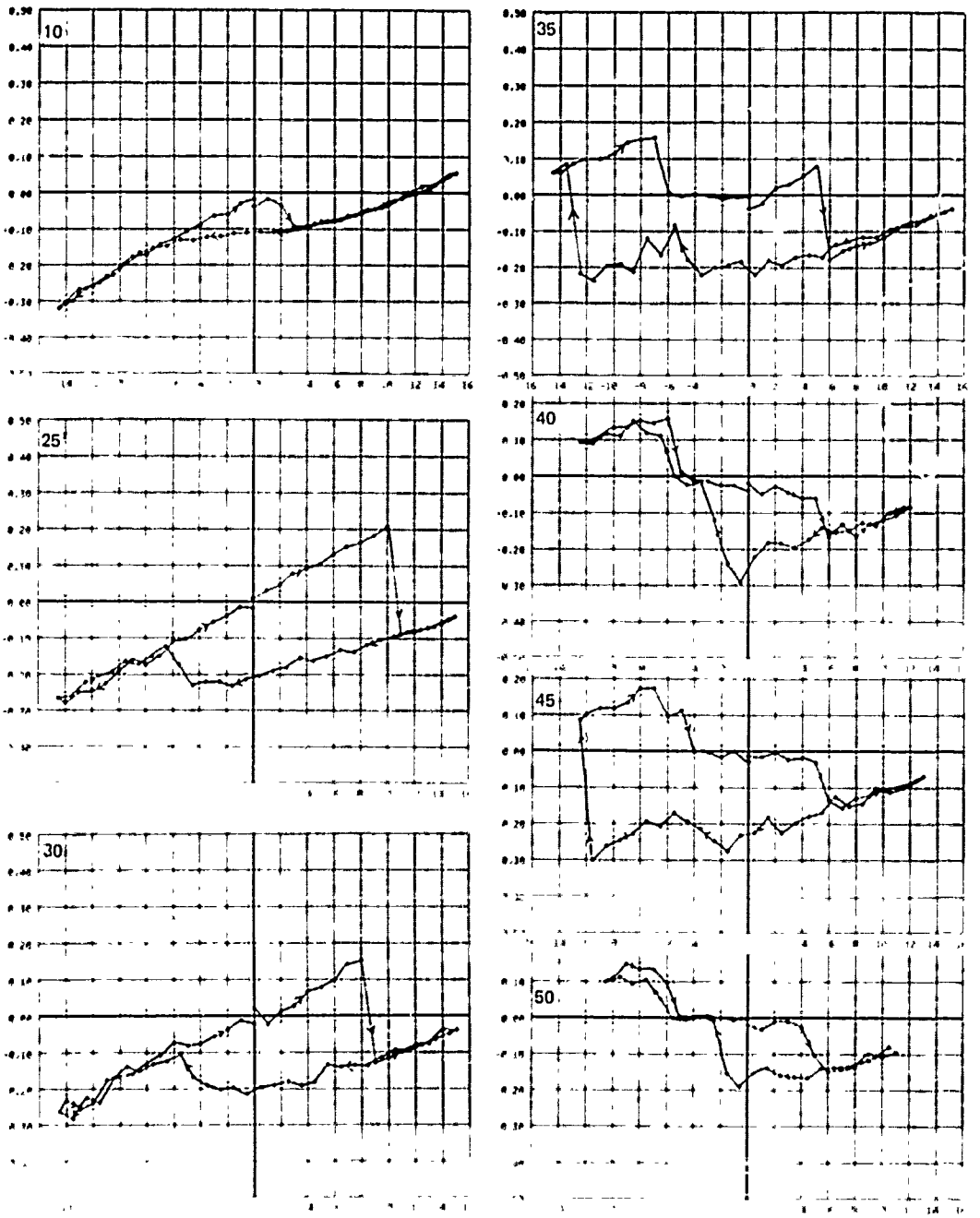

FIGURE 40a SIDEFORCE COEFFICIENT VS. SIDESLIP ANGLE, AIRBLEED STRUT, ATMOSPHERIC, WITHOUT FENCES, 10% C HOLES, PORT SIDE, 10, 25, 30, 35, 40, 45, 50 KTS.

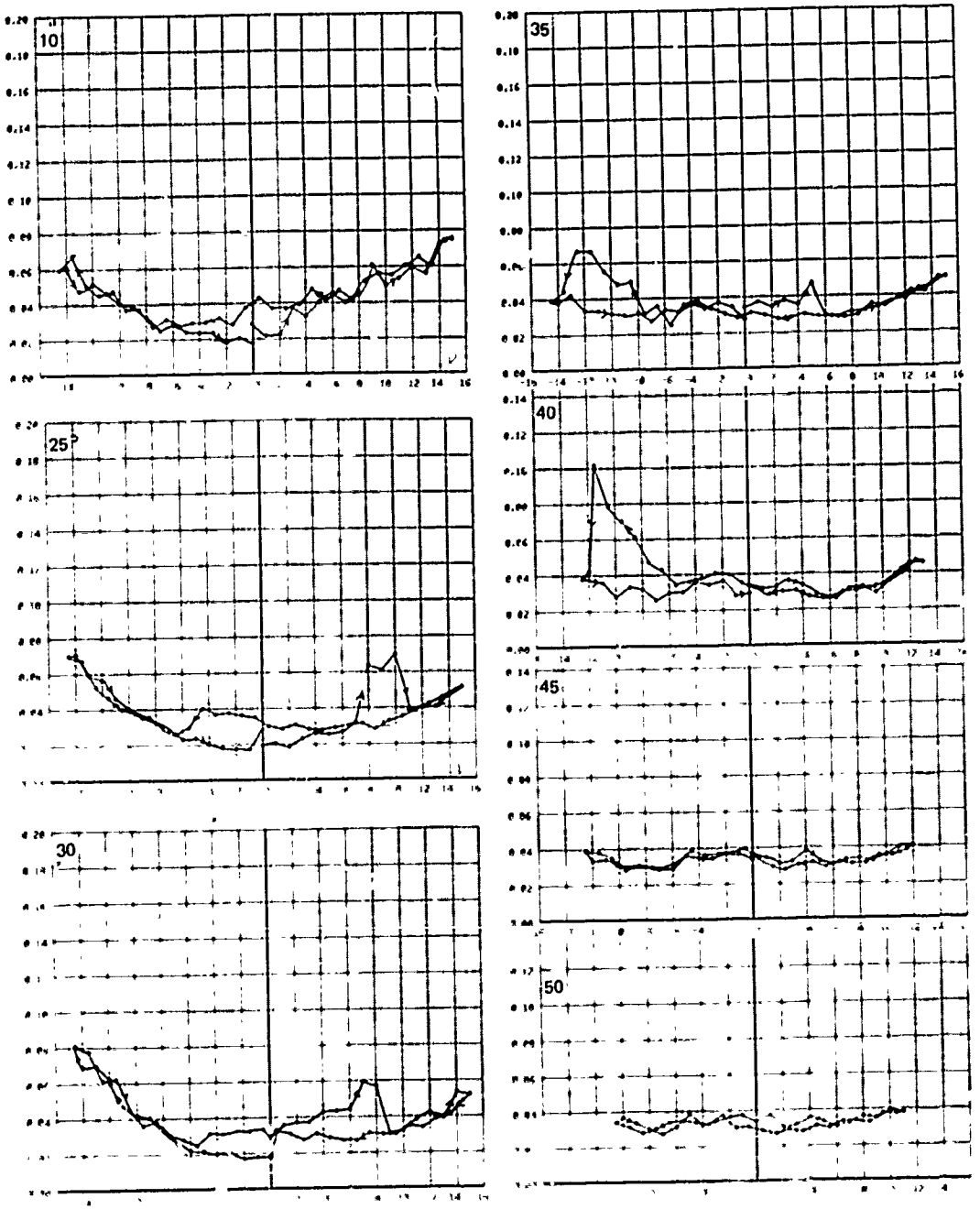

FIGURE 40b DRAG COEFFICIENT VS. SIDESLIP ANGLE, AIRBLEED STRUT, ATMOSPHERIC, WITHOUT FENCES, 10% C HOLES, PORT SIDE, 10, 25, 30, 35, 40, 45, 50 KTS.

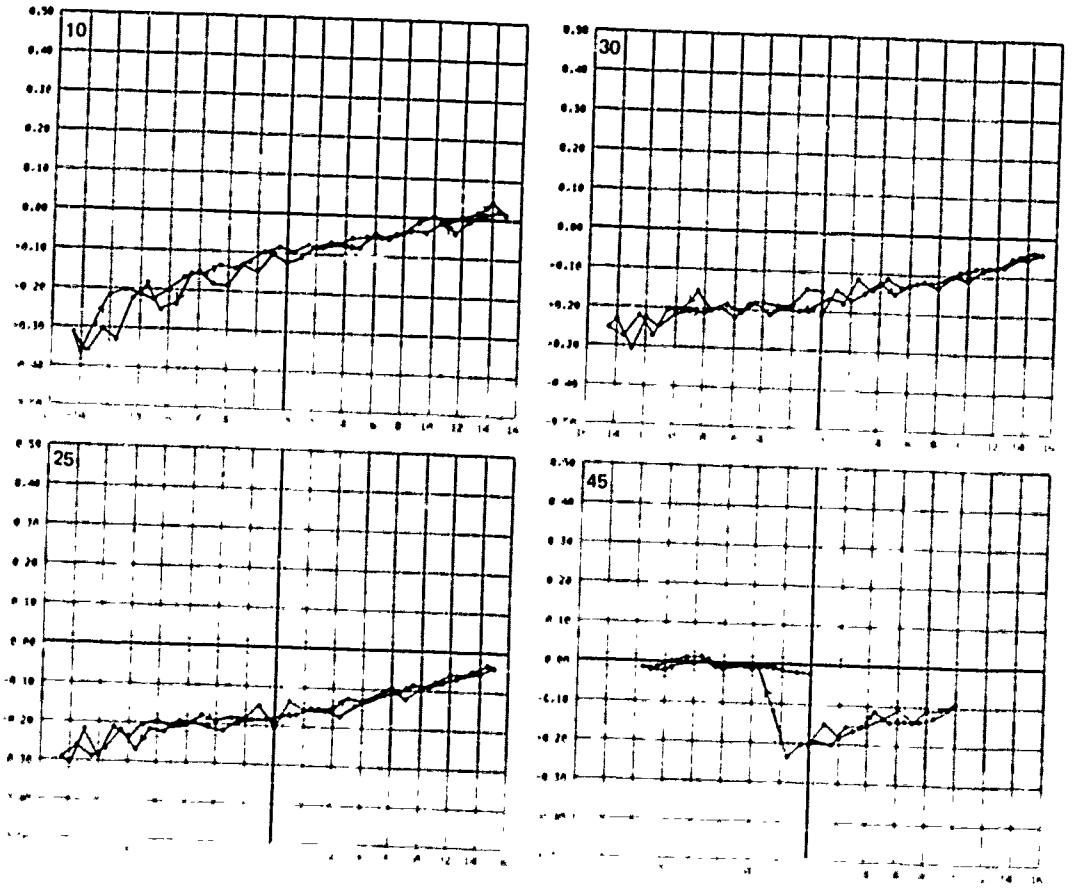

FIGURE 41a SIDEFORCE COEFFICIENT VS. SIDESLIP ANGLE, AIRBLEED STRUT, 20 SCFM (9.4 X $10^{-3}m^3/s$), WITHOUT FENCES, 25% C HOLES, PORT SIDE, 10, 25, 30, 45 KTS.

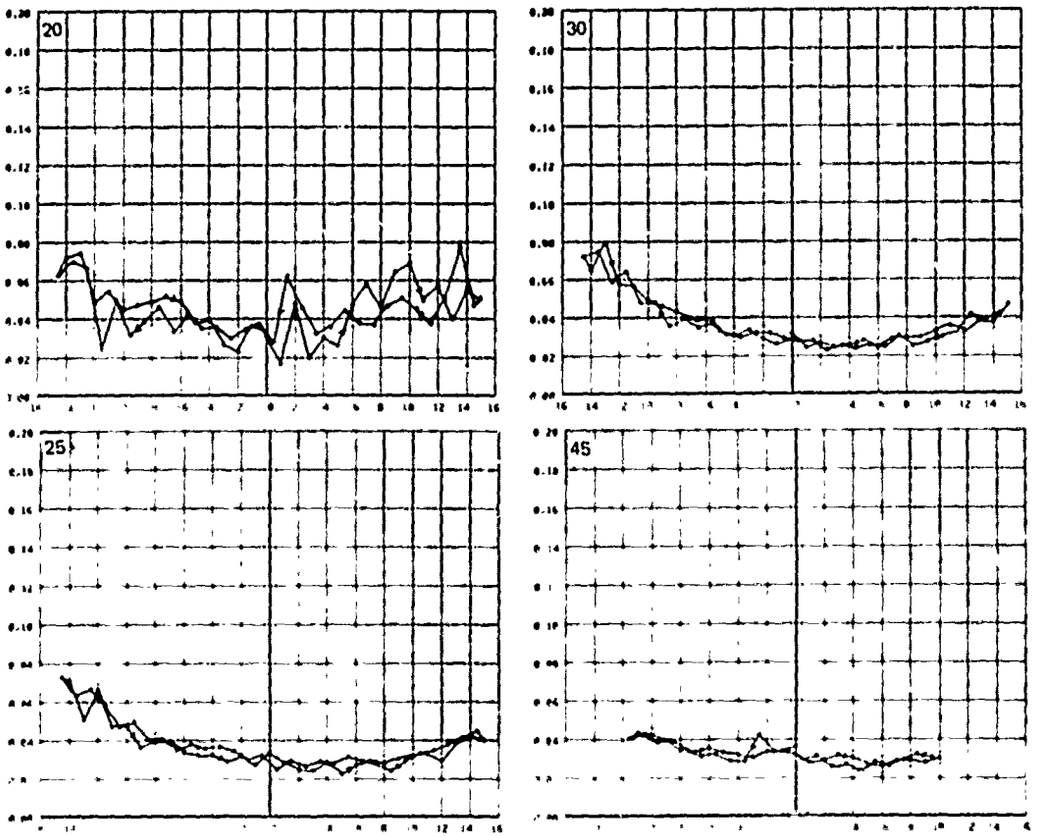

FIGURE 41b DRAG COEFFICIENT VS. SIDESLIP ANGLE, AIRBLEED STRUT, 20 SCFM (9.4 X $10^{-3}m^3/s$), WITHOUT FENCES, 25% C HOLES, PORT SIDE, 10, 25, 30, 45 KTS.

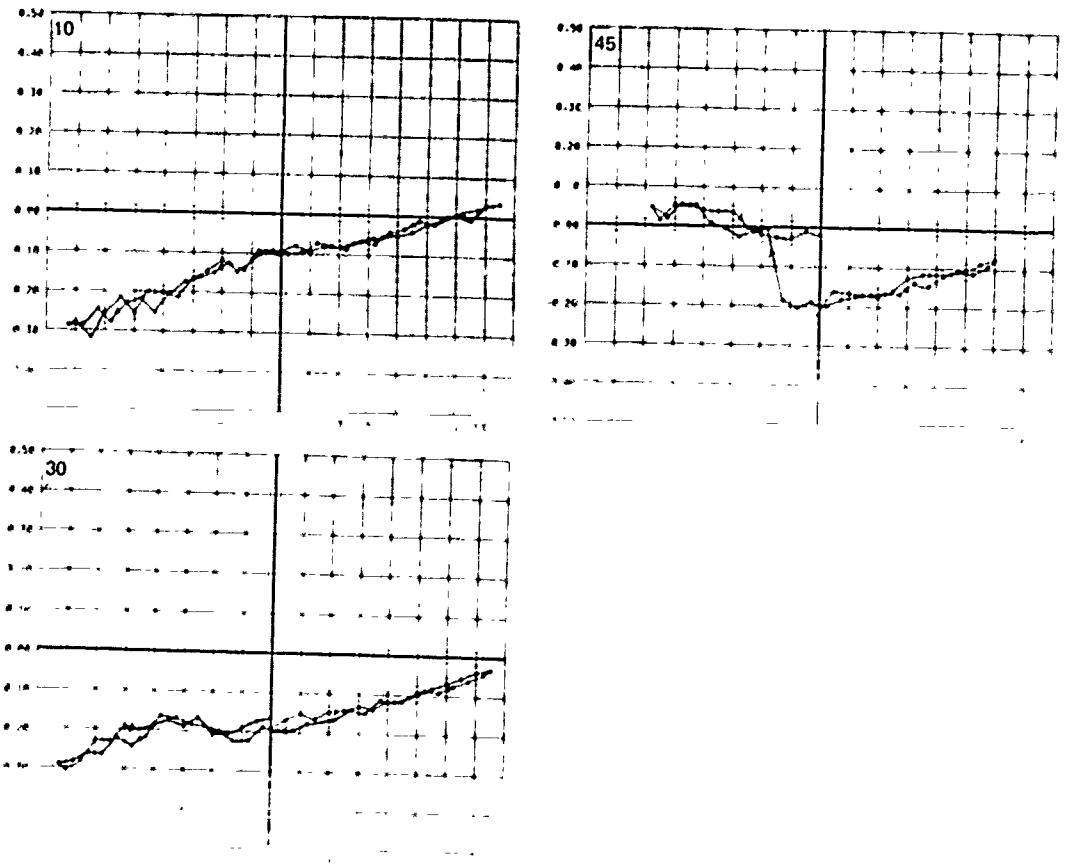

FIGURE 42a SIDEFORCE COEFFICIENT VS. SIDESLIP ANGLE, AIRBLEED STRUT, 10 SCFM (4.7 X 10^{-3} m^3/s), WITHOUT FENCES, 25% C HOLES, PORT SIDE, 10, 30, 45 KTS.

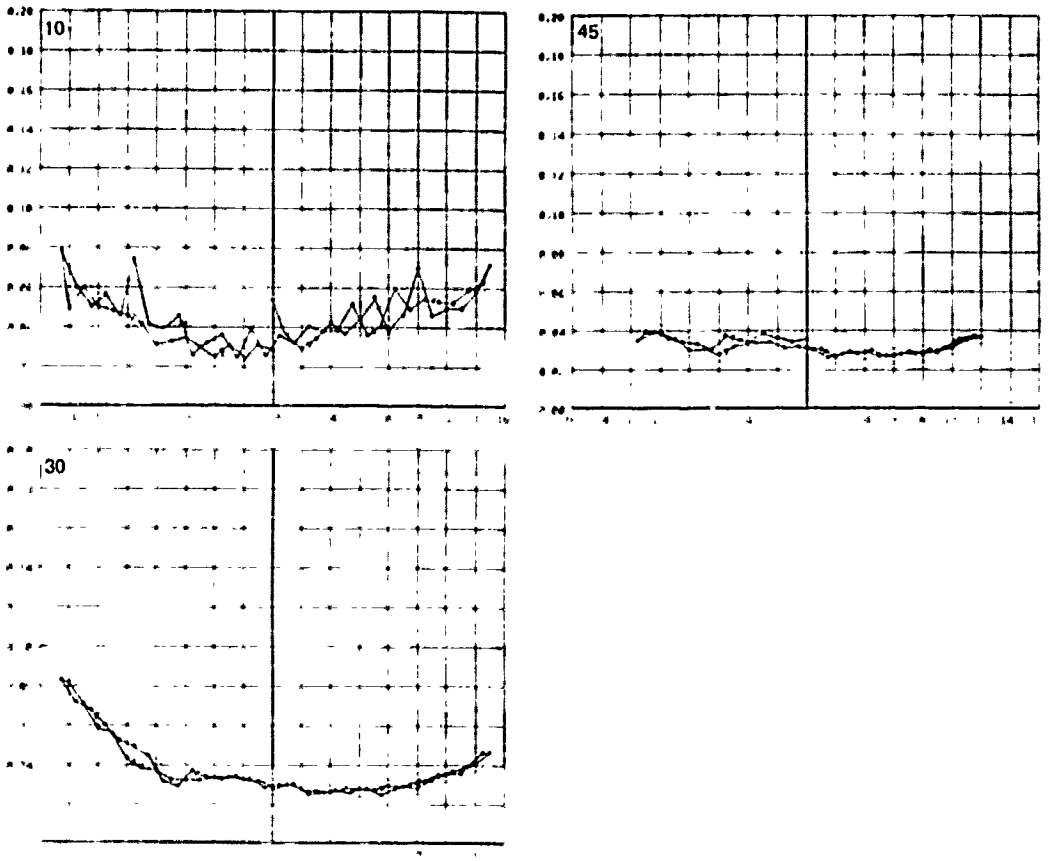

FIGURE 42b DRAG COEFFICIENT VS. SIDESLIP ANGLE, AIRBLEED STRUT, 10 SCFM (4.7 X $10^{-3}m^3/s$), WITHOUT FENCES, 25% C HOLES, PORT SIDE, 10, 30, 45 KTS.

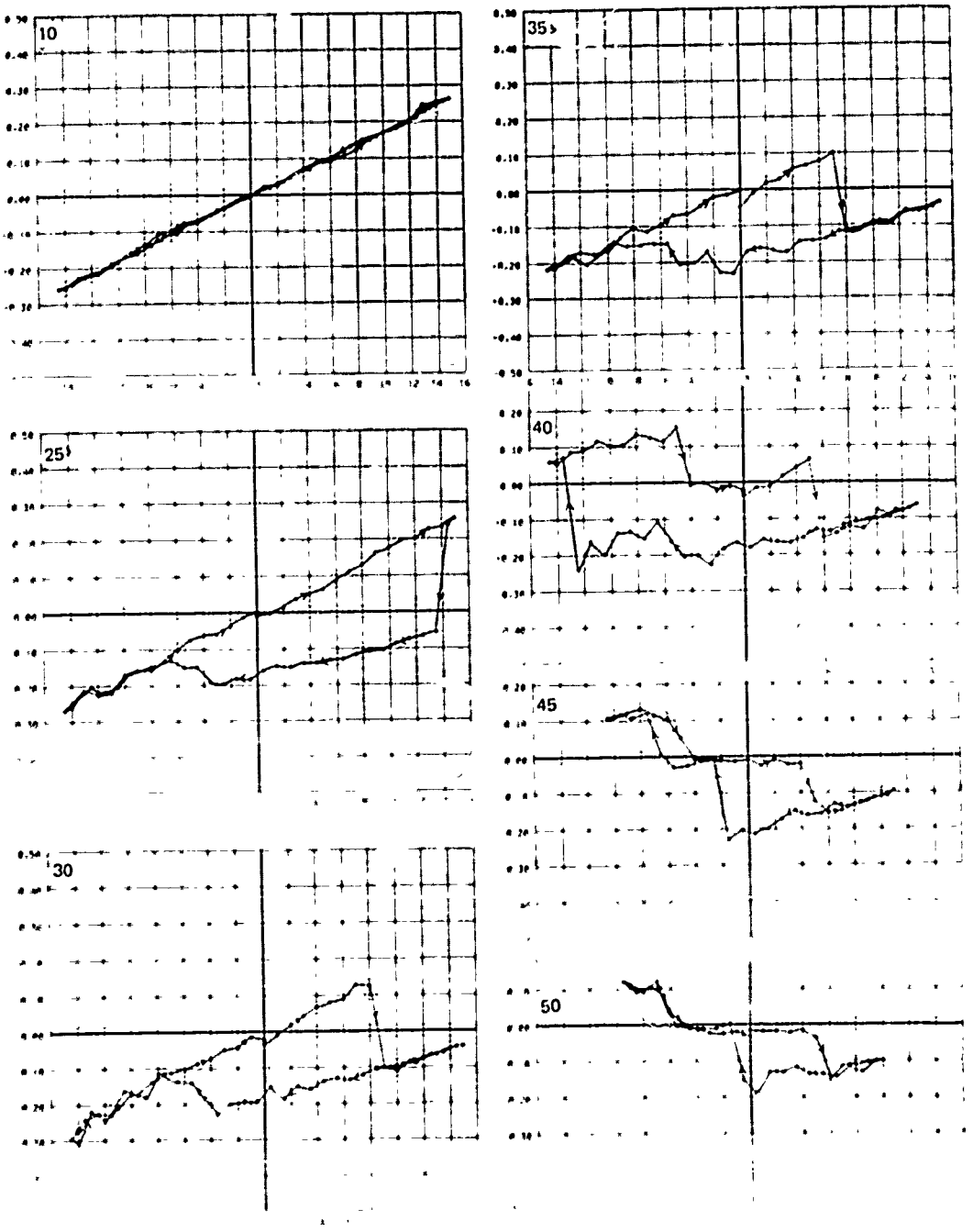

FIGURE 43a SIDEFORCE COEFFICIENT VS. SIDESLIP ANGLE, AIRBLEED STRUT, ATMOSPHERIC, WITHOUT FENCES, 25% C HOLES, PORT SIDE, 10, 25, 30, 35, 40, 45, 50 KTS.

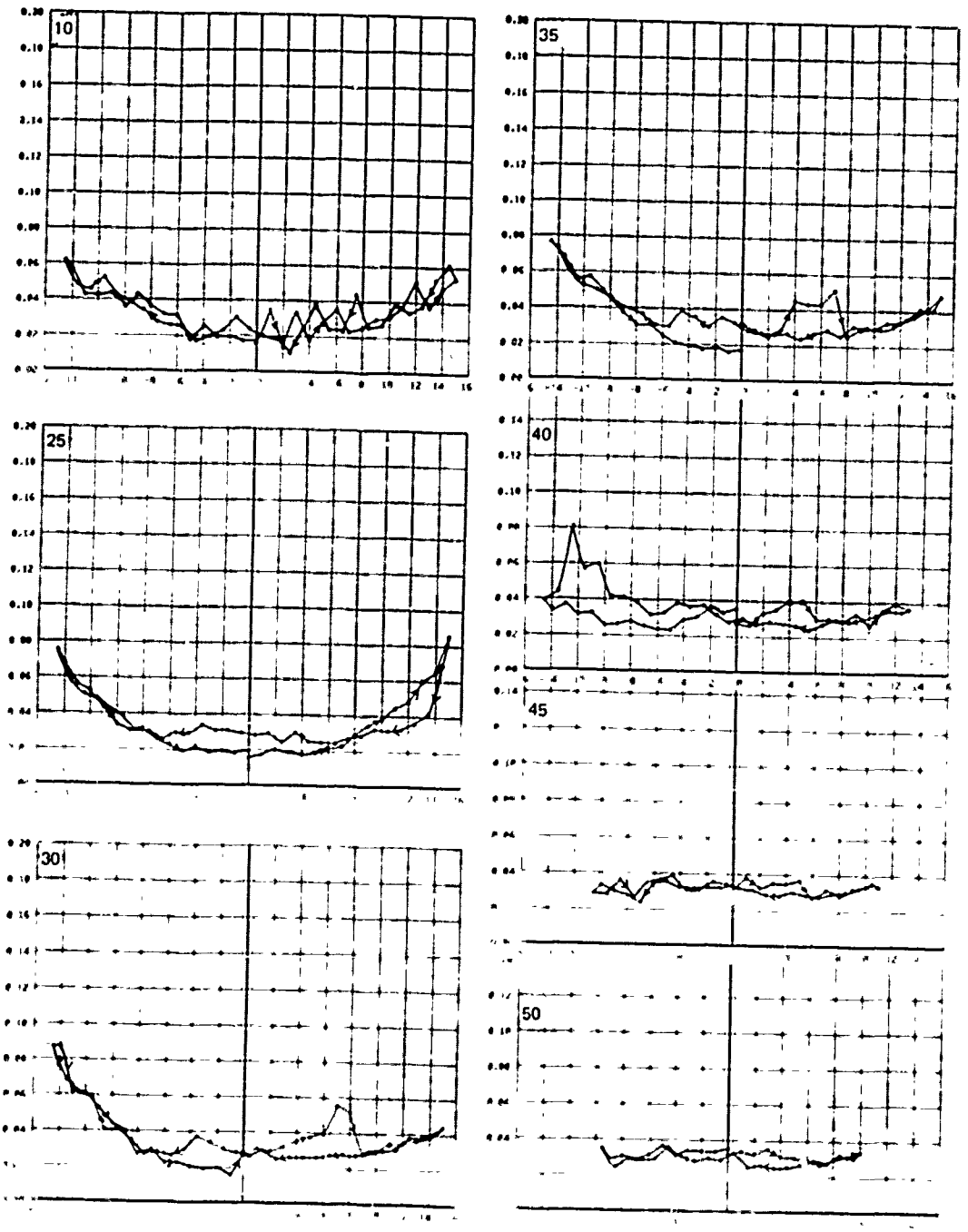

FIGURE 43b DRAG COEFFICIENT VS. SIDESLIP ANGLE, AIRBLEED STRUT, ATMOSPHERIC, WITHOUT FENCES, 25% C HOLES, PORT SIDE, 10, 25, 30, 35, 40, 45, 50 KTS.

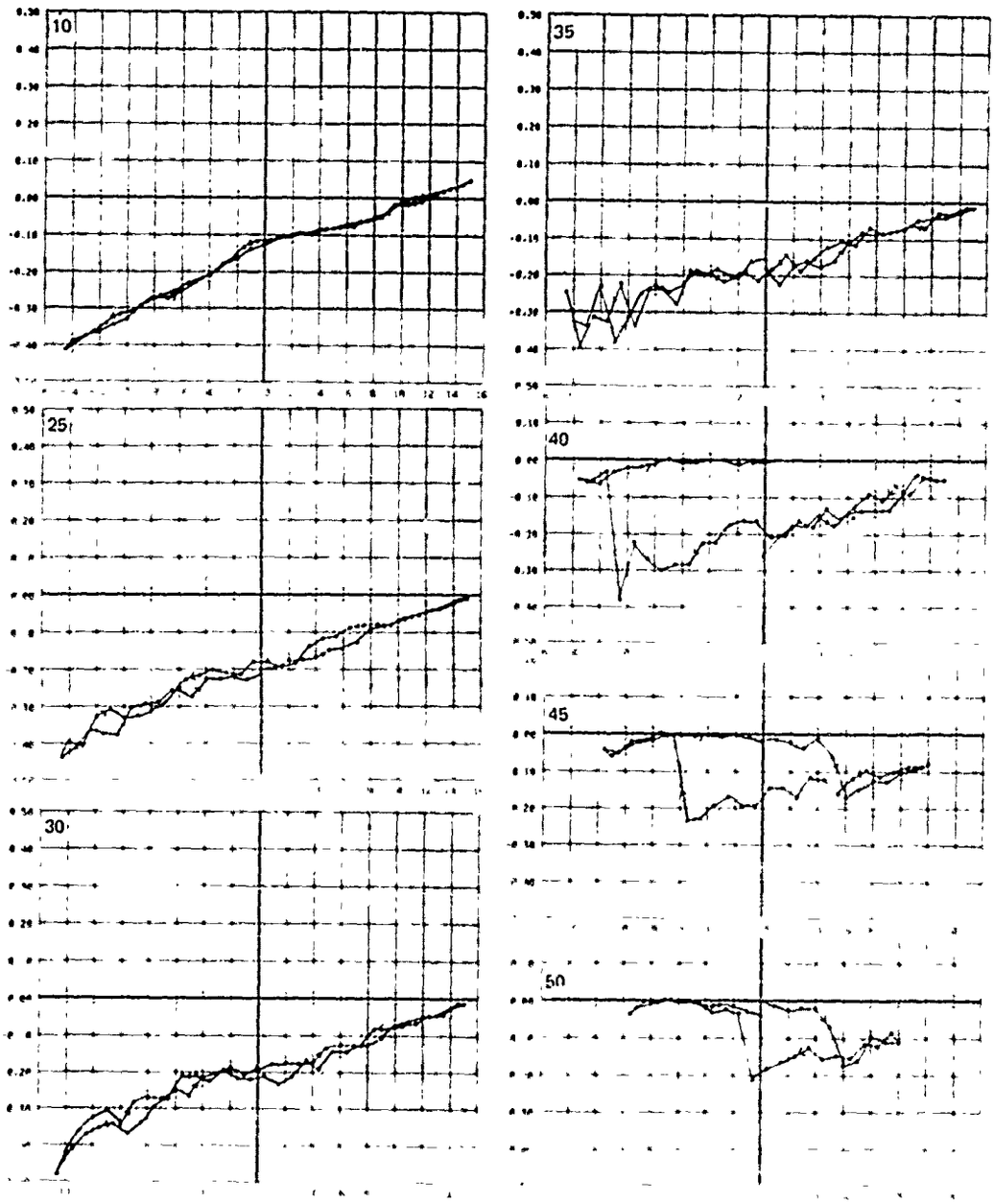

FIGURE 44a SIDEFORCE COEFFICIENT VS. SIDESLIP ANGLE, AIRBLEED STRUT, 20 SCFM (9.4 X 10^{-3} m^3/s), WITHOUT FENCES, MIDCHORD HOLES, PORT SIDE, 10, 25, 30, 35, 40, 45, 50 KTS.

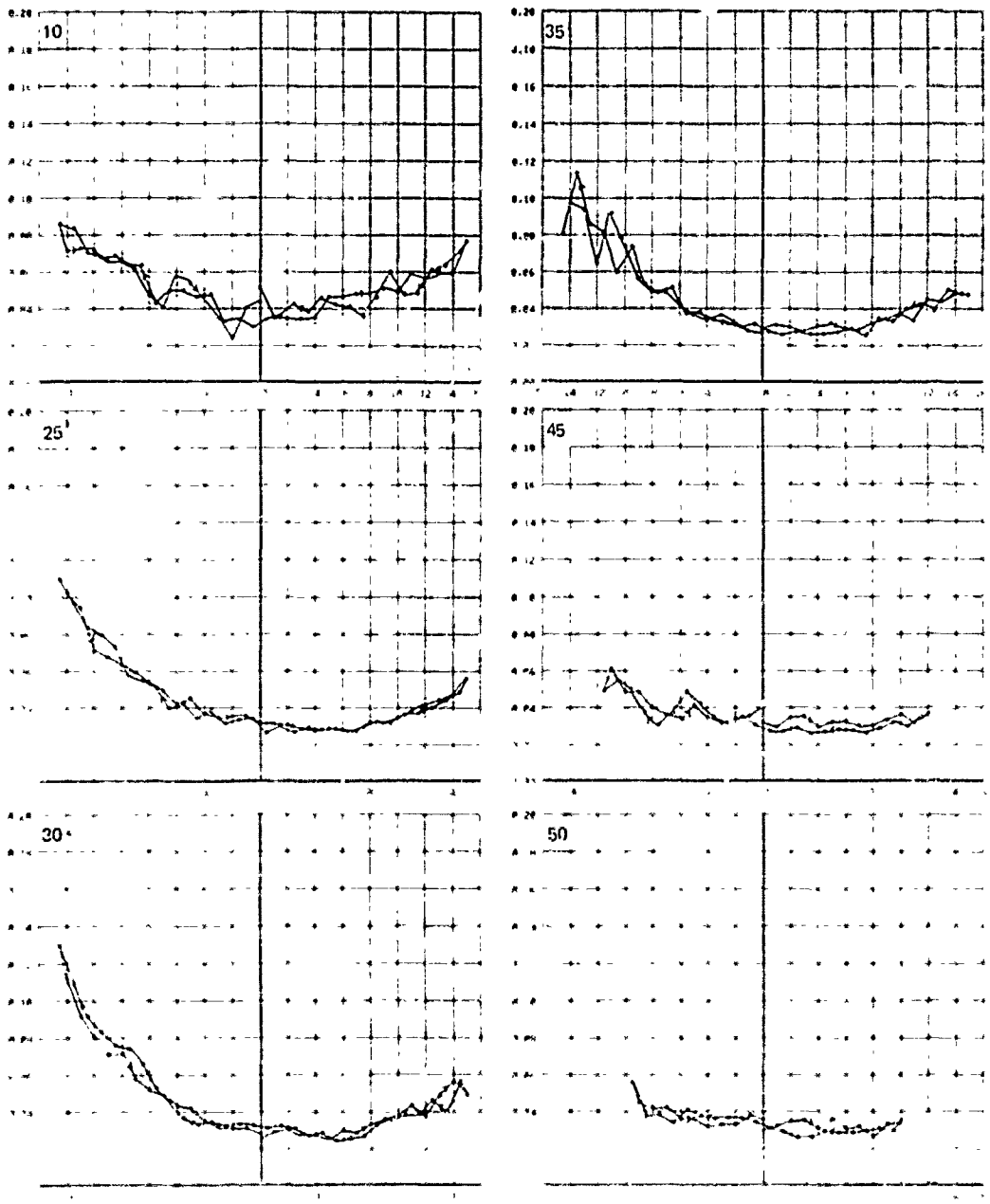

FIGURE 44b DRAG COEFFICIENT VS. SIDESLIP ANGLE, AIRBLEED STRUT, 20 SCFM (9.4 X 10^{-3} m^3/s), WITHOUT FENCES, MIDCHORD HOLES, PORT SIDE, 10, 25, 30, 35, 40, 45, 50 KTS

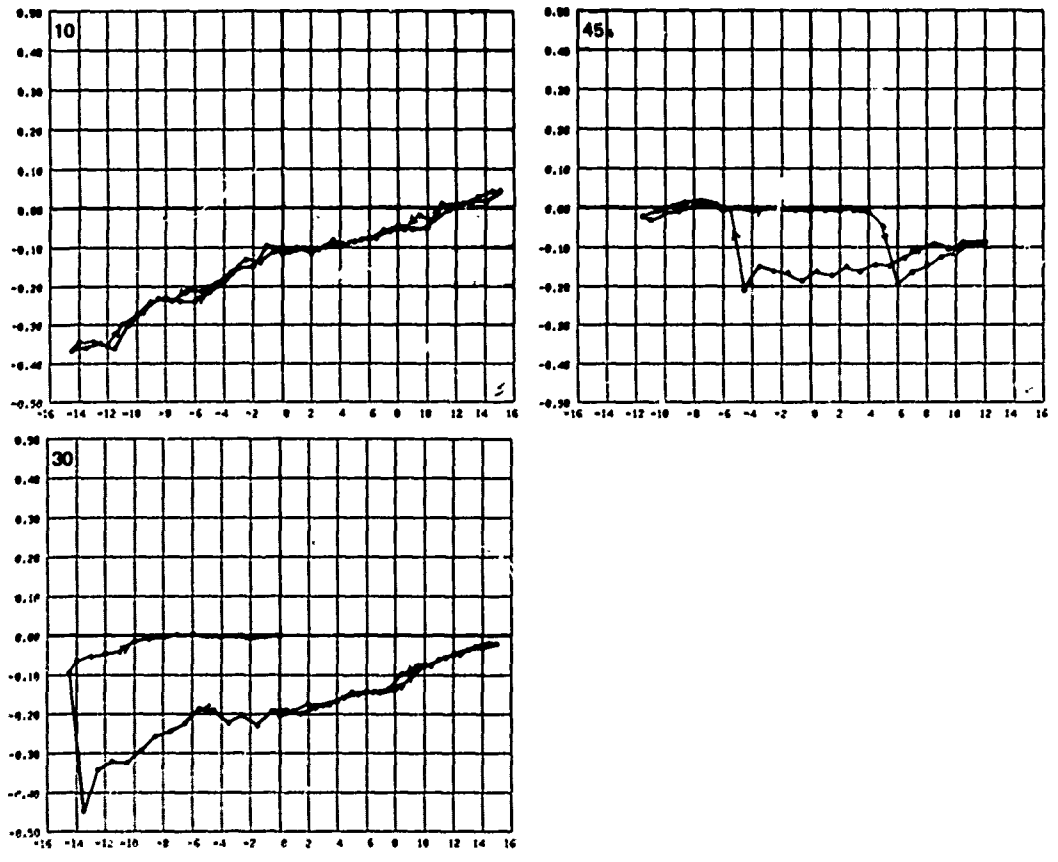

FIGURE 45a SIDEFORCE COEFFICIENT VS. SIDESLIP ANGLE, AIRBLEED STRUT, 10 SCFM (4.7 X $10^{-3}m^3/s$), WITHOUT FENCES, MIDCHORD HOLES, PORT SIDE, 10, 30, 45 KTS.

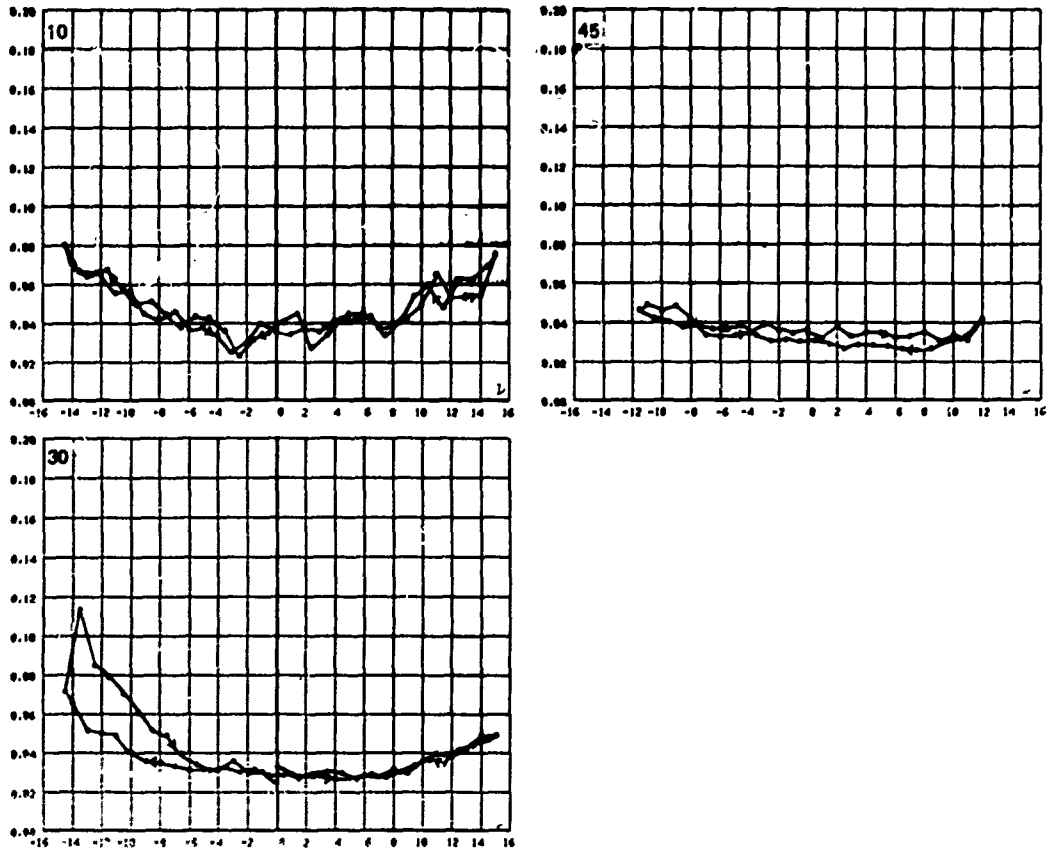

FIGURE 46b DRAG COEFFICIENT VS. SIDESLIP ANGLE, AIRBLEED STRUT, 10 SCFM (4.7 X $10^{-3}m^3/s$), WITHOUT FENCES, MIDCHORD HOLES, PORT SIDE, 10, 30, 45 KTS.

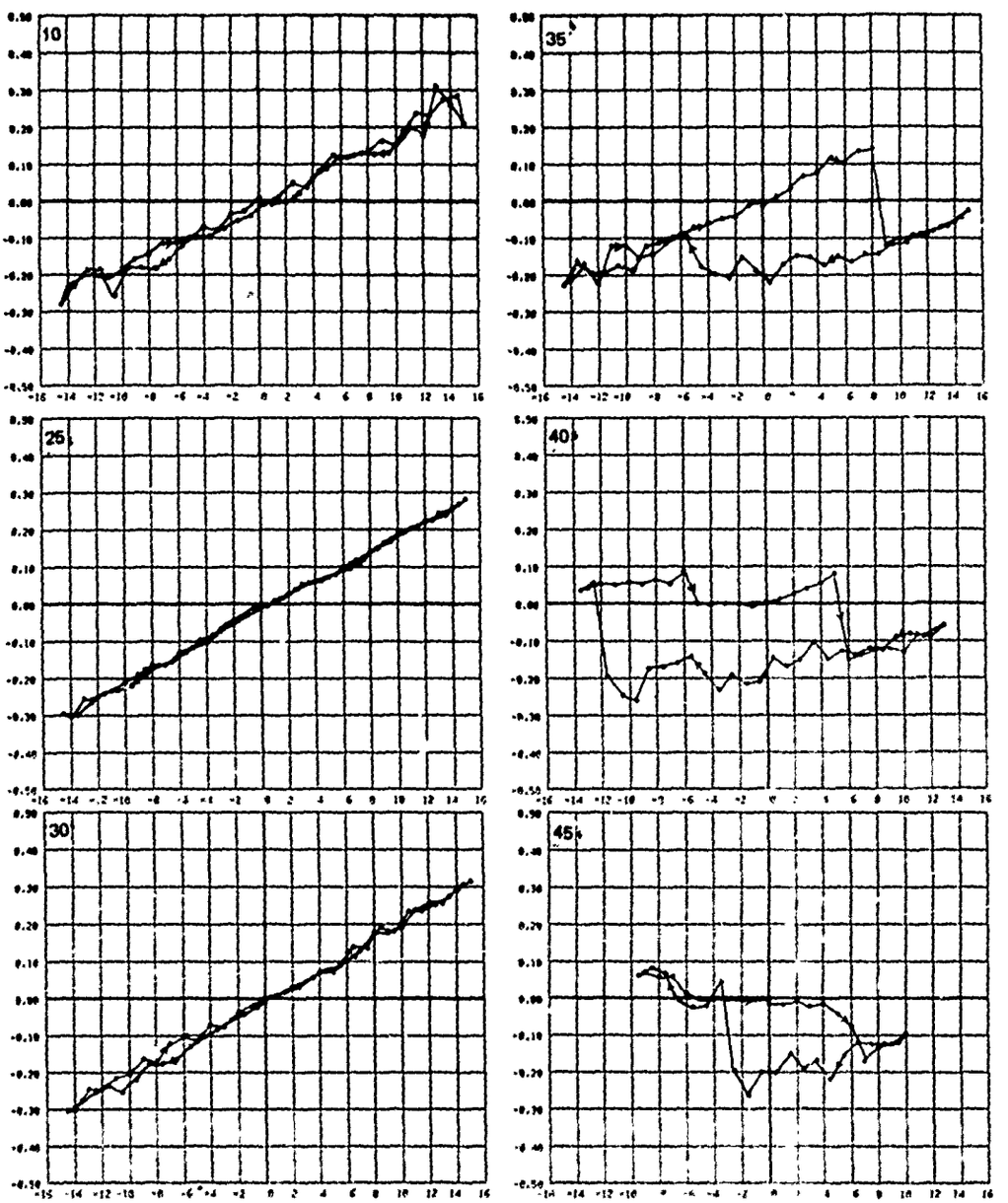

FIGURE 46a SIDEFORCE COEFFICIENT VS. SIDESLIP ANGLE, AIRBLEED STRUT, ATMOSPHERIC, WITHOUT FENCES, MIDCHORD HOLES, PORT SIDE, 10, 25, 30, 35, 40, 45 KTS.

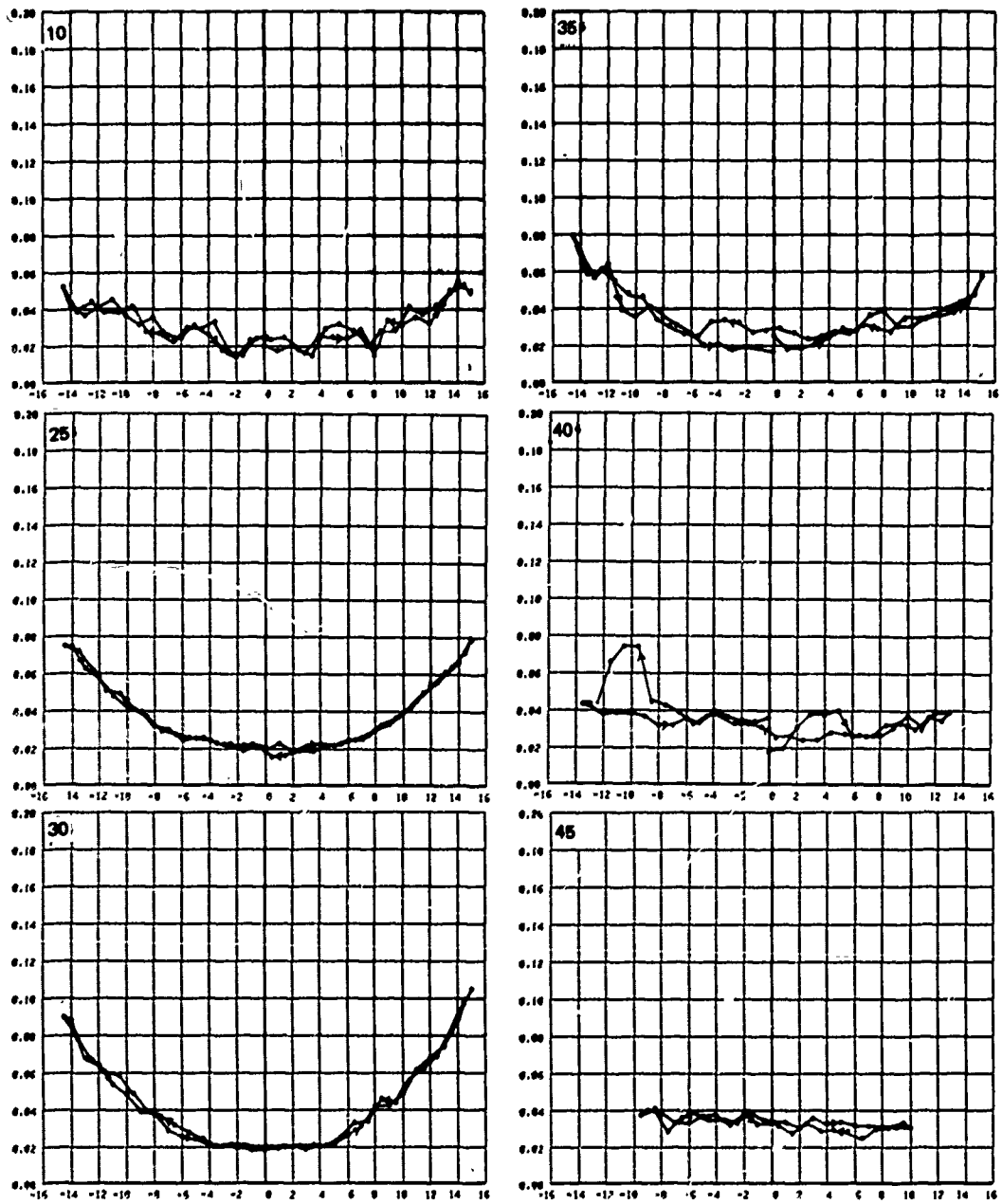

FIGURE 46b DRAG COEFFICIENT VS. SIDESLIP ANGLE, AIRBLEED STRUT, ATMOSPHERIC, WITHOUT FENCES, MIDCHORD HOLES, PORT SIDE, 10, 25, 30, 35, 40, 45 KTS.

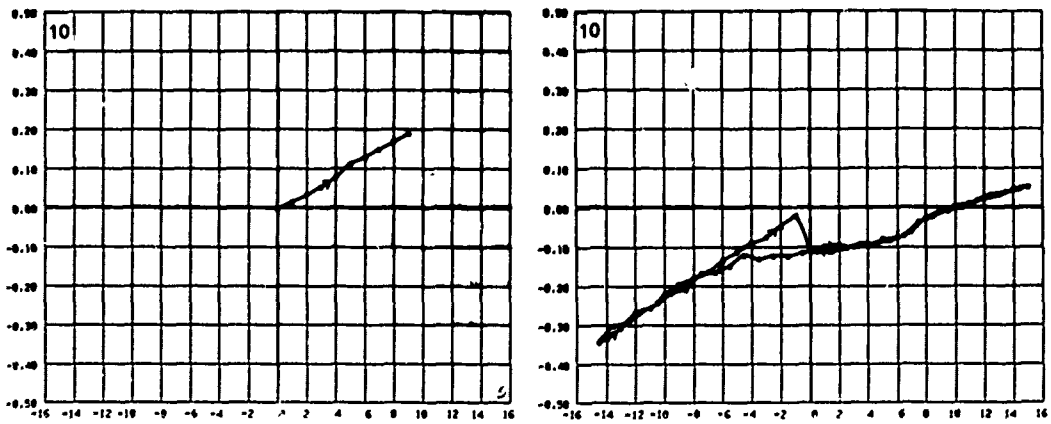

FIGURE 47a SIDEFORCE COEFFICIENT VS. SIDESLIP ANGLE, AIRBLEED STRUT, ATMOSPHERIC, WITHOUT FENCES, MIDCHORD HOLES, PORT SIDE, 10, 10 KTS. EXAMPLE OF CLEARED AND UNCLEARED HOLES.

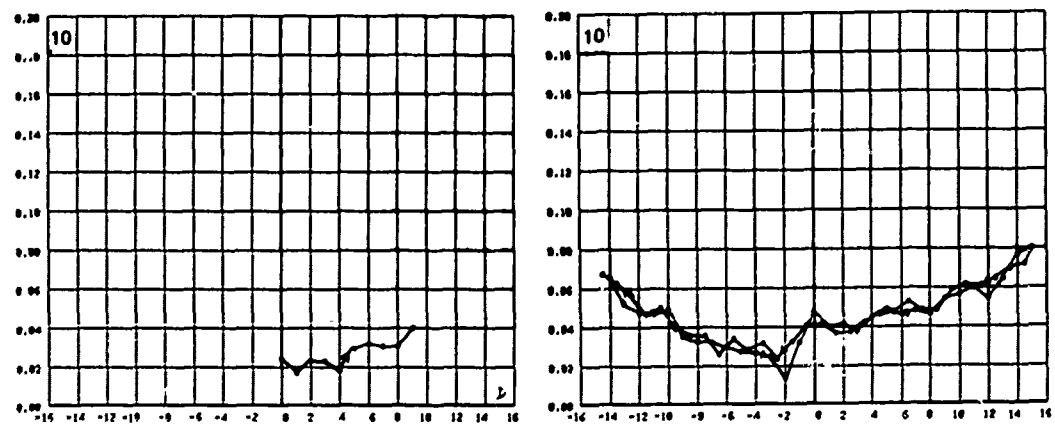

FIGURE 47b DRAG COEFFICIENT VS. SIDESLIP ANGLE, AIRBLEED STRUT, ATMOSPHERIC, WITHOUT FENCES, MIDCHORD HOLES, PORT SIDE, 10, 10 KTS. EXAMPLE OF CLEARED AND UNCLEARED HOLES.

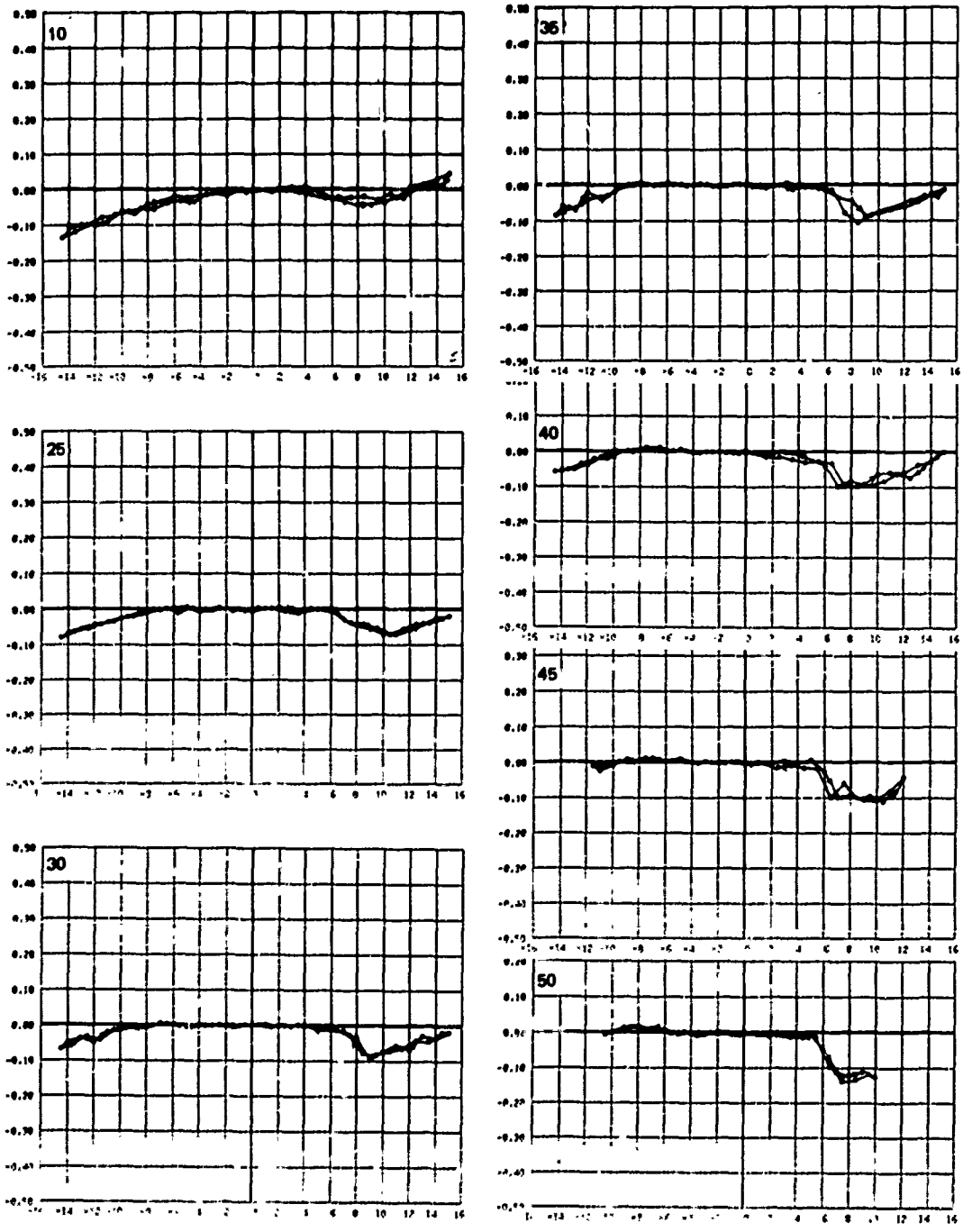

FIGURE 48a SIDEFORCE COEFFICIENT VS. SIDESLIP ANGLE, AIRBLEED STRUT, 35 SCFM (16.5 X 10^{-3} m^3/s), WITHOUT FENCES, ALL HOLES OPEN, PORT AND STARBOARD, 10, 25, 30, 35, 40, 45, 50 KTS.

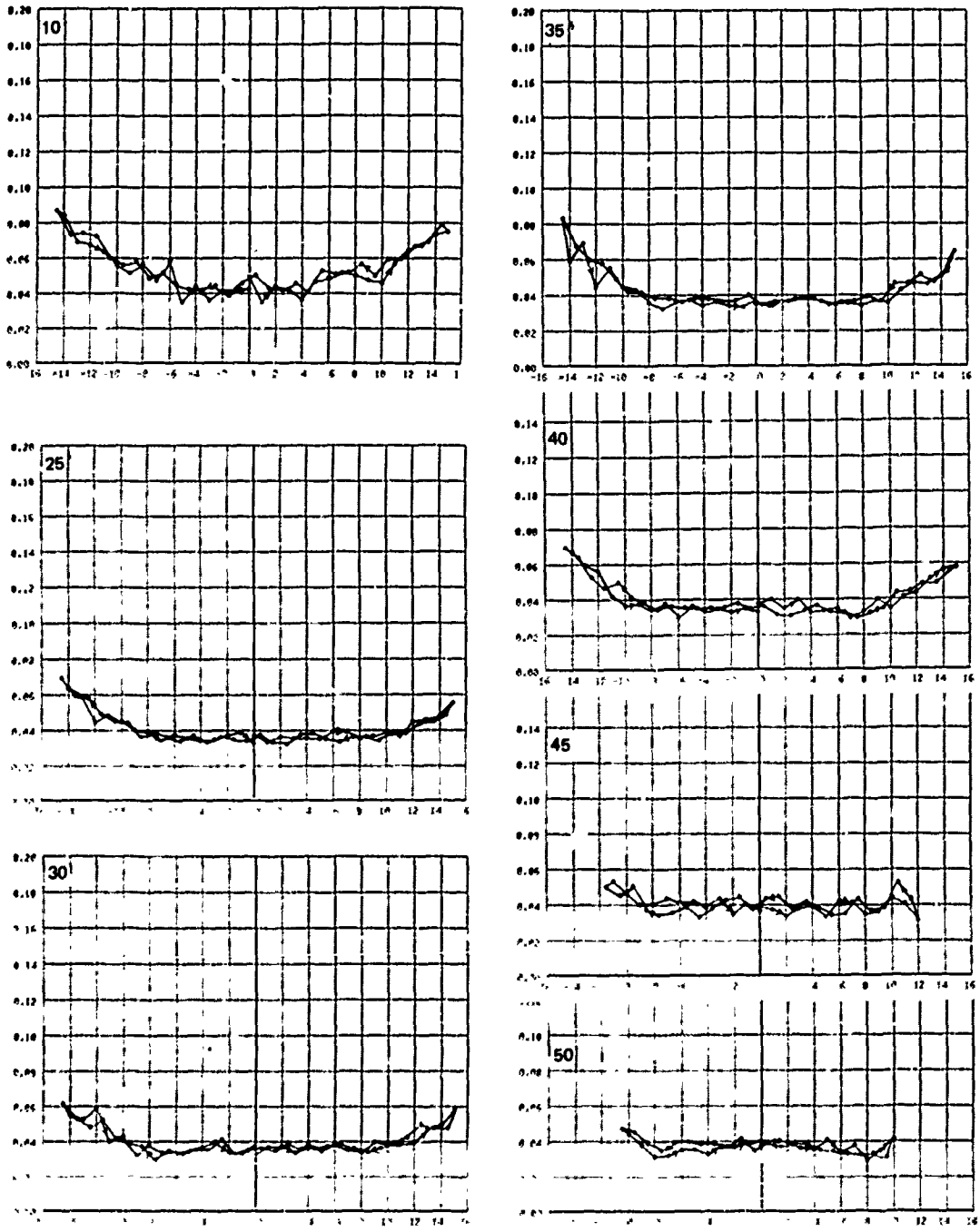

FIGURE 48b DRAG COEFFICIENT VS. SIDESLIP ANGLE, AIRBLEED STRUT, 35 SCFM (16.5 X 10^{-3} m^3/s), WITHOUT FENCES, ALL HOLES OPEN, PORT AND STARBOARD, 10, 25, 30, 35, 40, 45, 50 KTS.

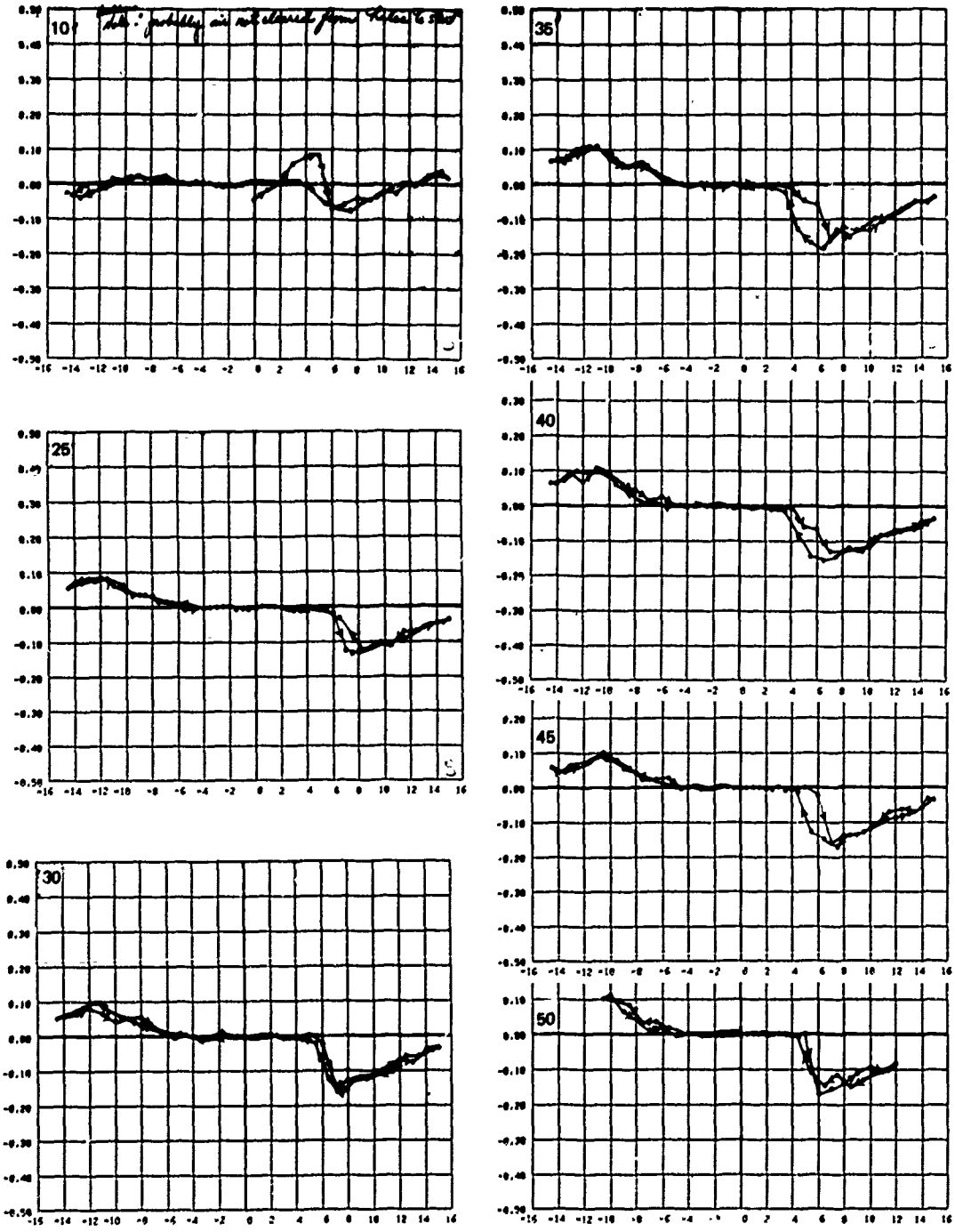

FIGURE 49a SIDEFORCE COEFFICIENT VS. SIDESLIP ANGLE, AIRBLEED STRUT, ATMOSPHERIC, WITHOUT FENCES, ALL HOLES OPEN, PORT AND STARBOARD, 10, 25, 30, 35, 40, 45, 50 KTS.

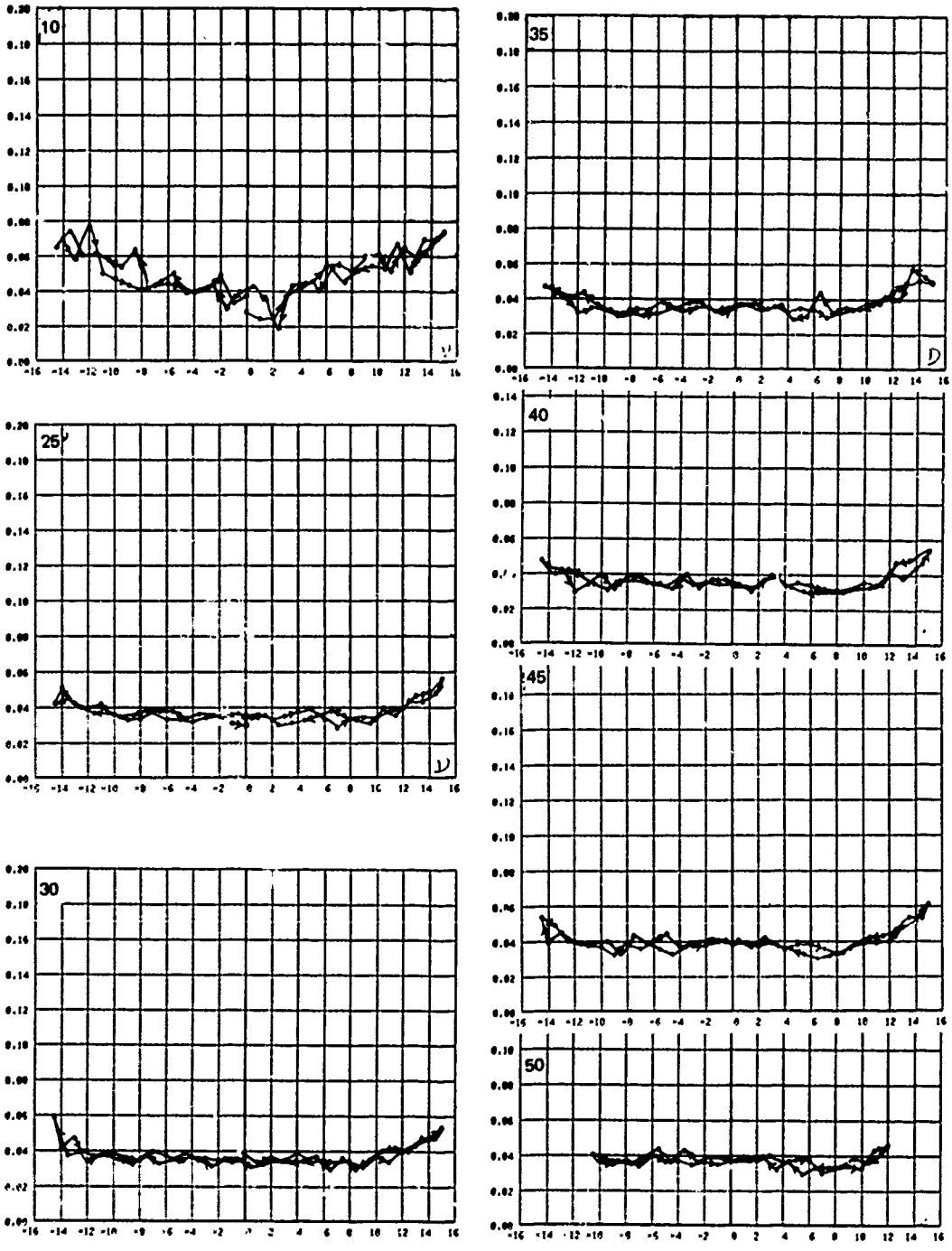

FIGURE 49b DRAG COEFFICIENT VS. SIDESLIP ANGLE, AIRBLEED STRUT, ATMOSPHERIC, WITHOUT FENCES, ALL HOLES OPEN, PORT AND STARBOARD, 10, 25, 30, 35, 40, 45, 50 KTS.

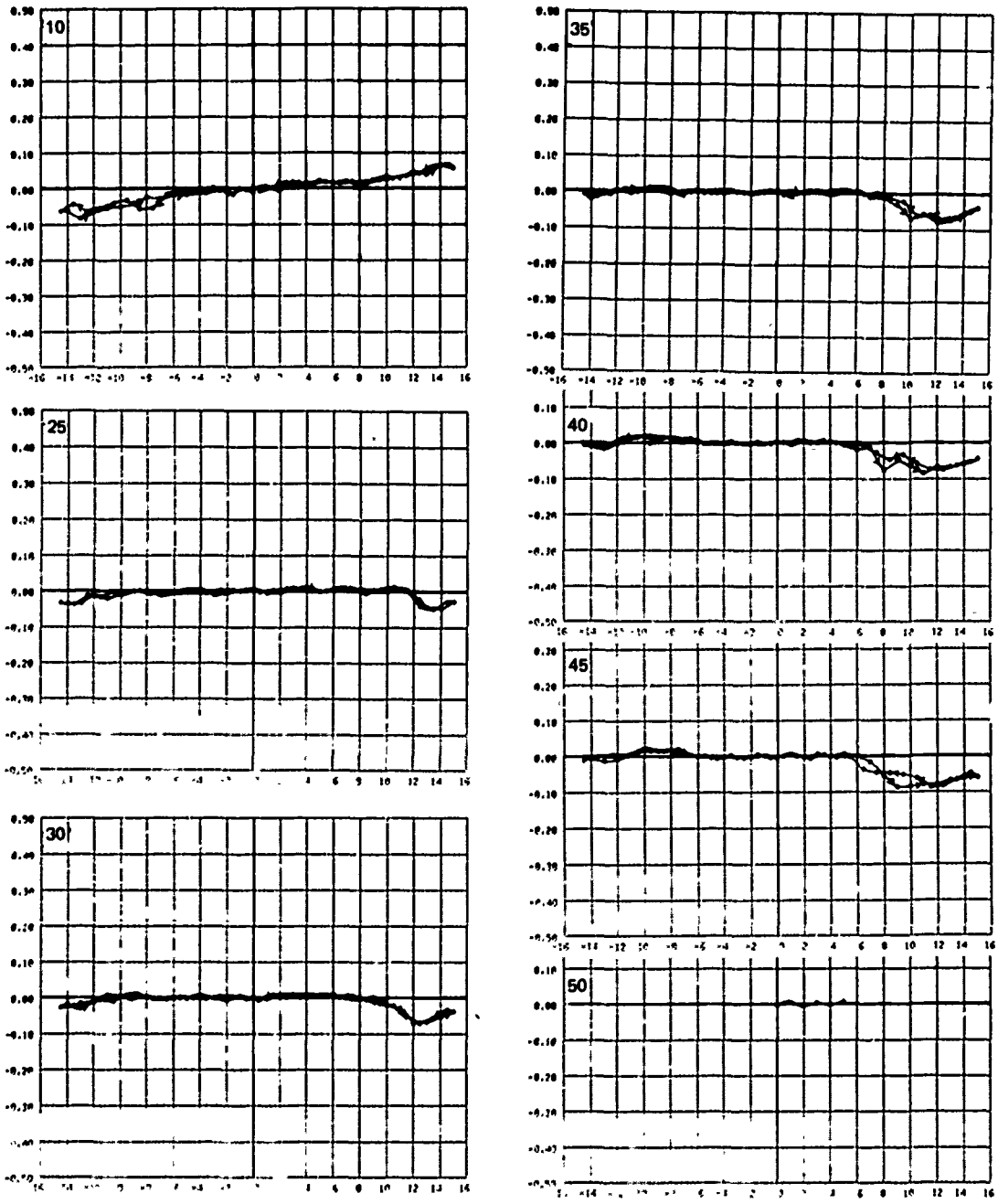

FIGURE 50a SIDEFORCE COEFFICIENT VS. SIDESLIP ANGLE, AIRBLEED STRUT, 35 SCFM, WITHOUT FENCES, LEADING EDGE HOLES OPEN BOTH SIDES, 10, 25, 30, 35, 40, 45, 50 KTS.

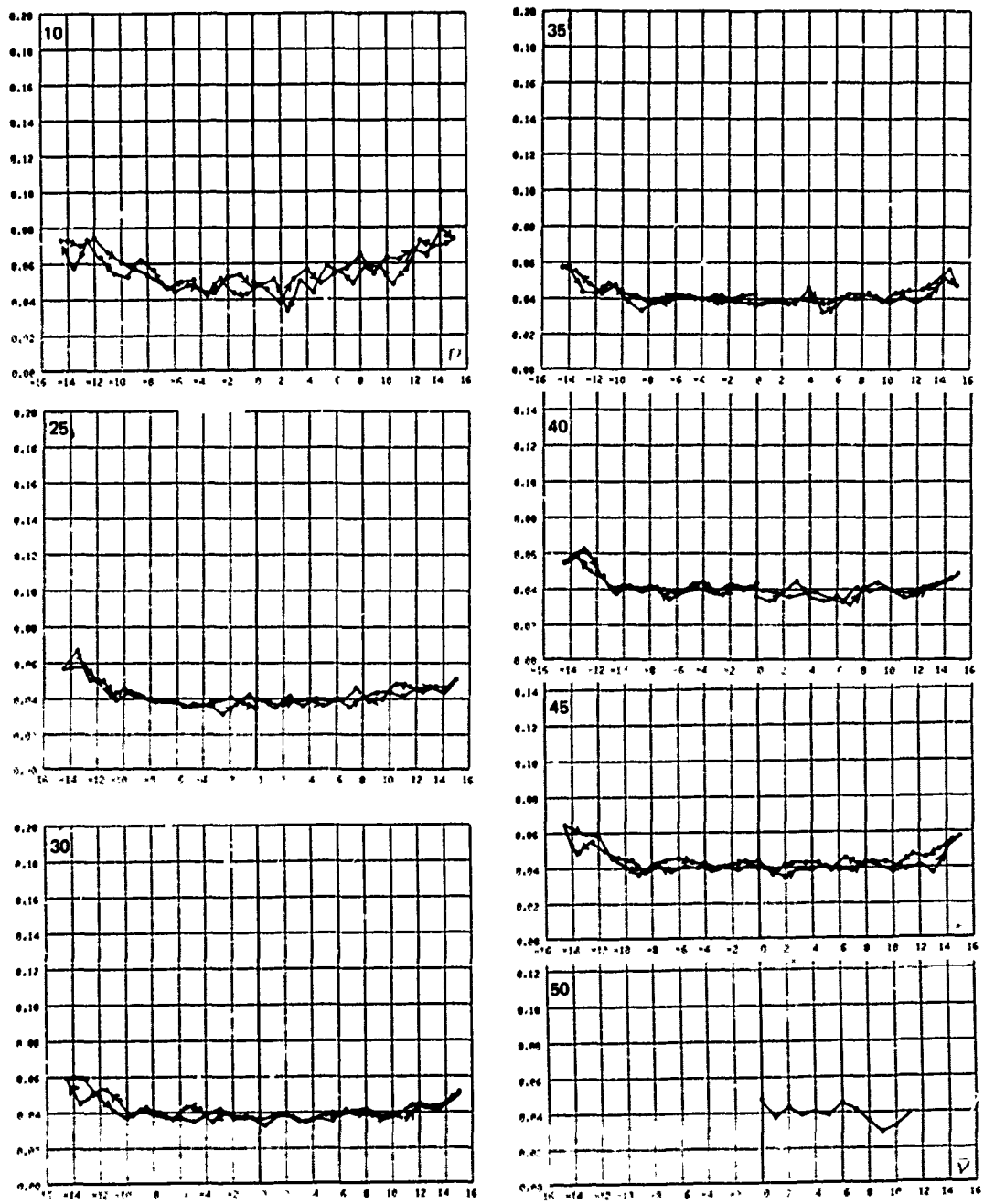

FIGURE 50b DRAG COEFFICIENT VS. SIDESLIP ANGLE, AIRBLEED STRUT, 35 SCFM, WITHOUT FENCES, LEADING EDGE HOLES OPEN BOTH SIDES, 10, 25, 30, 35, 40, 45, 50 KTS.

where A is the planform area

E denotes "endplate"

AR is the aspect ratio, taken in this case to be the strut submergence aspect ratio of 1.0

The area to be considered in the coefficient is the submerged planform area of the strut. In the present case $A_E/A \sim 0.5$, AR = 1.0. Therefore the endplate contribution to C_D is about 0.008 and the corrected value for the strut drag alone is 0.012. The drag for a similar strut tested in Reference 3 without endplate, which had the same maximum thickness and the same section aft of midchord, but which had a slightly finer nose section, was reported to be $C_D \cong 0.0075$.

It is possible that some drag may be induced by endplate lift because of the proximity of the endplate to the distorted free surface.

Both the drag and the sideforce curve slopes for the flapped model at zero incidence and zero flap angle (Figure 13) are similar to those for the plugged airbleed strut, including the phenomenon of reduced sideforce slope at speeds of 25 kts and above compared to 10 kts. The ventilation inception angles for the flapped model are much lower, as are the maximum sideforce coefficients attained at high speeds.

In sum, the value of the plugged airbleed model as a baseline for comparison with other airbleed strut configurations may be somewhat flawed. The drag appears slightly higher than might be expected, and the sideforce coefficients somewhat lower. The ventilation inception angles were also slightly lower. However, the overall behavior was approximately in agreement with previous tests.

Figures 26 and 27 show the results of 35 and 20 SCFM (16.5×10^{-3} m^3/s and 9.5×10^{-3} m^3/s) air forced through all the holes on the port side. Figure 28 shows the effect of allowing the holes to remain open, with the common manifold open to the atmosphere. The natural negative pressure at the ejection hole sites was sufficient to draw, at variable rates, about 2 - 3 SCFM of air through the supply hose and venturi throat for nealy all sideslip angles. The three Figures are nearly identical in the gross behavior of the force coefficients. At 10 kts, the sideforce coefficient at zero sideslip was about -0.10. The value at higher speeds was between -0.2 and -0.25. The coefficient slope at 10 kts for starboard sideslip angles was about the same as for the plugged hole case (Figure 25). For port angles, the slope was reduced.

Above 10 kts, the unventilated port angle coefficients continued to be about the same as the baseline case, but for starboard angles, ventilation of the starboard side usually occurred, which caused the sideforce to fall approximately to zero. Partial or full ventilation of the starboard side can be noted at remarkably small angles. This suggests that somehow the port side air made its way to the starboard side to provoke early ventilation. Another factor may have been the unusually low starboard side pressures implied by the large negative sideforce coefficients at negative sideslip angles. Sideforce coefficient is often a more reliable ventilation inception boundary than sideslip angle.

An explanation in detail of the ventilation behavior inferred from the force coefficients may be helpful in interpreting the Figures. In Figure 26, for example, at 10 kts, the run started with the port side vented. The situation remained the same as sideslip angle increased to 15 degrees, decreased to - 15 degrees, then increased to - 7 degrees. At - 7 degrees, the starboard side became partly ventilated, causing the sideforce coefficient to approach, but not reach, zero. The starboard side vent persisted to zero sideslip angle.

The next graph in Figure 26, for 25 kts, shows that the run began with the starboard side partial vent still existing. Between 6 and 7 degrees, the starboard vent washed off, and the force coefficient returned to the port side vented value. This situation was stable as sideslip angle increased from 7 to 15 degrees, then decreased to - 1½ degrees. From - 1½ to - 14½ degrees, partial vents, each successively more extensive, occurred until at - 14½ degrees, nearly full ventilation was present on the starboard side. Evidently the starboard vent continued to grow, or perhaps the portside vent decreased, even as sideslip angle increased. This was indicated by the sideforce coefficient approaching closer to zero, implying a symmetric flow pattern.

The remaining speeds can be interpreted in much the same way. Note that the 30, 35, 40 and 50 kt runs all started with starboard side vents left over from the previous runs. These vents washed out as sideslip angles became more positive, and were re-established at, mostly, negative sideslip angles.

It is interesting to note that the drag coefficient at zero sideslip angle in all three Figures was no different whether or not there was lift. For example, the plugged strut had a drag coefficient (Figure 25) of about 0.06 when the sideforce coefficient was 0.2. For the port aerated strut, at zero sideslip, the drag coefficient was about 0.03 whether the sideforce coefficient was zero or 0.2. In one case the air injection could be considered to increase drag, and in the other to decrease drag.

Figures 29, 30 and 31 show the results of the same conditions as the previous three Figures, except that four ventilation fences had been added, at the mean free surface and, at equal intervals of one quarter chord, one above and two below the surface.

The general trend, not obeyed in all cases, was for the fences to increase the sideforce coefficient slope at low speeds, to limit the hysteresis effects by reducing the excursions (maxima and minima) of the force coefficients, and to increase the drag. The notable exception to this generalization is shown in Figure 29 for the 35 kt, and to a certain extent, the 40 kt case for sideforce coefficient. The hysteresis and excursion is equally as large as for the unfenced case.

A possible explanation for the fence results is that the fences trapped air cavities, so that the change from one state to the next was never quite completed, and the state which resulted most of the time was a nondescript composite, which exhibited few extremes observed in the behavior of the unfenced airbleed strut. The reason for the exceptions noted in Figure 29 is probably that these were the initial runs of the fenced strut series, so the starboard side air pockets had not had a chance to become established. In fact, up to the 35 kt run in Figure 29, there had been no evidence of a starboard side vent. If this type of "damped" behavior is sought in a full scale craft, the penalty of an increase in drag coefficient of from 0.005 to 0.01 may be justified.

Before removing the fences and proceding to test the effects of individual rows of air ejection, some special purpose runs were made. Figure 32 shows the results of charging the air supply accumulator to near maximum capacity and allowing the air to be expelled at the maximum rate compatible with the airflow measurement system. This resulted in a maximum airflow of around 85 SCFM (40×10^{-3} m^3/s) which declined during the run to 35 SCFM (16×10^{-3} m^3/s), the maximum continuous rate sustainable by the supply compressor. This run was performed at 10 kts only. The principal difference between it and the similar runs was that a starboard side vent was provoked, showing that excessive air on the port side probably does affect the starboard side.

On the same Figure, the lower graphs show the results of releasing air in one second "bursts" every 10 seconds or so, a rate of about 95 SCFM (45×10^{-3} m^3/s), at a towing speed of 40 kts. In this case, no significant general differences were observed, although the points on the graph where the air is released are changed somewhat from the neighboring points. This shows that greatly increased airflow rates do not change the force characteristics appreciably. The technique of "bursting" the air may be useful if for some reason it is necessary to limit the amount of air ejected by the air bleed system, while still achieving substantially the same effect as continuous airbleed.

Figure 33 shows the effect of turning off a valve between the air supply accumulator and the strut. The effect is much the same as for those runs with active air bleed at the same speeds, 10 and 40 kts. Apparently the air remaining in the manifold and supply hose, plus

air sucked in through the above-water holes in the strut was sufficient to create substantially the same effect as vigorous air ejection. The implication for full scale application is that, while it may be easy to provoke ventilation, it is not so easy to turn it off.

Figures 34 through 47 show the results of ejecting air from between hole rows 5, 10, 25 and 50 percent of chord aft of the leading edge. Again, no major difference in behavior was noted. The principal minor variations were: the starboard side did not become ventilated at as small a sideslip angle at the low and intermediate speeds, especially in the case of the mid-chord holes; with just atmospheric air as the supply, there was somewhat more hysteresis and the results were more erratic than with all the portside holes open; with atmospheric air alone, if the midchord holes were not cleared of water before a run, they would not spontaneously clear until a "natural" vent occurred; no single row of holes functioned as well with atmospheric air supply if is was not cleared prior to the run. A comparison of runs made with midchord holes cleared and not cleared is shown in Figure 46.

In general, it can be said that, with active air injection, there was little to choose between any hole pattern. With minimal air supply, holes distributed over the chord functioned better than holes at any specific chordwise location.

For the final airbleed tests, a row of holes was opened up on the starboard side, 5 percent of chord aft of the leading edge. Figures 48 and 49 show the results of airbleed through all holes, port and starboard. Figures 51 through 53 show the results of just the forward 5 percent chord rows of holes on both sides open.

In Figure 48, the sideforce coefficient exhibited the same tendencies as for runs during which both sides of the strut were ventilated. However, at large port angles, the coefficients behaved more as if just the port side were vented, indicating that the starboard side was "starved". Even at large starboard angles, the port side seems to have had the better air supply.

More symmetry is apparent in Figure 49 for atmospheric air supply. At large port angles, the starboard side seems to have been starved, but the converse was also true. Even in this case, it is still evident that the port side had the more adequate air supply.

For all cases of starboard and port side airbleed, the drag coefficient was nearly independent of sideslip angle, and slightly increased above the comparable value obtained with blowing on only one side at zero sideslip angle. The drag coefficient was about 0.035 to 0.040, compared to a plugged-strut zero sideslip value of 0.02.

During blowing on both sides from the 5 percent chord holes only, the sideforce coefficients were quite symmetric, showing signs of starvation on both the port and starboard tacks. This was pronounced in the atmospheric supply case, Figure 53, less so for 10 SCFM (4.7×10^{-3} m^3/s) airflow rate, and hardly noticeable at the 20 SCFM (9.4×10^{-3} m^3/s) rate.

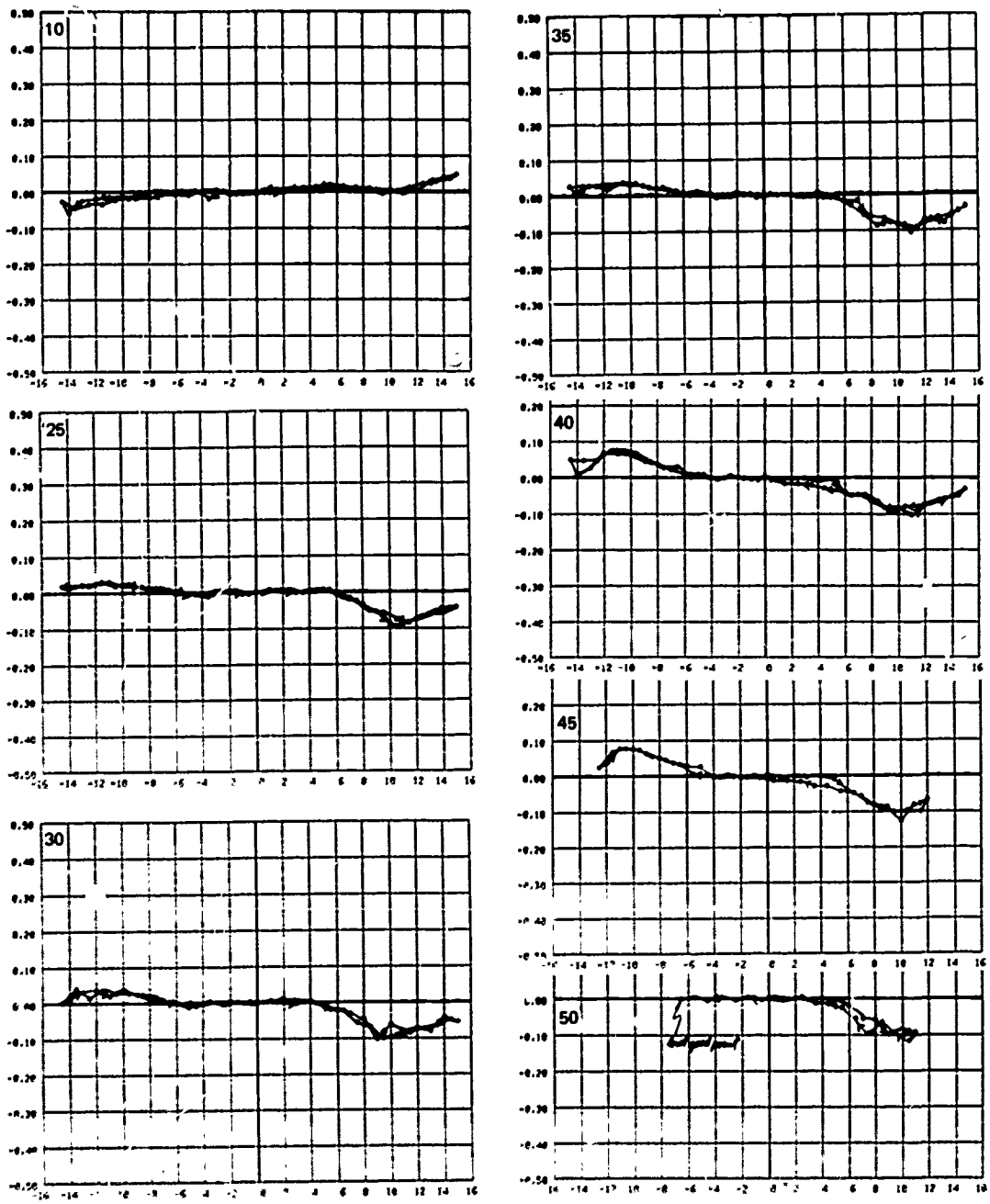

FIGURE 51a SIDEFORCE COEFFICIENT VS. SIDESLIP ANGLE, AIRBLEED STRUT, 20 SCFM (9.4 X 10^{-3} m^3/s), WITHOUT FENCES, LEADING EDGE HOLES OPEN BOTH SIDES, 10, 25, 30, 35, 40, 45, 50 KTS.

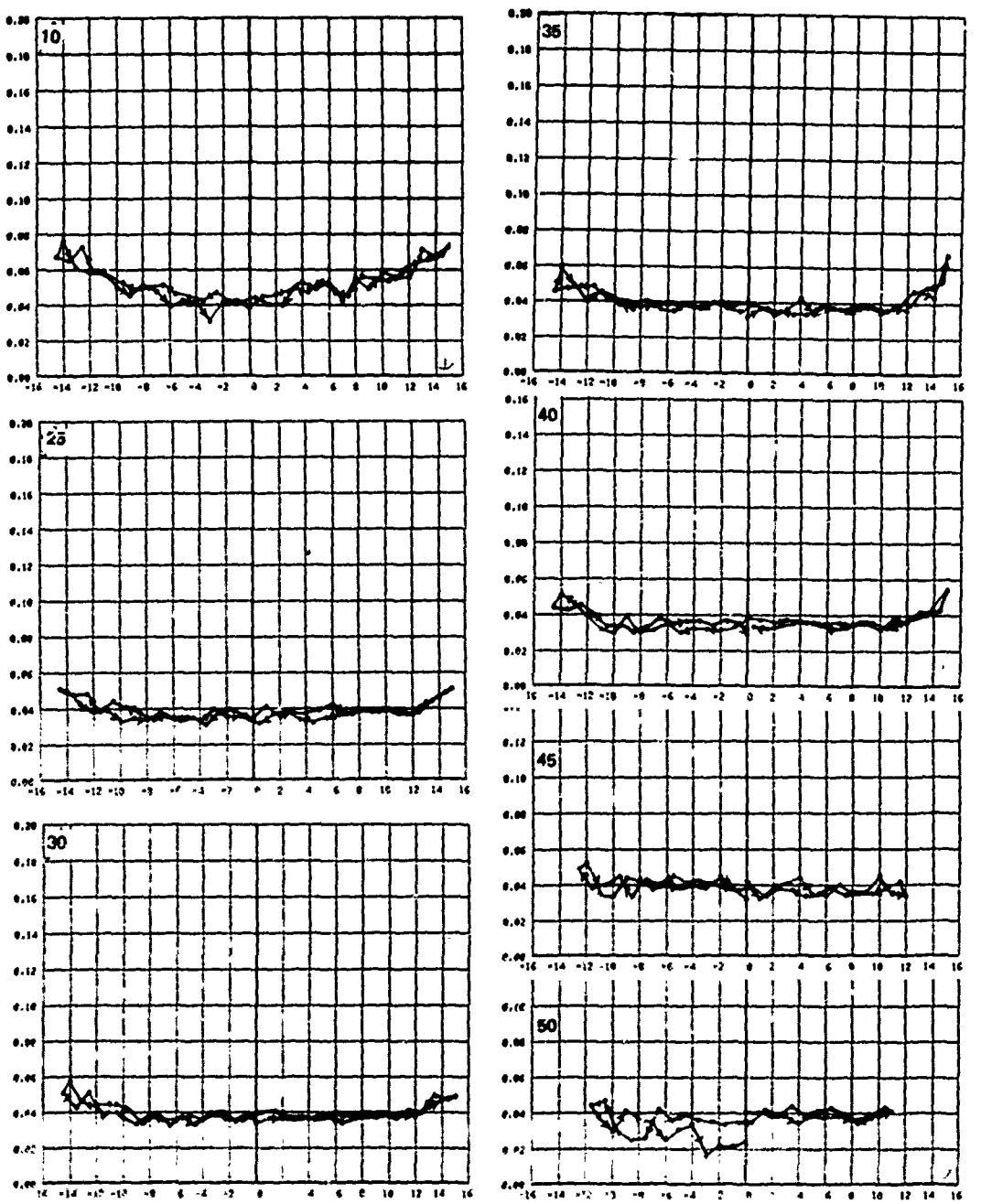

FIGURE 51b DRAG COEFFICIENT VS. SIDESLIP ANGLE, AIRBLEED STRUT, 20 SCFM (9.4 X $10^{-3}m^3/s$), WITHOUT FENCES, LEADING EDGE HOLES OPEN BOTH SIDES, 10, 25, 30, 35, 40, 45, 50 KTS.

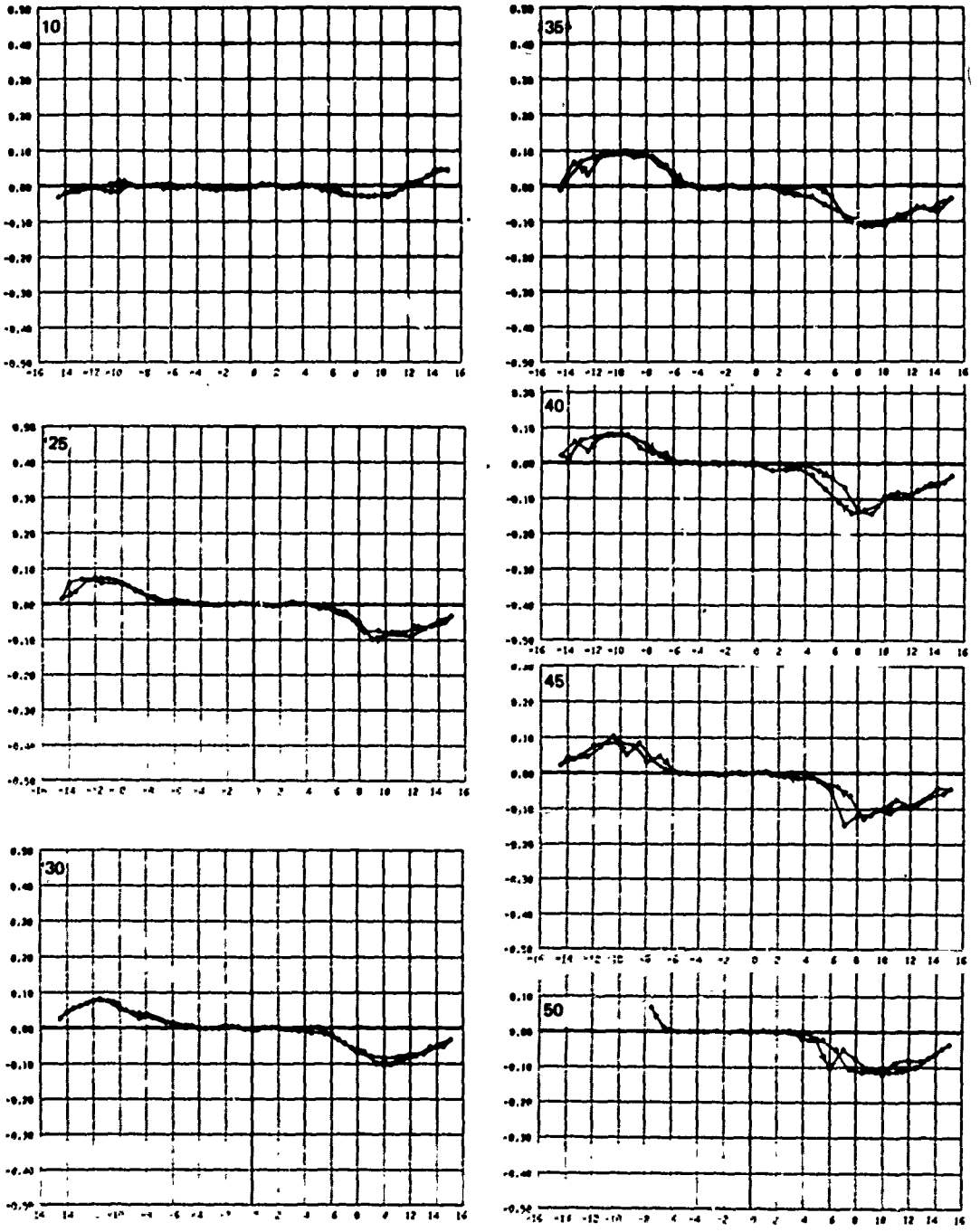

FIGURE 52a SIDEFORCE COEFFICIENT VS. SIDESLIP ANGLE, AIRBLEED STRUT, 10 SCFM (4.7 X $10^{-3}m^3/s$), WITHOUT FENCES, LEADING EDGE HOLES OPEN BOTH SIDES, 10, 25, 30, 35, 40, 45, 50 KTS.

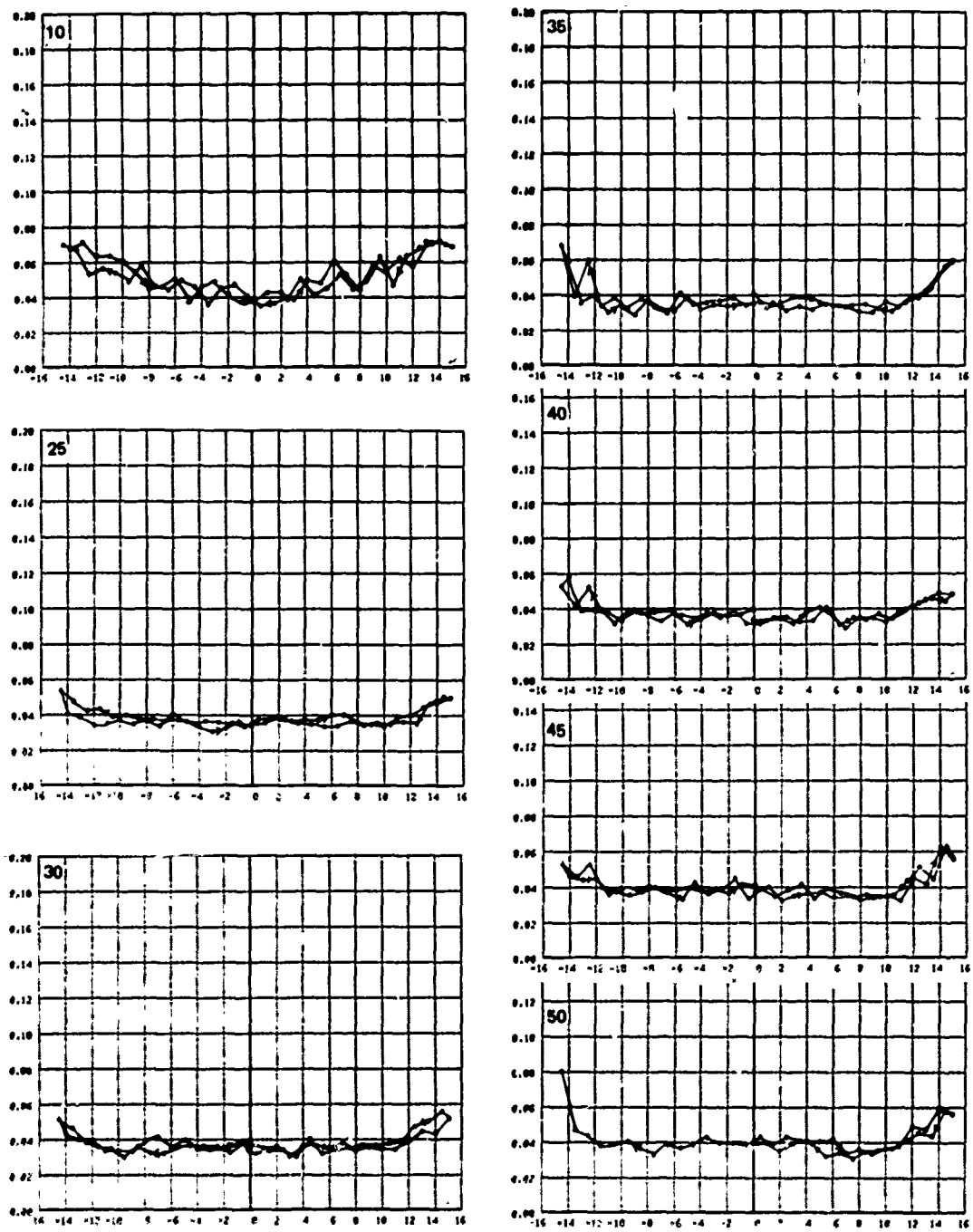

FIGURE 52b DRAG COEFFICIENT VS. SIDESLIP ANGLE, AIRBLEED STRUT, 10 SCFM (4.7 X 10^{-3} m^3/s), WITHOUT FENCES, LEADING EDGE HOLES OPEN BOTH SIDES, 10, 25, 30, 35, 40, 45, 50 KTS.

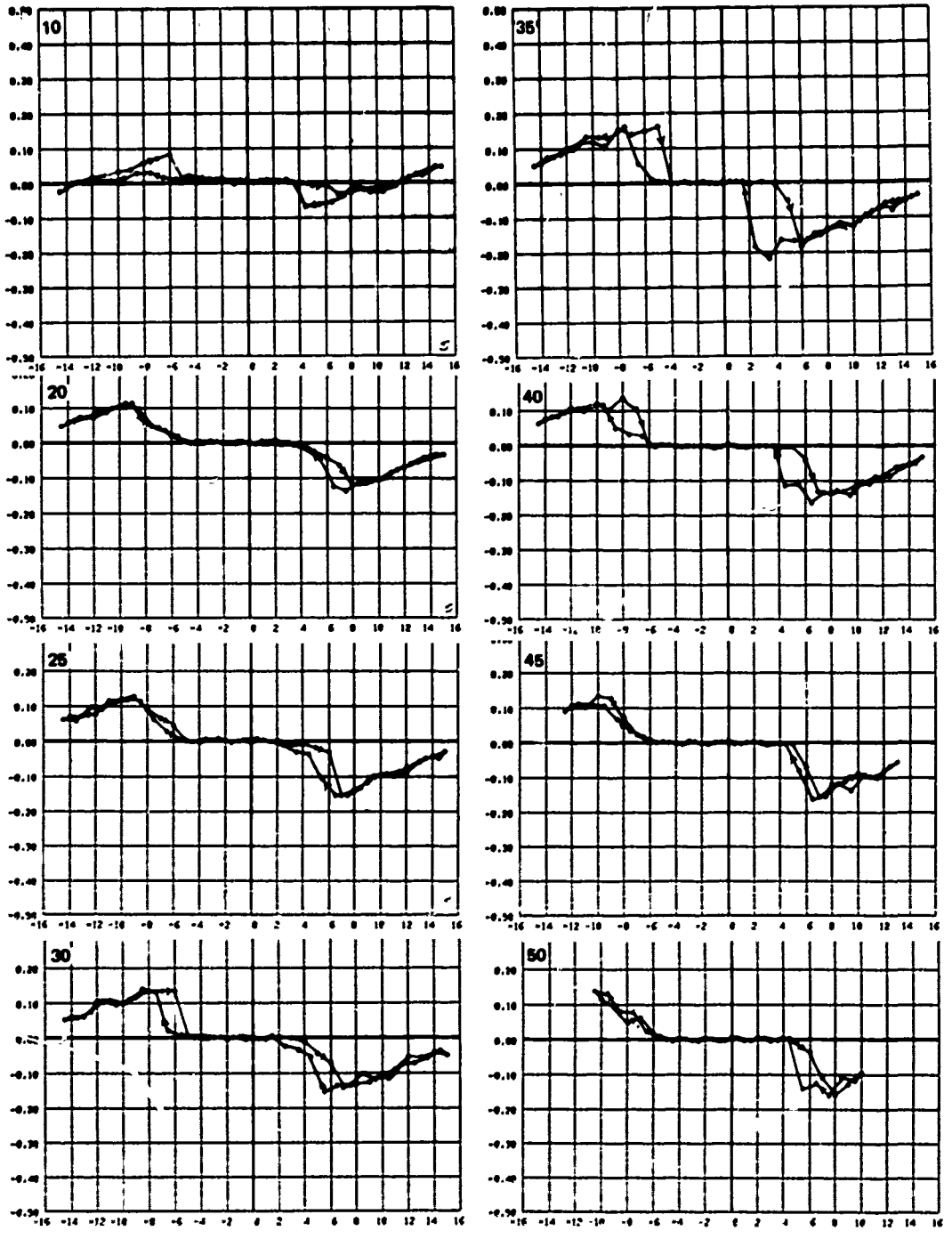

FIGURE 53a SIDEFORCE COEFFICIENT VS. SIDESLIP ANGLE, AIRBLEED STRUT, ATMOSPHERIC, WITHOUT FENCES, LEADING EDGE HOLES OPEN BOTH SIDES, 10, 20, 25, 30, 35, 40, 45, 50 KTS.

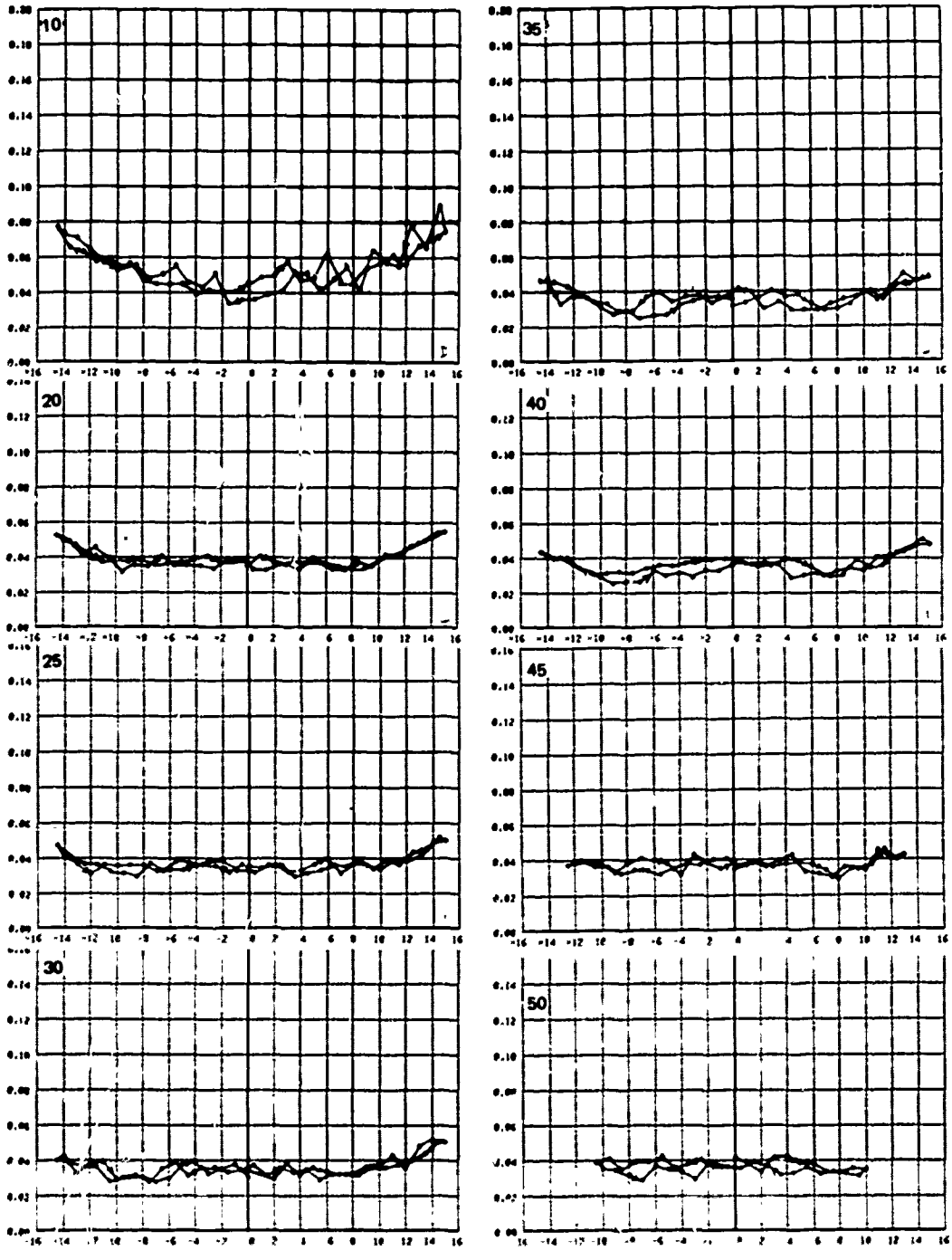

FIGURE 53b DRAG COEFFICIENT VS. SIDESLIP ANGLE, AIRBLEED STRUT, ATMOSPHERIC, WITHOUT FENCES, LEADING EDGE HOLES OPEN BOTH SIDES, 10, 20, 25, 30, 35, 40, 45, 50 KTS.

An extremely interesting and significant phenomenon occurred at the 35, 20, and 10 SCFM (16.5×10^{-3}, 9.4×10^{-3}, 4.7×10^{-3} m^3/s) flowrates at 50 kts. At 20 and 10 SCFM, on the starboard sweep, large unsteady forces occurred which overloaded the analog-to-digital converter and prevented further data acquisition. At 35 SCFM, on the port sweep, extremely large unsteady forces were registered which not only overloaded the electronics, but were distinctly and disturbingly felt by the test operators.

Since the unsteady forces on the starboard tack were experienced in an angular region where air starvation is presumed to have been a problem, it is likely that they were caused by the vented cavity shrinking to a length of the order of one chord. This is known to create severe oscillations (e.g., Reference 11).

The unsteady forces encountered at fairly low port angles present more of a puzzle, particularly since they occurred at the 35 SCFM airflow rate, the maximum generally applied. It is possible that having so much air exiting at a very forward position created an instability of the attachment point of the flow, which alternately vented and wetted each side of the strut in a coupled oscillation. The involvement of both sides of the strut could explain the subjective sense of unusual severity of the oscillation. Evidently, multiple chordwise positions of the air holes prevent the oscillations, since they were not observed prior to the 5 percent chord airbleed runs. This may be a problem that will have to be examined before a full scale system is designed.

CONCLUSIONS OF THE AIRBLEED AND FENCE EXPERIMENT

- A small amount of airbleed can affect sideforce coefficients by an amount equal to a change in sideslip angle of nearly 12 degrees ($\Delta C_s = \pm 0.2$).
- Airbleed on both sides of a strut can effectively reduce sideforce to near zero even for sideslip angles of 15 degrees.
- For continuous airbleed from both sides of a strut, the drag penalty referenced to a baseline condition in this experiment was 75 to 100 percent (about 4 percent of overall drag).
- Unsteady forces due to cavity oscillations can be a problem if air ejection is limited to a single chordwise position.
- Chordwise location of air ejection is not a significant parameter, except perhaps for oscillations.
- Multiple-row air ejection compared to single row at a single chordwise position gives more consistent results and requires less or no blowing pressure.

SPOILERS

A device similar in effect to a split flap is the flow "spoiler" shown in Figure 54. As suggested by its name, the spoiler derives part of its effect by changing the circulation by "spoiling" the flow past a certain point. This might prevent the negative pressures from developing on the low pressure side of an airfoil, for example. Spoilers can be retractable or permenantly fixed. The advantage of a spoiler-type flap would be the predictability of its ventilation characteristics. Spoilers of the type shown in Figure 54 applied to a surface-piercing strut would probably be ventilated at their base as soon as they were deployed. For fixed spoilers on both sides of a surface-piercing strut, the expected behavior would be similar to that of a blunt-based strut, as shown by comparing the data of Dailey[6] and Nelka.[7]

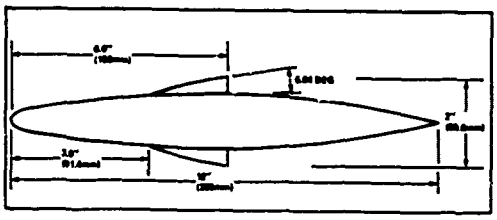

Figure 54 – Spoilers on NACA-16-012 Surface-Piercing Strut

Spoilers could be applied in two ways. A retractable spoiler could be extended on either side of a surface-piercing strut as necessary to counteract undesirable forces or to generate a desired side force. Or, permanent spoilers could be attached to both sides, which would be expected to limit the maximum sideforce that could be developed in either direction. However, based on experience with blunt based struts, the sideforce developed prior to ventilation is likely to be a linear function of sideslip angle.

In applying spoilers to a given situation, there are several unknowns among which are: the sideslip angle at which ventilation takes place; the conditions under which the trailing part of the strut would be completely enclosed in the ventilated cavity; the effectiveness of a given spoiler in producing or reducing sideforce; the control power required to actuate a spoiler. To clarify these points, an experimental program was necessary.

THE SPOILER EXPERIMENT

The Model. The flapped model was fitted with two spoilers as shown in Figure 54. After testing, the port spoiler was removed and the strut filled and smoothed to its original contour. The spoilers were identical to those used by Nelka in Reference 7. They were mounted so that the spoiling effect took place at mid chord, rather than at 70 percent of chord aft, as in Nelka's experiment. The angle subtended by the spoilers was nearly 7 degrees.

They were designed to provide a favorable pressure gradient as the flow followed the "ramp" starting at the spoiler leading edge, so that premature separation would not occur.

Test Conditions. As in the previous test, the strut was mounted at a radius of 1.30 chords and towed on the Rotating Arm through a range of speeds tested from 10 to 50 kts, corresponding to angular velocities of 0.14 to 0.7 rad/s. The strut was tested with spoilers on both sides and on the starboard side alone. The data acquisition system was identical to that used before.

RESULTS AND DISCUSSION OF THE SPOILER EXPERIMENT

Figure 55 shows the results of the test with spoilers on both sides of the NACA 16-012 strut. The sideforce coefficient curve is virtually identical to the 10 kt slope recorded for the previous two models tested in their baseline condition. That is, the 16-012 strut with zero flap and the plugged airbleed strut.

However, unlike the flapped and airbleed strut, the coefficient slope remained practically unchanged at the higher speeds. Unfortunately, the range of sideslip angles tested was limited by the tendency of the spoilers to aggravate the spray problem.

The only occurrence of ventilation that seriously affected the force coefficient happened at 15 degrees and 35 kts. This is quite good compared to the airbleed and flap models at similar speeds and equivalent to the unmodified 16-012 strut as tested by Nelka.[7] The post-vented sideforce coefficient was less changed compared to ante-vented conditions than either Nelka's unmodified 16-012 or his spoiler strut, which had spoilers farther aft.

The behavior of the force coefficients also compared favorably with a blunt based strut, similar to the NACA 16-012, truncated at midchord, tested by Dailey. The sideforce coefficient slope was not as great as that measured by Dailey for the blunt based strut. In fact, it was less than half. However, the ventilation boundary angles were greater and the force changes were much smaller than those associated with the blunt based strut.

The increase in zero sideslip drag caused by the addition of spoilers was about 50 percent, compared to the previously tested baseline strut. The absolute change in drag coefficient was about 0.01, less than for continuous airbleed.

Figure 56 shows the results of the tests of the NACA 16-012 with the spoiler on the starboard side only. The change in lift coefficient at zero sideslip was 0.2, equivalent to a change in sideslip angle of about 8 degrees. This was about the same as the change in lift generated by airbleed. The ventilation angle with port sideslip angle was slightly lower than in the case with the dual spoiler, and the force changes are greater. However, for starboard

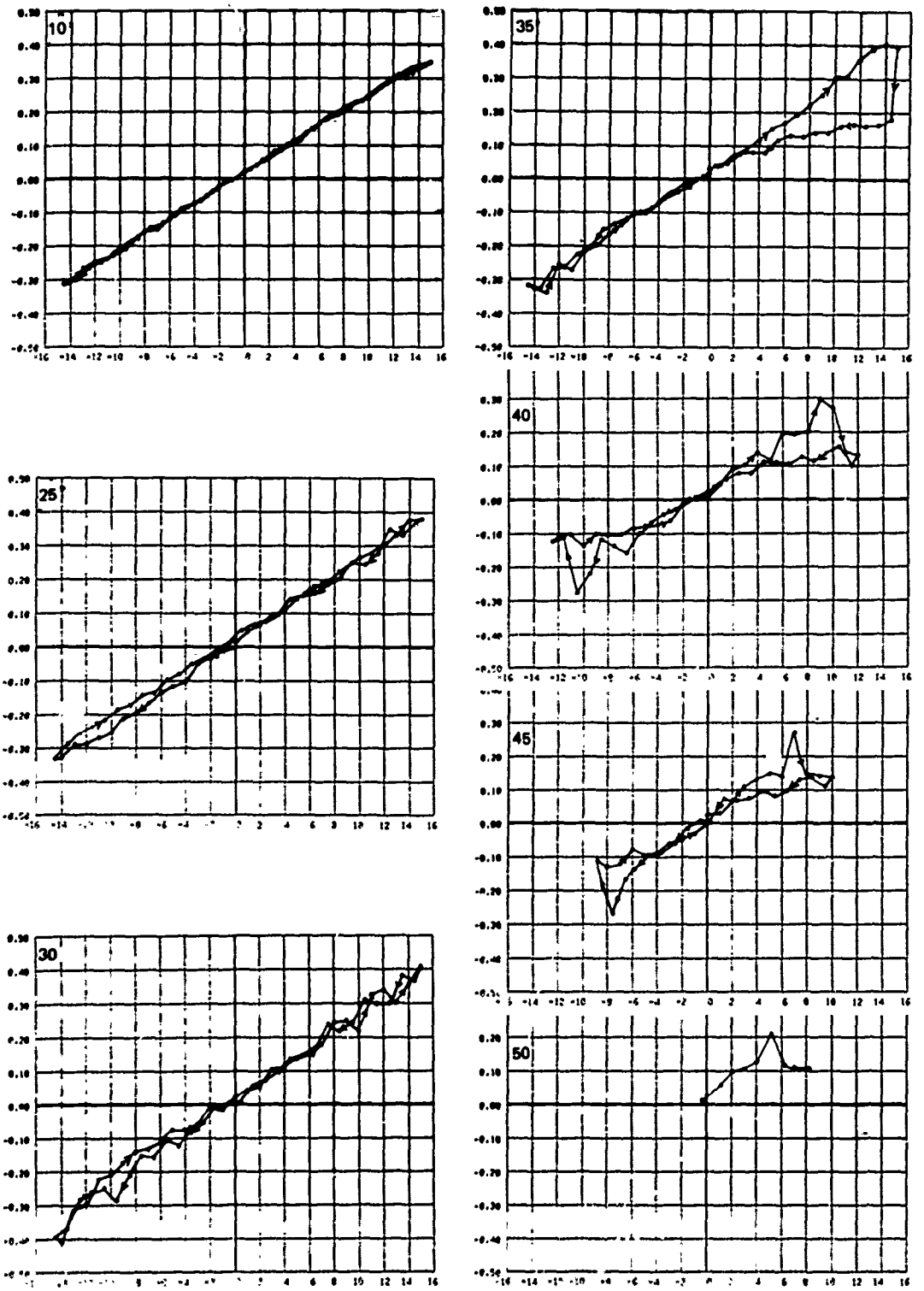

FIGURE 55a SIDEFORCE COEFFICIENT VS. SIDESLIP ANGLE, SPOILER STRUT, WITHOUT FENCES, SPOILER BOTH SIDES, 10, 25, 30, 35, 40, 45, 50 KTS.

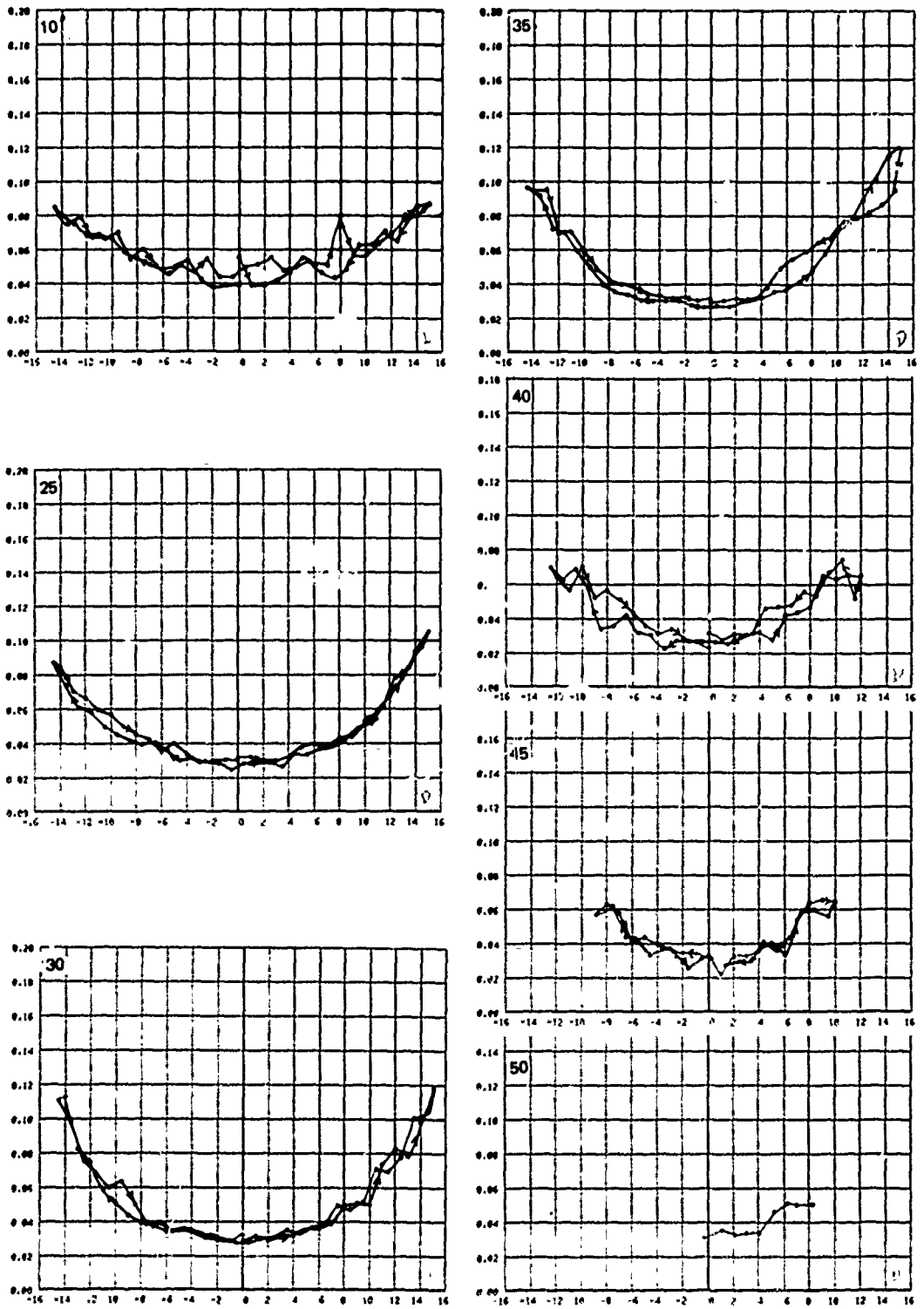

FIGURE 56b DRAG COEFFICIENT VS. SIDESLIP ANGLE, SPOILER STRUT, WITHOUT FENCES, SPOILER BOTH SIDES, 10, 25, 30, 35, 40, 45, 50 KTS.

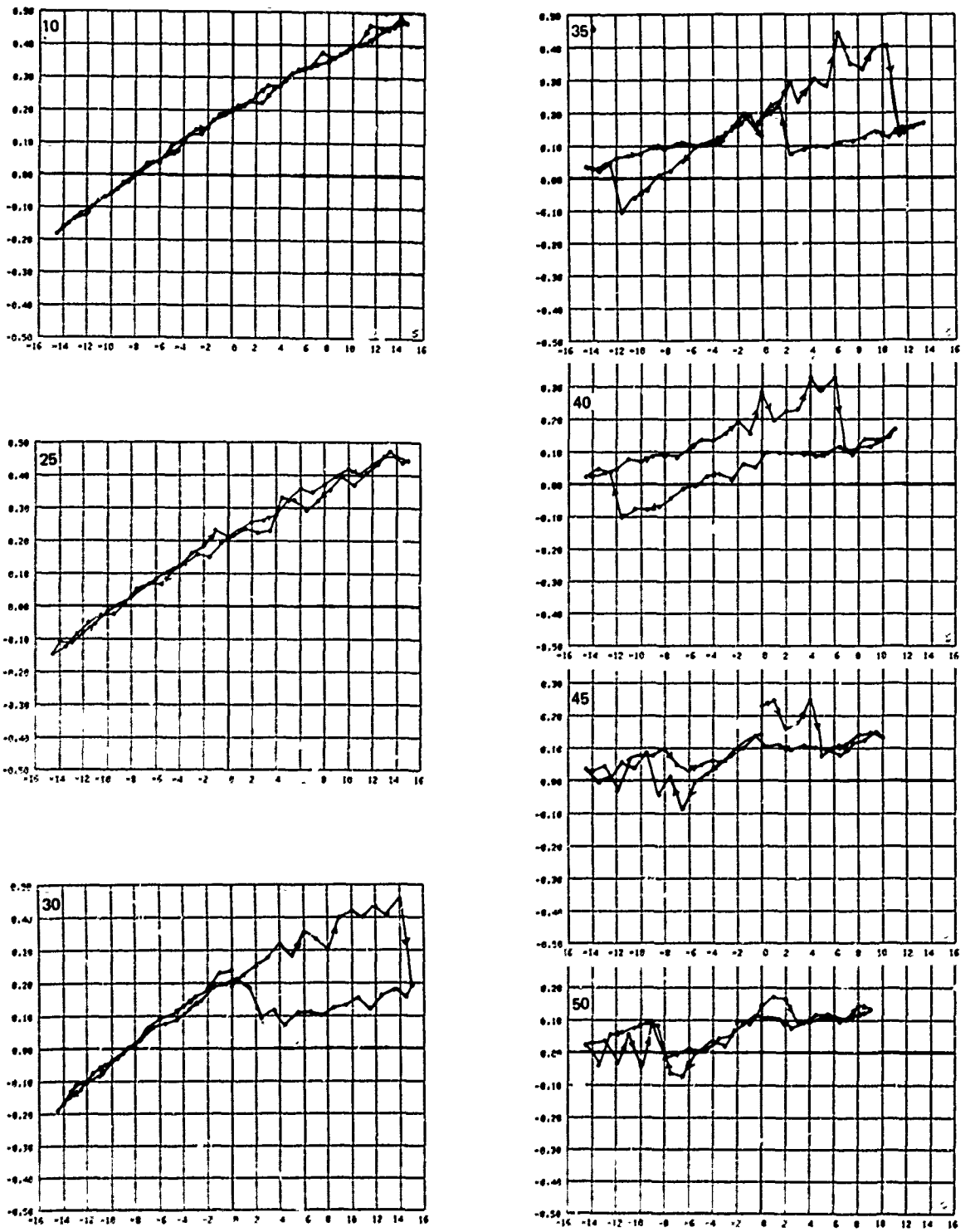

FIGURE 56a SIDEFORCE COEFFICIENT VS. SIDESLIP ANGLE, SPOILER STRUT, WITHOUT FENCES, SPOILER STBD SIDE, 10, 25, 30, 35, 40, 45, 50 KTS.

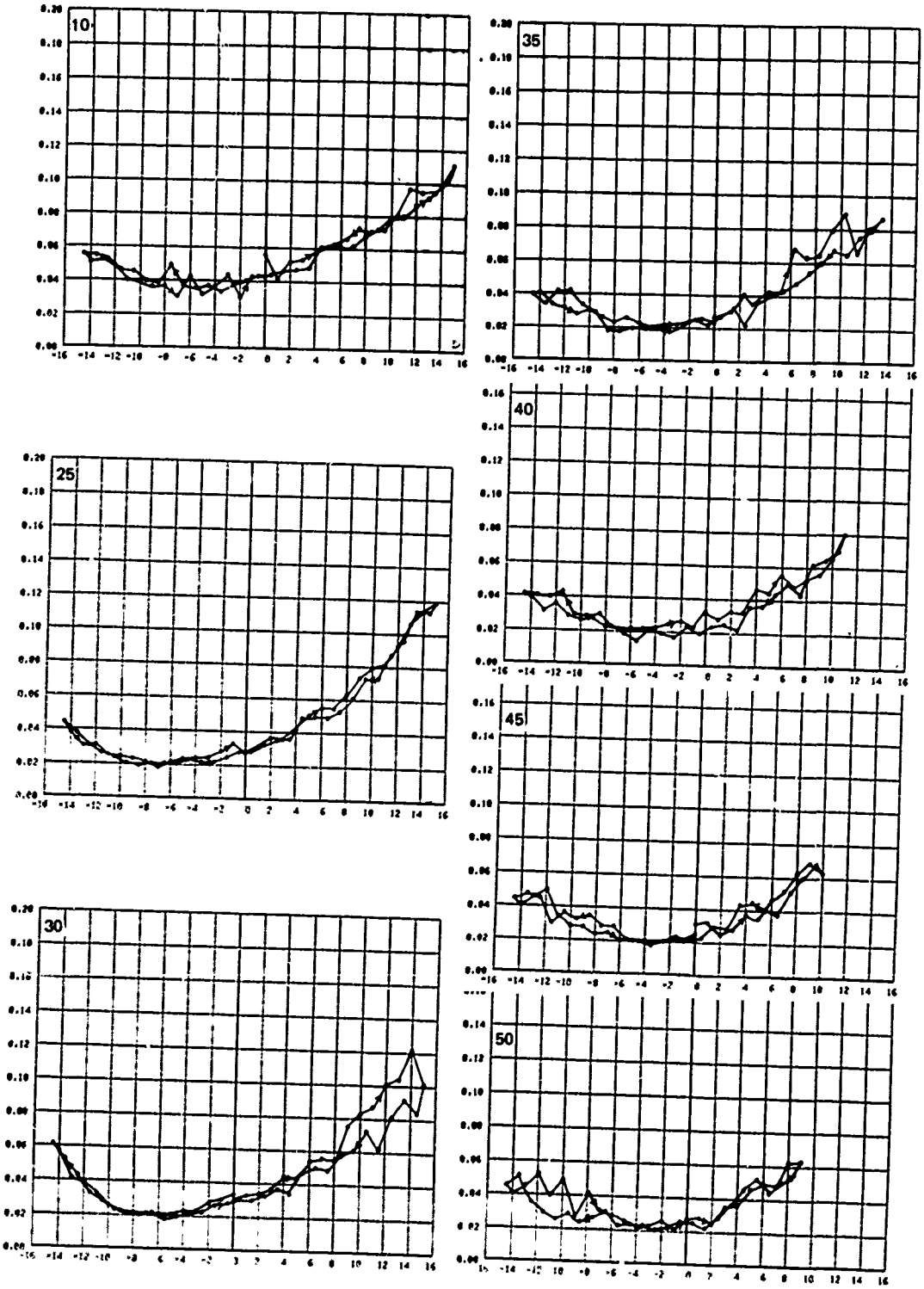

FIGURE 56b DRAG COEFFICIENT VS. SIDESLIP ANGLE, SPOILER STRUT, WITHOUT FENCES, SPOILER STBD SIDE, 10, 25, 30, 35, 40, 45, 50 KTS.

sideslip angle, which is the postulated condition for the use of a retractable starboard side spoiler, either ventilation does not occur until a very large angle, or the force changes accompanying it are not very great.

Interestingly, the drag penalty compared with the baseline case is nil, even with the spoiler deployed. Obviously, there would be little or no drag penalty associated with a properly designed retracted spoiler, but control power would be necessary for actuation.

CONCLUSIONS OF THE SPOILER EXPERIMENT

- A retractable midchord spoiler is a feasible method of reducing sideforce on a surface-piercing strut to nearly zero, and minimizing the adverse effects of ventilation.
- The drag penalty for a single spoiler was below the resolution of the present experiment.
- Fixed midchord spoilers can minimize sideforce anomalies associated with partial and full ventilation to achieve a measure of linearity of response of sideforce to sideslip angle. Spoilers at midchord were more effective than spoilers farther aft.
- The drag penalty associated with double spoilers was about 50 percent of the baseline value at zero sideslip angle.

GENERAL CONCLUSIONS

- Flaps, airbleed or retractable spoilers could be used to affect or nearly eliminate the side-force experienced by a surface piercing strut at an angle of sideslip.
- The flap has the disadvantage that it would be ineffective or detrimental at small angles. Unless air can be prevented from travelling down the hinge intersection, a substantial drag penalty will be incurred.
- Airbleed has many potential advantages, including simplicity. There would be a substantial drag penalty for continuous airbleed. Intermittent airbleed poses control problems, which would be aggravated by the tendency of the air not to cease its effect when shut off.
- Single or double spoilers, while not as positive in reducing sideforce as airbleed, have little or no drag penalty associated with them. Single-sided spoilers would necessarily be retractable, an added complication. It is not known whether the response of a retractable spoiler would be proportional to its extention.

LIST OF REFERENCES

1. Abbott, I.H., and A.E. von Doenhoff, *"Theory of Wing Sections,"* Dover Publications, Inc., New York (1959).

2. Jacobs, E.N. and R.M. Pinkerton, *"Pressure Distribution over a Symmetrical Airfoil Section with Trailing Edge Flap,"* Langley Memorial Aeronautical Laboratory Report No. 360 (Apr 1930).

3. Rothblum, R.S., D.A. Mayer, and G.M. Wilburn, *"Ventilation, Cavitation, and Other Characteristics of High-Speed Surface-Piercing Struts,"* Naval Ship Research and Development Center Report 3023 (Oct 1972).

4. Swales, P.D., R.C. McGregor, R.S. Rothblum, *"The Influence of Fences on Strut and Foil Ventilation,"* 10th ONR Symposium, Boston (1974).

5. Layne, D.E., *"Effects of External Stiffeners on the Ventilation, Force and Cavitation Characteristics of a Surface-Piercing Hydrofoil Strut,"* Naval Ship Research and Development Center Report SPD-621-01 (Apr 1975).

6. Dailey, N.L., *"Experimental Investigation of the Ventilation and Force Characteristics of a Blunt-Based Surface-Piercing Strut,"* Naval Ship Research and Development Center Ship Performance Department Report 479-H-01 (Feb 1973).

7. Nelka, J.J., *"Effects of Mid-Chord Flaps on the Ventilation and Force Characteristics of a Surface-Piercing Hydrofoil Strut,"* Naval Ship Research and Development Center Report 4508 (Nov 1974).

8. Dailey, N.L., M.F. Jeffers, R.S. Rothblum, *"Ventilation and Force Characteristics of the NACA 16-012 Surface-Piercing Strut in Cavitating Flow,"* Naval Ship Research and Development Center Ship Performance Department Report 479-H-03 (Aug 1972).

9. Von Schertel, Hanns, *"Comparative Tests Between an Air Stabilizer and a Conventional Supramar PT50,"* Supramar, Ltd (1967).

10. Von Schertel, Hanns. *"Experimental Investigation of Air-Fed Hydrofoils,"* Supramar, Ltd (Aug 1964).

11. Lang, T.G., D.A. Daybell, and K.E. Smith, *"Water-Tunnel Tests of Hydrofoils with Forced Ventilation,"* NAVORD Report NOTS TP 2363 (Nov 1959).

12. Von Schertel, Hanns, *"Hydrofoil Boats as a New Means of Transportation,"* paper presented to New York Metropolitan Section of SNAME (30 Oct 1958).

13. Hoerner, S.F., *"Fluid-Dynamic Drag,"* published by author (1965).

DTNSRDC ISSUES THREE TYPES OF REPORTS

(1) DTNSRDC REPORTS, A FORMAL SERIES PUBLISHING INFORMATION OF PERMANENT TECHNICAL VALUE, DESIGNATED BY A SERIAL REPORT NUMBER.

(2) DEPARTMENTAL REPORTS, A SEMIFORMAL SERIES, RECORDING INFORMATION OF A PRELIMINARY OR TEMPORARY NATURE, OR OF LIMITED INTEREST OR SIGNIFICANCE, CARRYING A DEPARTMENTAL ALPHANUMERIC IDENTIFICATION.

(3) TECHNICAL MEMORANDA, AN INFORMAL SERIES, USUALLY INTERNAL WORKING PAPERS OR DIRECT REPORTS TO SPONSORS, NUMBERED AS TM SERIES REPORTS; NOT FOR GENERAL DISTRIBUTION.